DISSERTATION

HAZARD AREA MAPPING DURING EXTREME RAINSTORMS IN SOUTH KOREAN MOUNTAINS

Submitted by

Jaehoon Kim

Department of Civil and Environmental Engineering

In partial fulfillment of the requirements

For the Degree of Doctor of Philosophy

Colorado State University

Fort Collins, Colorado

Fall 2012

Doctoral Committee:

Advisor: Pierre Y. Julien

Chester C. Watson
Christopher I. Thornton
Lee H. MacDonald

ABSTRACT

HAZARD AREA MAPPING DURING EXTREME RAINSTORMS

IN SOUTH KOREAN MOUNTAINS

The concern for climate change has increased worldwide. Localized rain storms with high intensity and short duration have been observed in the United States, Europe, Australia, and China. South Korea is one of the countries that have also been impacted by extreme rainfall events during typhoons. Extreme rainstorms have caused major damage from landslides and debris flows in the South Korean mountains.

The Duksan Creek watershed in South Korea was selected to simulate surface runoff using TREX during the extreme rainstorm precipitation event from July 14 to July 16, 2006. The maximum hourly rainfall was 62 mm on July 15 in 2006. The three hour rainfall from 08:00 AM to 11:00AM on this day was 168 mm. This rainstorm triggered 518 landslides and caused major infrastructure damage from debris flows. The three hour rainfall precipitation has a 100 year return period.

The TREX model was calibrated in two mountainous regions of South Korea. The relative percent difference of time to peak and peak discharge on the Naerin Stream and the Naesung Stream were 6.25 %, -2.58 % and 1.90 %, -0.25 %, respectively. The TREX simulation at the Duksan Creek was performed at a 30 m resolution with distributed data on topography (DEM), soil type, and land use. The peak discharge from the TREX simulation at the Duksan Creek watershed was 452 m^3/s. This value was compared to the results of several other methods and the relative percent difference was -1.1 %. The peak discharge was also compared with

specific peak discharge measurements and this value corresponds to the range of values for similar watersheds.

The TREX model can calculate the distribution of infiltration depth. The infiltration depth calculation typically ranged from 0.2 m to 0.3m with maximum value of 1.2 m. Based on the infinite slope analysis, such infiltration depths correspond to a critical slope angle of 25° to 29°. This range of the critical slope angle was comparable to the angle of 26° from the field investigations and from the analysis of satellite images and aerial photographs at the Duksan Creek. Several different hazard mapping methods were compared including a landslide hazard map from the Korea Forest Institute (KFRI), SINMAP, and TREX. The result of the relative predictability of TREX was slightly better an improvement of 24.6 % than the result of SINMAP.

The maximum shear stress could also be calculated by the TREX model. Values of shear stress typically ranged between 0.223 kPa to 0.895 kPa in the tributaries and 1.79 kPa to 17 kPa in the main channel. Based on a critical shear stress analysis, a 1 m diameter boulder reaches incipient motion at a shear stress of 0.895 kPa.

ACKNOWLEDGEMENTS

I am very thankful to my advisor, Dr. Pierre Julien for his great guidance, warm encouragement, and excellent suggestions. I would also like to thank to my committee members: Dr. Chester Watson, Dr. Christopher Thornton of the Department of Civil and Environmental Engineering and Dr. Lee MacDonald of the Department of Forest and Rangeland Stewardship for their directions, comments, and assistance during my studies at Colorado State University.

I also thank CSU staffs including Jenifer Davis, Laurie Alburn, Linda Hinshaw, Karleene Schindler, and Nicole Martinez for their kindness and help. Special thanks extend to Dr. Changwoo Lee, Yongdeok Cho, Kiyong Lee, Dr. Un Ji, Dr. James Halgren, Jazuri Abdullah, Junchul Lee, Dr. Sangki Park, Dr. Jongseok Lee, Sophia Linn, Stephen Chignell, and Anthony Sanchez for data collection, support, and comments on my dissertation. Without their assistance, I could not have finished this research.

I would like to thank all members at the Forest Water Resources Lab in Yeungnam University including Dr. Heonho Lee for their encouragement. I would also like to thank to all Korean alumni of CSU, all Korean students in the Department of Civil Engineering at CSU, people at Korea Institute of Construction Technology, people at the Engineering Research Center at CSU, Chad Martin, Carmen Bernedo, and all my friends in South Korea for their support.

Special thanks to all members of Dr. Julien's Rising Stars including Dr. Seema Shah-Fairbank, Dr. Mark Velleux, Kiyoung Park, Nur Shazwani Muhammad, and Andy Steininger.

Finally, my deepest thanks extend to all my family members including my parents, parents-in-law, and my siblings, and especially my wife Sukhyun Kwon and my daughter Nahyun for their support, encouragement, and unconditional love.

TABLE OF CONTENTS

LIST OF TABLES

LIST OF FIGURES

CHAPTER 1 INTRODUCTION

1.1 PROBLEM STATEMENT

Extreme events occur worldwide and the concern for this is continued to increase. The main extreme events in the world are temperature and precipitation. The change in amount and frequency for extreme event are observed in the United States, Europe, Australia, and China.

South Korea is one of the countries that have been affected by extreme precipitation. The average annual precipitation in Korea is about 1,245 mm (1974 to 2003) and two third of this is concentrated in the summer season. During the past 10 years two typhoons and one heavy rainfall went through and severely damaged the Korean peninsula. The amount of damages with typhoon Rusa in 2002, typhoon Maemi in 2003, and heavy rainfall in 2006 was 5.1 billion dollars, 4.2 billion dollars, and 1.8 billion dollars respectively.

This rainfall pattern due to typhoon and heavy rainfall has caused surface runoff and severe mountain disaster including debris flow and landslides. There are three main causes for landslides, which are geological, morphological, and human causes. The geological cause is weak or sensitive materials, weathered materials, and adversely oriented discontinuities such as faults. The morphological cause is tectonic or volcanic uplift, glacial rebound, and fluvial, wave, or glacial erosion of slope toe or lateral margins. Human cause includes excavation of the slope or its toe, loading of the slope or its crest, and mining.

When it comes to water, slope saturation due to water is a primary cause of landslide. As rainfall infiltrates into soils, it increases pore pressure of soils fully saturated and reduces shear strength on the slip surface. Landslides in Korea usually are induced by intensive rainfall in summer season (Kim et al., 2000).

Figure 1.1. Damaged area in Inje County in Gangwon Province, South Korea

Duksan Creek is located in Inje County in Gangwon-do in Korea. This site is surrounded by high and steep mountains. Residents in this area usually live near the main channel of Duksan Creek.

By the extreme event in July 2006, 17 people were dead and 12 people were missed in Inje County (Lee and Yoo, 2009). All residential areas were swept out due to landslide and debris flow, and people in this area were isolated for three days without any assistance.

The researches for the problems due to extreme event have not been sufficiently studied in South Korea. Thus, hazard area mapping using distributed modeling would be beneficial in South Korea.

1.2 OBJECTIVE

The objectives of this research are to analyze the characteristics of surface runoff in the mountainous area from extreme events using numerical methods for hazard mapping. To accomplish this study, the following analyses will be performed:

- Two dimensional surface runoff modeling of extreme event on the Duksan Creek watershed.
- Landslide hazard area mapping using the TREX simulation and infinite slope model and compare to the TREX results with the SINMAP and Korea Forest Research Institute (KFRI) map.
- Debris flow hazard area mapping using shear stress and compare to shear stress results with field investigation measurements

1.3 APPROACH

The TREX (Two Dimensional Runoff Erosion and Export) model is physically-based computer model that is designed to simulate hydrology, sediment transport, and chemical transport. This model is used in this study to investigate the effect of surface runoff in the mountainous area and hazard area mapping.

This dissertation consists of 6 chapters. Chapter 1 describes an introduction. Chapter 2 presents literature review of extreme event, debris flow and landslides studies, existing models,

and TREX model theory. Chapter 3 identifies site description and analyzes extreme event, Chapter 4 carried out TREX calibration and simulation. Chapter 5 shows hazard area mapping. Chapter 6 describes includes countermeasures for mountainous hazard area. Finally, chapter 7 presents conclusions.

CHAPTER 2 LITERATURE REVIEW

2.1 EXTREME EVENTS

2.1.1 Introduction

There are three different methods for identifying extreme rainfall. The first method is related to the actual rainfall amounts. Karl et al. (1996) focused an extreme change analysis on the daily precipitation event. They found the proportional increase of the total annual precipitation from 1-day extreme events exceeding more than 2 inches or 50.8 mm in a United States area from 1910 to 1994. Using U.S. Climate Extremes Index indicators, they suggested the value of an extreme one day precipitation as twice its value to 101.6 mm. Groisman et al. (1999) defined a "heavy" precipitation threshold as a daily precipitation exceeding 50.8 mm in the countries of the Unites States, Mexico, China, and Australia and exceeding 25.4 mm in the countries of Russia, Canada, Norway, and Poland.

The second method is to examine the frequency of precipitation events. Groisman (2001) showed the maps with values of the maximum daily precipitation associated with the 90^{th} (heavy) and 99^{th} (very heavy) percentiles of precipitation in days.

The third method is to use return period. Kunkel et al. (1999) analyzed the trends of 1 to 7 days extreme precipitation events with one year or a longer return period, because these events had high correlation with hydrologic flooding. Groisman (2001) showed the maps with values of the maximum daily precipitation associated with 1 year (heavy) and 20 year (very heavy) return periods. Spierre and Wake (2010) examined the recurrence intervals of 10, 5, and 1 year of one day events for each station across the Northeast United States for extreme event analysis.

In South Korea, the Korea Meteorological Administration introduces a severe rainfall storm as a huge amount of rainfall with short duration and small area. Generally, the amount of rainfall could be over 30 mm per hour, over 80 mm per day, or 10 % of annual mean precipitation. The duration of rainfall would be a few minutes to a few hours. The area could be the radius of 10 km to 20 km. The Korea Meteorological Administration provides criteria for heavy rain advisory and heavy rain warning with respect to duration and amount of rainfall and these criteria are summarized in Table 2.1.

Table 2.1. The criteria of heavy rainfall (KMA, http://kma.go.kr/weather/warning/standard.jsp)

	Heavy rain advisory	Heavy rain warning
Rainfall duration (hr)	6	6
Amount of rainfall (mm)	>70	>110
Rainfall duration (hr)	12	12
Amount of rainfall (mm)	>110	>180

2.1.2 Trend in the World

The concern about extreme events continues to increase in the world. The main extreme events are temperature and precipitation, and these patterns are the change of frequency and intensity as a result of climate change due to human influences. Table 2.2 summarizes change in extreme phenomena over the world. For mid-latitude regions, heavy precipitation events have increased since 1951 and for the United States and the United Kingdom, the precipitation events over a 10 year return period have also increased.

Table 2.2. Change in extremes for phenomena over the world (Solomon et al., 2007)

Phenomenon	Change	Region	Period	Confidence
Low-temperature days/nights and frost days	Decrease, more so for nights than days	Over 70% of global land area	1951–2003 (last 150 years for Europeand China)	Very likely
High-temperature days/nights	Increase, more so for nights than days	Over 70% of global land area	1951–2003	Very likely
Cold spells/snaps (episodes of several days)	Insufficient studies, but daily temperature changes imply a decrease			
Warm spells (heat waves) (episodes of several days)	Increase: implicit evidence from changes of daily temperatures	Global	1951–2003	Likely
Cool seasons/ warm seasons (seasonal averages)	Some new evidence for changes in inter-seasonal variability	Central Europe	1961–2004	Likely
Heavy precipitation events (that occur every year)	Increase, generally beyond that expected from changes in the mean (disproportionate)	Many mid-latitude regions (even where reduction in total precipitation)	1951–2003	Likely
Rare precipitation events (with return periods > ~10 yr)	Increase	Only a few regions have sufficient data for reliable trends (e.g., UK and USA)	Various since 1893	Likely (consistent with changes inferred for more robust statistics)
Drought (season/year)	Increase in total area affected	Many land regions of the world	Since 1970s	Likely
Tropical cyclones	Trends towards longer lifetimes and greater storm intensity, but no trend in frequency	Tropics	Since 1970s	Likely; more confidence in frequency and intensity
Extreme extratropical storms	Net increase in frequency/intensity and poleward shift in track	Northern Hemisphere land	Since about 1950	Likely
Small-scale severe weather phenomena	Insufficient studies for assessment			

Karl et al. (1996) found that one day precipitation exceeding 50.8 mm increased between 1910 and 1994. Karl and Knight (1998) verified that the increase in precipitation is primary due to the heavy and extreme daily precipitation events. Kunkel et al. (1999) found the increase trends in one year seven day events of 3 % per decade

and in five year seven day events of 5 % per decade. These data were confirmed with statistical significance. Kunkel et al. (2003) analyzed extreme precipitation events and indicated that the frequency of extreme precipitation events has been largely increased in the United States since the 1920s and 1930s.

Klein Tank et al. (2002) found a positive trend in the mean amount per wet day in Europe between 1946 and 1999. Klein Tank and Konnen (2003) confirmed that all Europe-average indices of wet extremes were increased between 1946 and 1999.

Haylock and Nicholls (2000) examined three indices of extreme rainfall including extreme frequency, extreme intensity, and extreme percent in Australia. They found that extreme events were more frequent and intense during years with high rainfall. Alexander et al. (2007) found that trends in extreme precipitation were highly correlated with trends in mean and indicated that the rate of change of extreme was faster in relation to the mean in Australia.

Wang and Zhou (2005) observed the trend in extreme events in China between 1961 and 2001. The pattern of extreme daily precipitation events increased significantly in the southwest, northwest, and east of China, and decreased significantly in central, north and northeast China. For the Yangtze River basin, the extreme precipitation events increased by 10 % to 20 % every 10 years in summer. Xu et al. (2011) found that extreme precipitation amounts in China increased by 10.9 mm between 1990 and 2007.

Easterling et al. (2000) showed the map where significant changes in heavy precipitation have occurred during past decades in the world.

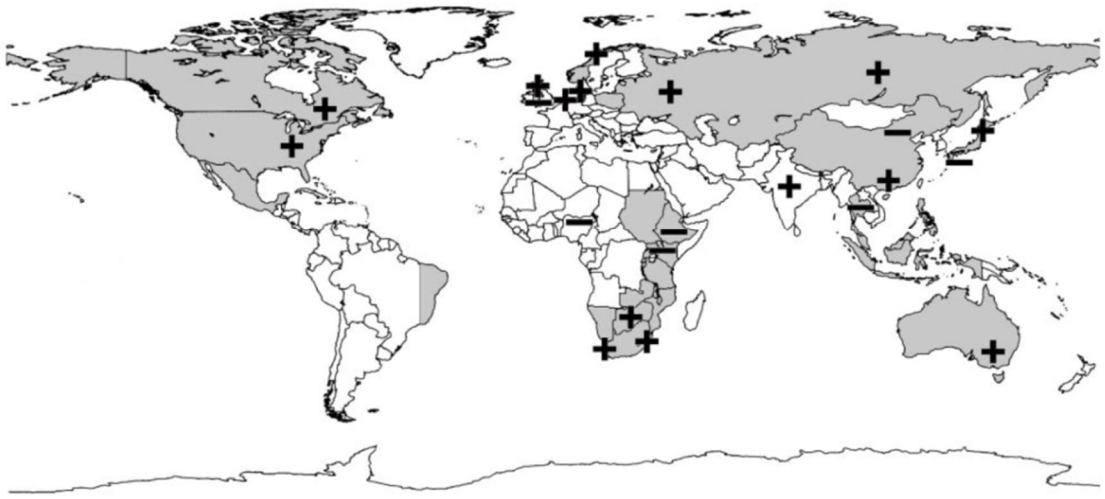

Figure 2.1. Regions where significant changes in heavy precipitation have occurred during the past decades (Easterling et al., 2000)

2.1.3 Trend in South Korea

The annual precipitation amount in South Korea is 1,245 mm and has seasonal variation. Two thirds of precipitation occurs between June and September during the rainy typhoon season. One fifth of the annual precipitation occurs between November and April. This precipitation pattern causes frequent floods and droughts (MLTM, 2006). The trend of mean annual precipitation in South Korea is shown in Figure 2.2.

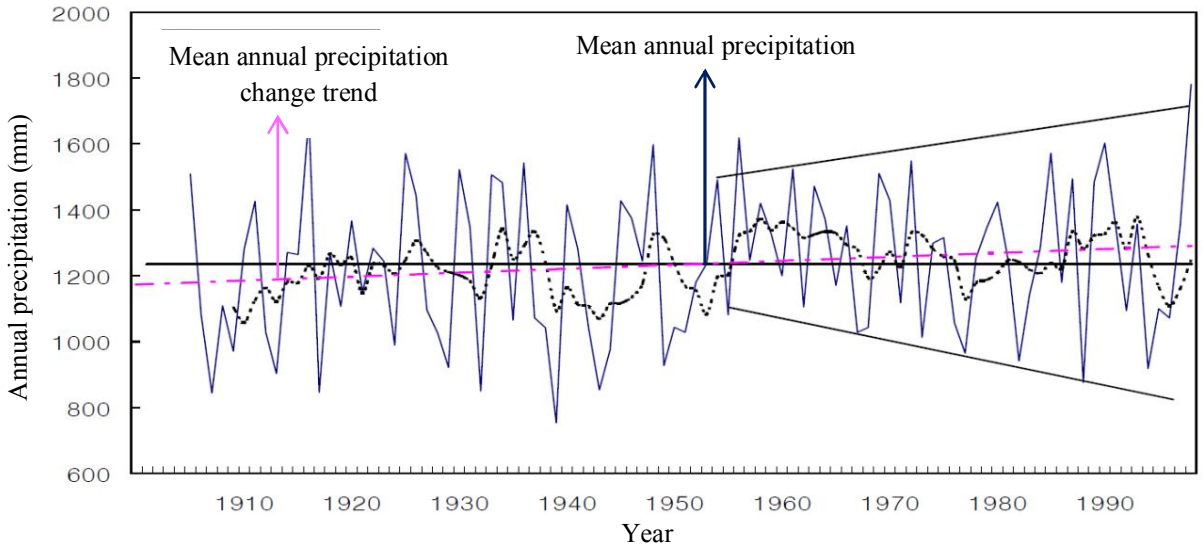

Figure 2.2. The mean annual precipitation change in South Korea (MLTM, 2001)

The trend of mean annual precipitation change has slightly increased since 1905, but the variation range of mean annual precipitation has increased since 1955.

Jung et al. (2002) studied 46 years of daily precipitation record and confirmed that extreme precipitation events have significantly increased in South Korea. Chang and Kwon (2007) examined 187 stations in Korea between 1973 and 2005 and tried to mapping of 90th percentile of summer daily precipitation total. He also indicated that the number of precipitation days exceeding 50mm and 30 mm increased at all stations. Jung et al. (2011) investigated 183 weather station data between 1973 and 2005. They found that annual precipitation increase was mainly caused by the mean summer precipitation increase. This pattern was related to the trend of frequency and intensity of heavy precipitation. Thus, they concluded that the increase in annual precipitation was significantly associated with the increase in heavy rainfall events during the summer season.

Cha (2010) examined the characteristics of the precipitation in South Korea from 1954 to 2009. The severe rain storm occurs 20.8 times per year and the number of severe rain storm has increased since the late 1990's. In July 2006, 22 times of severe rain storm occurred and these events were caused by three typhoons including Ewiniar, Bilis, and Gaemi. Typhoon Bilis vanished out in China, however it supplied a lot of water vapor to Korea peninsula continuously and activated a rain front in July 14 to July 20 in 2006.

The severe rain storms bring severe damage and this trend has been increased in South Korea. When this damage focuses on mountainous stream areas damage patterns can include landslide and debris flows. The next section will deal with landslide and debris flows due to extreme precipitation.

2.2 LANDSLIDES AND DEBRIS FLOWS

2.2.1 Definition

Debris flow is water flow with massive earth material generated by rainfall. Varnes (1958) defined debris flow as rapidly moving, gravity induced slurries of granular solids, water, and air. Debris flows can be all types of flows including rock debris, but mudflows refer to finer size debris. Varnes (1958) also defined mudflows as the mixture of water and sediment material that has at least 50 % solids (sand size or smaller) by weight.

A landside is the downward and outward movement of slope forming material. Cruden (1991) defined the definition of a landslide as the movement of a mass of rock, debris, or earth down a slope. Varnes (1978) described the dimension and geometry of a landslide and terminology for landslides.

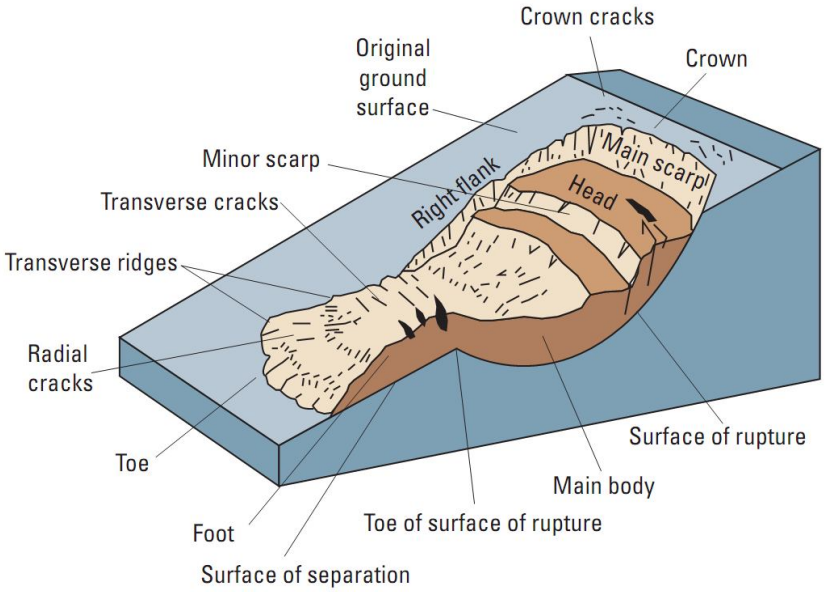

Figure 2.3. Terminology for landslide features (modified from Varnes, 1978)

There is no criterion to describe landslides by size, but Cornforth (2005) provided landslide size by the area of landslides. It is summarized in Table 2.3.

Table 2.3. Grouping landslides by area in plan

Descriptor	Area (ft^2)	Area (m^2)
Very small	< 2000	<200
Small	2,000 - 20,000	200 - 2,000
Medium	20,000 - 200,000	2,000 - 20,000
Large	200,000 - 2,000,000	20,000 - 200,000
Very large	2,000,000 - 20,000,000	200,000 - 2,000,000
Huge	> 20,000,000	> 2,000,000

Fell (1994) classified landslide sizes by volume and it is shown in Table 2.4.

Table 2.4. Size classification for landslides

Size class	Size description	Volume (m^3)
2	Extremely small	<500
2.5	Very small	500 - 5,000
3	Small	5,000 - 50,000
4	Medium	50,000 - 250,000
5	Medium-large	250,000 - 1,000,000
6	Very large	1,000,000 - 5,000,000
7	Extremely large	> 5,000,000

2.2.2 Classification and Causes

Highland et al. (2008) classified landslides into six basic types: falls, topples, slides, spreads, flows, and combination of two or more. These landslide types are shown in Table 2.5.

Table 2.5. Types of landslides (Modified from Varnes, 1978)

TYPE OF MOVEMENT		TYPE OF MATERIAL		
		BED ROCK	ENGINEERING SOILS	
			Predominantly coarse	Predominantly fine
FALLS		Rock fall	Debris fall	Earth fall
TOPPLES		Rock topple	Debris topple	Earth topple
SLIDES	ROTATIONAL	Rock slide	Debris slide	Earth slide
	TRANSLATIONAL			
LATERAL SPREADS		Rock spread	Debris spread	Earth spread
FLOWS		Rock flow (deep creep)	Debris flow (soil creep)	Earth flow
COMPLEX		Combination of two or more principal types of movement		

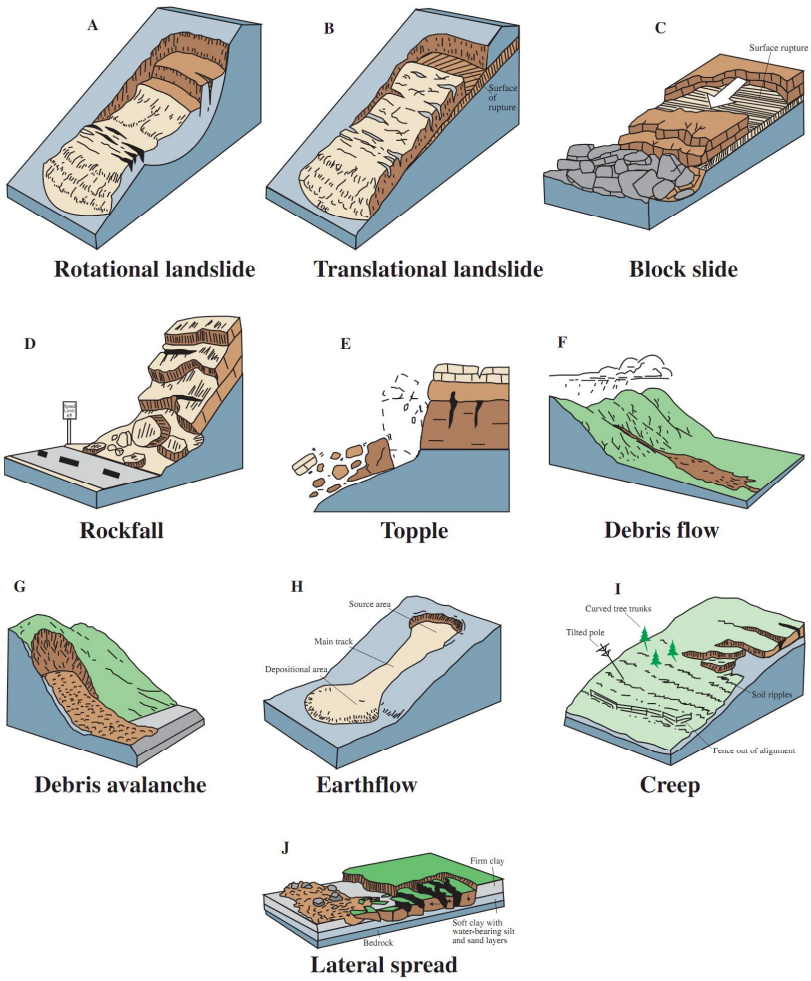

Figure 2.4. The types of landslides (USGS, http://pubs.usgs.gov/fs/2004/3072/fs-2004-3072.html)

A rockfall starts from the detachment of soil or rock, or both, from steep slopes along a surface with little or no shear displacement. It occurs on steep or vertical slopes and travels very rapidly. Slope undercut by natural processes, such as streams and rivers, or differential weathering, are the main reason for the rockfall

Topple is known as the forward rotation out of a slope of a soil or rock mass. The places of occurrence are volcanic terrain, streams, or rivers with steep banks due to gravity, water, or ice in cracks in the mass. It moves extremely slowly to extremely rapidly.

Slide is downslope movement of soil or rock. A translational landslide is one example of slides and one of the most common types of landslides. The cause of this landslide is primarily intense rainfall or rise in ground water within the slide due to rainfall and snowmelt. It moves slowly at the initial time (1.5 m/month) but rapidly (1.5 m/day) under extreme conditions.

Spread is an extension of a cohesive soil or rock mass. Lateral spread is one example. It occurs on very low slopes or flat terrain. Saturation of an underlying weak layer due to precipitation or snow melt is one reason. It moves moderately, or sometimes rapidly.

Flow is a spatially continuous movement. Debris flow belongs to this movement. It occurs in steep gullies and canyons. The reason for debris flow is intense surface water flows due to heavy precipitation or rapid snowmelt.

2.2.3 Landslides with Rainfall

From the review of the landslides above, most landslides had a close relationship with water. Especially saturated soil due to precipitation is the primary cause for landslides and the research for landslides concerning rainfall needs to be reviewed.

Montrasio and Valentio (2008) developed a simplified, physically based stability model for the assessment of the safety factor of slopes for rainfall induced shallow landslides and applied this method in the Emilia Romagna region in Italy. The stability was lowest in the maximum daily rainfall depth. Muntohar and Liao (2009) estimated the occurrence time of a slope failure using the Green and Ampt model and the infinite slope method. For rain infiltration induced slope failure, a slope tends to have a slip surface at a depth of about 1.5–3.0 m below the surface. Casagli et al. (2006) investigated two landslides in Pistoia in Italy, and the most critical time step for failure was a few hours following the rainfall peak. Shieh et al. (2009) applied

effective rainfall intensity and effective accumulation precipitation as the index to establish the rainfall criteria of debris flow occurring after the earthquake.

On the other hand, the disasters due to rainfall in mountainous areas are increasing, and the research for this is also on going. The most common types of landslides in Korea are debris flow, rock fall, planar slide, rock creep, and rotational slide (Kim, 2000). Among them, debris flow that occurs along the mountainous valley is a dominant type of landslide. Initially, it starts from a translational slide and then changes to debris flow. Therefore, most debris flow is related to translational slides. Kim et al. (1998) researched landslides in the northern part of South Korea. The debris flow of 66 % was caused by intensive rainfall. The bedrock was granite which was more weathered than metamorphic rock. These properties increased water permeability and then raised shear stress. Kim et al. (2009) investigated 10 landslides since 1990. The landslide occurrence depended on the rainfall intensity rather than rainfall duration. The shallow translational slides were dominant in the granite bedrock area. Park (2008) studied the characteristics of landslides from debris flow in Gangwon Province. The landslides of 55 % were debris flow and the causes for landslides were saturated soil and infiltration.

2.2.4 Landslide Models

The research for the quantification of landslide hazards is classified as the statistical method and the deterministic method. The statistical method is based on the frequency of landslides and is difficult to apply to different areas. The deterministic method relies on physics and mechanics, and the prediction parameters can be topographic, geologic, soil, and rainfall. Several landslide models have been developed since the 1990's, and five models were reviewed.

The first model is the Stability INdex MAPing (SINMAP) for shallow landslide (Pack et al., 1998a, Pack et al., 1998b, Pack et al., 2001, Pack et al., 2005). This model combines the infinite slope model with a hydrological model. It provides 6 kinds of stability index. Mohr-Coulomb failure criterion was applied to limit equilibrium equation and failure slide is assumed to parallel with earth surface. The limitation of this model is that it cannot be applied to deep seated instability, including deep earthflows and rotational slumps, and it needs field information such as soil and climate properties.

The second model is the SHAllow Landsliding STABility Model (SHALSTAB). This model is a physically based model for the topographic control on shallow landsliding (Dietrich and Montgomery, 1998). The hydrological model is TOPOG which predicts the soil saturation from steady state rainfall in a spatially constant thickness of cohesionless soils on each topographic element. The limitation is that several parameters, including soil cohesion, were skipped to compute slope instability.

The third model is Level I Stability Analysis (LISA). This model was developed by Hammond et al. (1992) for the U.S. Forest Service and a Monte Carlo simulation was used to estimate a probability of slope failure. The limitation of this model is that LISA cannot simulate the size or number of failure on a particular landform, or the likely locations of failures, or the type of failure.

The fourth model is the Distributed Shallow Landslide Analysis Model (dSLAM). This model was developed by Wu and Sidle (1995 and 1997) and is a distributed, physically based slope stability model. This model is based on an infinite slope model, a kinematic wave groundwater model and a continuous change vegetation root strength model. This model assumes that infiltration capacity is larger than rainfall intensity, therefore, hortonian flow was

not considered. The limitation of this model is that many parameters, including effective soil cohesion, the cohesion attributed to root strength, and vegetation surcharge, are used to obtain slope stability.

The fifth model is the Transient Rainfall Infiltration and Grid-Based Regional Slope Stability Model (TRIGRS) by Baum et al. (2008) for the U.S. Geological Survey. This model is based on a Fortran program for calculating transient pore pressure changes and factor of safety. Infiltration was analyzed by an analytical solution of the Richards' equation. Input data that are hard to obtain in this model are soil depth and initial water-table depth for running this program. The results are also very sensitive to the initial conditions. This model is not applicable for use on slopes steeper than 60°.

From the review of landslide models, SINMAP was used to simulate landslide in Duksan Creek watershed because the input parameters of this model are simple compared to other models and the results of SINMAP are represented to stability index (factor of safety) that is easy to compare with the TREX simulation results.

2.3 EXISTING MODELS

There are three types of basic watershed models and they are lumped parameter model, advanced lumped parameter (semi distributed) model, and distributed model. The lumped parameter model is the entire watershed expressed as one container with constant parameters. The rational method is one example. The advanced lumped parameter model divides the watershed into small sub basins, and parameters vary with sub basins. Examples of this method are HEC-HMS (Hydrologic Engineering Center - Hydrologic Modeling System), HSPF (Hydrologic Simulation Program-Fortran), SWAT (Soil and Water Assessment Tool), and

KINEROS (Kinetic Runoff and Erosion). The distributed model represents watersheds as raster cells with parameters that are fully distributed in space. SHETRAN, CASC2D (CASCade 2 Dimensional model), GSSHA (Gridded Surface/Subsurface Hydrologic Analysis), and TREX (Two Dimensional Runoff Erosion and Export) are the examples of the distributed model. Each model has its advantages and limitations, and it is necessary to review the existing models before further steps are taken.

2.3.1 Lumped Parameter Model

Kuichling (1889) estimated design discharge for small watershed up to 200 acres (80 hectares). The assumption of this method is if the intensity of rainfall is constant, the entire drainage area influences the peak discharge as elapsed time passes. The rainfall intensity is uniform at the entire watershed, and the assumption of uniform distribution is reasonable for small area. The equation for calculating discharge consists of runoff coefficient, rainfall intensity, and drainage area. The runoff coefficient for forest land use is 0.05 to 0.25.

2.3.2 Advanced Lumped Parameter Models

2.3.2.1 HEC-HMS

HEC-HMS (Hydrologic Engineering Center - Hydrologic Modeling System) is designed to simulate the precipitation-runoff processes of dendritic watershed systems (Scharffenberg and Fleming, 2010). This model is good for a wide range of geographic areas. HEC-HMS divides the entire watershed into several sub basins. The hydrograph produced by this model can be used with water availability, urban drainage, flow forecasting, future urbanization impact, reservoir spillway design, flood damage reduction, floodplain regulation, and systems operation.

The limitation of HEC-HMS is to simulate evaporation and infiltration at the same time and to compute soil erosion and sediment transport.

2.3.2.2 HSPF

HSPF (Hydrologic Simulation Program-Fortran) was developed from the Stanford watershed model in the early 1960's (Bicknell et al., 1996). Using continuous rainfall and other meteorological records, HSPF can compute hydrology and water quality parameter on a watershed. This model can simulate interception, infiltration, soil moisture, surface runoff, interflow, base flow, snowpack depth and water content, snowmelt, evapotranspiration, groundwater recharge, dissolved oxygen (DO), biochemical oxygen demand (BOD), temperature, pesticides, fecal coliforms, sediment detachment and transport, sediment routing by particle size, channel routing, reservoir routing, constituent routing, pH, nitrogen and phosphorus compounds, and plankton. The routing can be done by the modified form of the kinematic wave equation. This model has been applied to a large area covering 160,000 km^2 in the Chesapeake Bay watershed, and to small areas of a few acres near Watkinsville, Georgia. The sediment can be computed but metals cannot be simulated by this model.

2.3.2.3 SWAT

SWAT (Soil and Water Assessment Tool) was developed to predict the impact of land management practices on water, sediment, and agricultural chemical yields in large complex watersheds with varying soils, land use and management conditions over long periods of time (Neitsch et al., 2009). This model is a physically based model and can simulate rainfall, infiltration, flow routing through basin stream (including lateral flow, groundwater flow, and transmission losses), sediment and chemical transport through ponds, reservoirs, and streams. For the purpose of the modeling, the entire watershed can be divided into a number of sub basins.

It is beneficial to use sub basins when they have different land uses or soil types. For each sub basin input information can be grouped or organized into the following categories: climate, hydrologic response unit, ponds/wetlands, groundwater, and main channel. The benefits of this model are that watersheds without stream gage data can be modeled and that the relative impact of alternative input data such as changes in management practices, climate, vegetation, etc. on water quality or other variables of interest can be quantified. Since SWAT is a long term yield model it cannot simulate detailed, single event flood routing.

2.3.2.4 KINEROS

KINEROS (Kinetic Runoff and Erosion) is an event oriented, physically based model (Woolhiser et al, 1990). This model can simulate interception, infiltration, surface runoff, and erosion from small agricultural and urban watersheds. The watershed surface and channel network are expressed by a cascade of planes and channels. The general approach of KINEROS is to divide the entire watershed into a channel branching system with plane elements. The parameters, including rainfall input and initial conditions, may be different for each plane. The kinematic wave approximation and Manning roughness are applied to simulate one dimensional flow routing. KINEROS may be beneficial to determine the effects of various artificial features such as urban developments, small detention reservoirs, or lined channels on flood hydrographs and sediment yield. This model is event oriented and does not have components to describe evaporation and soil water movement between storms. Thus, it cannot maintain a hydrologic water balance between storms.

2.3.3 Distributed Model

2.3.3.1 SHETRAN

SHETRAN starts from SHE (Systeme Hydrologiqure Europeen) and it is a fully distributed and physically based model (Ewen et al., 2000). SHETRAN consists of three components including water flow, sediment transport, and contaminant transport. The main processes in this model are: interception, evaporation and transpiration, infiltration, snowpack and snowmelt, groundwater seepage discharge, sediment erosion and deposition, advection, dispersion, and decay. The Saint-Venant equation and diffusion approximation are used for channel flow and overland flow. The variable saturated flow equation (3D) is used in subsurface flow. The source code of SHETRAN is not open to the public.

2.3.3.2 CASC2D

CASC2D (including CASC2D-SED) (Julien et al. 1995; Johnson et al. 2000; Rojas, 2002; Julien and Rojas, 2002; Rojas et al. 2003) is two dimensional, fully distributed, physically based, and an event-oriented model that simulates rainfall, interception, infiltration, overland flow, channel flow, sediment erosion, and deposition. For surface waters, flow routing is accomplished using diffusive wave approximation and is two dimensional overland and one dimensional in channels. This model does not include groundwater flow, but it can be coupled with GIS-based data.

CASC2D has been applied to a wide variety of spatial scales from large river basins (12,000 km^2) to moderate watersheds (560 km^2) (Molnár and Julien, 2000) to small watersheds (20-30km^2) (Rojas, 2002). The modified Kilinc-Richardson equation is used to determine overland erosion, and the Engelund-Hansen equation is used to compute channel erosion. The source code of CASC2D is open to the public.

2.3.3.3 GSSHA

GSSHA (Gridded Surface/Subsurface Hydrologic Analysis) is a spatially-distributed, physically-based hydrologic model (Downer and Ogden, 2004). GSSHA has its origin in CASC2D. GSSHA can simulate stream flow generated by both infiltration-excess and saturation-excess mechanisms, as well as exfiltration and groundwater discharge to stream. GSSHA can represent lateral groundwater flow with two dimensional vertically averaged approximation for water movement in saturated zone. Interaction between stream and groundwater and exfiltration are calculated using Darcy's law. The source code of CASC2D is open to public.

2.3.3.4 TREX

TREX (Two-Dimensional Runoff, Erosion and Export) is a spatially distributed, physically based model that can simulate precipitation, interception, snowpack and snowmelt, infiltration, transmission loss, overland flow, channel flow, soil erosion, sediment transport, and chemical transportation, and fate at the watershed scale (Velleux et al. 2008; England et al. 2007; Velleux et al. 2006; Velleux, 2005). TREX has its origin with CASC2D (Johnson et al. 2000; Rojas, 2002; Julien and Rojas, 2002) for surface hydrology and sediment transport and combines chemical transport from the WASP/IPX series of water quality models (Ambrose et al. 1993; Velleux et al. 2001)

Hydrologic processes include precipitation and interception, snowpack and snowmelt infiltration and transmission loss, infiltration and transmission loss, storage, and overland and channel flow. Precipitation can be set up to one station rainfall or distributed rainfall stations in terms of time and space. Interception and surface storage may be computed as equivalent depths. Infiltration and transmission loss was calculated by Green and Ampt (1911) relationship.

Overland flow is two dimensional and simulated by the diffusive wave approximation. Channel flow is one dimensional and computed by the diffusive wave approximation.

Sediment processes are composed of advection and diffusion, erosion and deposition, and bed elevation change. The parameters are solid concentrations in overland, soil, stream flow, and stream bed sediment. Any number of particle sizes can be simulated.

Chemical transport and fate processes consist of chemical partitioning and phase distribution, chemical advection, erosion and deposition, infiltration and transmission loss, and mass transfer and transformation. The variables are chemical concentrations in overland runoff, soil, stream flow, and stream bed sediment. Any number of chemicals can be simulated.

Water, sediment, and chemicals can come into streams by overland flow and return to overland by water level exceeded from bank height. TREX source code, manual, and references are open to the public.

Existing models were reviewed to determine an appropriate model to simulate surface runoff and sediment effect from heavy rainfall with short duration in steep, mountainous areas. For this research, the model requirements for simulating the study site were summarized below:

1. Model can analyze fully distributed parameters
2. Model can simulate single heavy intense rainfall with short duration
3. Model can compute sediment transport with heavy intense rainfall
4. Model can be compatible with GIS

From the model requirements above, TREX was selected to simulate the Duksan Creek watershed, and the theoretical background is reviewed in the next section.

2.4 TREX MODEL THEORY

The TREX model is a spatially distributed model that can evaluate watershed hydrology, sediment transport, and contaminant transport. Since the first objective of this research is to simulate extreme event on the Dusan Creek TREX model theory is focused on watershed hydrology. The hydrologic process includes: (1) rainfall and interception, (2) infiltration and transmission loss, (3) storage, and (4) overland and channel flow.

2.4.1 Rainfall and Interception

The hydrologic cycle starts from precipitation. When it reaches the ground surface, it is initially intercepted by vegetation on the land. When an ambient temperature is below 0°C, snow is formed (Maidment, 1993). Precipitation includes both rainfall and snowfall. Since snowfall can be represented as an equivalent depth (or volume) of water, it may be expressed as equivalent precipitation. The total volume of water reaching the near surface is:

$$\frac{\partial V_g}{\partial t} = i_g \; A_s \qquad (2.1)$$

where: V_g = gross precipitation water volume [L^3]
i_g = gross precipitation rate [LT^{-1}]
A_s = surface area over which precipitation occurs [L^3]
t = time [T]

Interception is gross precipitation that wets and adheres to vegetation until it is returned to the atmosphere through evaporation. The amount of water intercepted depends on (1) the storm water character; (2) the species, age, and density of prevailing plants and trees; and (3) the season of the year (Viessman and Lewis, 2003). Interception is dominant when the precipitation

is in an early period and the rainfall intensity is low. Conceptually, interception may be expressed as a volume. The net rainfall volume is the difference between the gross rainfall volume and the volume lost to interception.

$$V_i = \left(S_i + E\, t_R\right) A_s \tag{2.2}$$

$$\begin{aligned} V_n &= V_g - V_i \qquad for: V_g > V_i \\ V_n &= 0 \qquad\qquad for: V_g \le V_i \end{aligned} \tag{2.3}$$

where: V_i = interception volume [L^3]
S_i = interception capacity of projected canopy per unit area [L^3L^{-2}]
E = evaporation rate [LT^{-1}]
t_R = precipitation event duration [T]
V_n = net precipitation volume reaching the surface [L^3]

Note that when the total cumulative volume of precipitation during an event is less than the volume of interception, the net precipitation on the ground surface is zero. For a single storm event, the interception volume recovered by evaporation may be neglected. Net volume of precipitation can be represented as a net precipitation rate:

$$i_n = \frac{1}{A_s}\frac{\partial V_n}{\partial t} \tag{2.4}$$

where: i_n = net (effective) precipitation rate at the surface [LT^{-1}]

2.4.2 Infiltration and Transmission Loss

Infiltration is the process that precipitation moves downward from the ground surface to the subsurface. The infiltration rate is affected by hydraulic conductivity, capillary action, and gravity as the soil matrix goes to saturation. Many relationships has been studied to explain infiltration that are presented by Green and Ampt (1911), Richards (1931), Philip (1957), and Smith and Parlange (1978). The Green and Ampt equation was used for TREX because this equation provides an exact analytical solution using approximate physical theory. The assumption of this equation is that the wetting front is a sharp boundary which divides soil moisture content below from saturated soil moisture content above, the wetted zone increases as infiltration begins, and the ponded depth is negligible. The Green and Ampt equation can be represented as (Li et al. 1976; Julien, 2002):

$$f = K_h \left(1 + \frac{H_c \left(1 - S_e\right) \theta_e}{F} \right) \tag{2.5}$$

where: f = infiltration rate [LT^{-1}]
K_h = effective hydraulic conductivity [LT^{-1}]
H_c = capillary pressure (suction) head at the wetting front [L]
θ_c = effective soil porosity = $\left(\varphi - \theta_r\right)$ [dimensionless]
φ = total soil porosity [dimensionless]
θ_r = residual soil moisture content [dimensionless]
S_e = effective soil saturation [dimensionless]
F = cumulative (total) infiltrated water depth [L]

The water in the channel can be lost due to transmission loss. The rate of transmission loss may be influenced by several factors. The capillary suction head can be important with unsaturated sediment in the ephemeral channel. Woodward (2007) described the relationship for

transmission loss. Abdullrazzak and Morel-Seytoux (1983) made use of the Green and Ampt (1911) equation for transmission loss. The transmission loss may be expressed as:

$$t_l = K_h \left(1 + \frac{(H_w + H_c)(1 - S_e)\theta_e}{T} \right) \qquad (2.6)$$

where: t_l = transmission loss rate [LT^{-1}]
K_h = effective hydraulic conductivity [LT^{-1}]
H_w = hydrostatic pressure head (depth of water in channel) [L]
H_c = capillary pressure (suction) head at the wetting front [L]
θ_c = effective sediment porosity = $(\varphi - \theta_r)$ [dimensionless]
φ = total sediment porosity [dimensionless]
θ_r = residual sediment moisture content [dimensionless]
S_e = effective sediment saturation [dimensionless]
T = cumulative (total) depth of water transported by transmission loss [L]

Water was not completely changed to air on soil void spaces in the infiltration process. Hydraulic conductivities are generally smaller than saturated hydraulic conductivities due to air in soil porous and they can be affected by surface crusting in bare soils and macropores in vegetation areas (Rawls et al. 1983; Rawls et al. 1993)

It may be overlooked that infiltration capacity by evaporation and percolation recovery to the initial condition can occur after a single storm. Transmission loss due to evaporation or other processes can also be negligible for a single storm.

2.4.3 Storage

Water can be stored in concave areas on the land surface. The storage depth can be represented as a threshold limiting the occurrence of overland flow. If the water depth is lower than the depression area overland flow is zero. The water in the depression area can still infiltrate and evaporate. Stream water in channel may also be stored in the depression area, which is called to dead storage. Water in the dead storage can still infiltrate and evaporate.

2.4.4 Overland and Channel Flow

Overland flow is initiated when the water depth on the overland exceeds water level in the depression area. Conservation of mass and momentum is the governing equation in overland flow. Two dimensional continuity equation in partial differential form is (Julien et al. 1995; Julien, 2002):

$$\frac{\partial h}{\partial t} + \frac{\partial q_x}{\partial x} + \frac{\partial q_y}{\partial y} = i_n - f + W = i_e \qquad (2.7)$$

where: h = surface water depth [L]
q_x , q_y = unit discharge in the x- or y-direction = $Q_x / B_x , Q_y / B_y$ [L^2T^{-1}]
Q_x , Q_y = flow in the x- or y-direction [L^3T^{-1}]
B_x , B_y = flow width in the x- or y-direction [L]
W = unit discharge form/to a point source/sink [L^2T^{-1}]
i_e = excess precipitation rate [LT^{-1}]

A momentum equation can be derived by relating the net forces per unit mass to flow acceleration. This form may be expressed as the Saint Venant equations and can be simplified be neglecting local and convective acceleration components of momentum. The diffusive wave approximation is:

$$S_{fx} = S_{0x} - \frac{\partial h}{\partial x} \tag{2.8}$$

$$S_{fy} = S_{0y} - \frac{\partial h}{\partial y} \tag{2.9}$$

where: S_{fx}, S_{fy} = friction slope (energy grade line) in the x- or y-direction [dimensionless]

S_{0x}, S_{0y} = ground surface slope in the x- or y-direction [dimensionless]

The overland flow equations for continuity and momentum need five hydraulic variables in terms of a depth-discharge relationship to solve the overland flow equation. The assumption in this flow is that turbulent and resistance may be described by the Manning equation (S.I. units) and the relationship of the depth-discharge are (Julien et al. 1995; Julien, 2002):

$$q_x = \alpha_x \, h^{\beta} \tag{2.10}$$

$$q_y = \alpha_y \, h^{\beta} \tag{2.11}$$

$$\alpha_x = \frac{S_{fx}^{1/2}}{n} \tag{2.12}$$

$$\alpha_y = \frac{S_{fy}^{1/2}}{n} \tag{2.13}$$

where: α_x, α_y = resistance coefficient for flow in the x- or y-direction [$L^{1/3}T^{-1}$]

β = resistance exponent = 5/3 [dimensionless]

n = Manning roughness coefficient [$TL^{-1/3}$]

Channel flow occurs when water depth in the channel exceeds water level in dead storage. The governing equation for channel flow is conservation of mass and momentum. Channel flow

is represented by one-dimension in the watershed. The one-dimensional continuity equation for gradually varied flow along a channel is (Julien et al. 1995; Julien 2002):

$$\frac{\partial A}{\partial t} + \frac{\partial Q}{\partial x} = q_l \tag{2.14}$$

where: A_c = cross sectional area of flow [L^2]
Q = total discharge [L^3T^{-1}]
q_l = lateral unit flow (into or out of the channel) [L^2T^{-1}]

The diffusive wave approximation can be used for the friction slope. For the channel flow equation for continuity and momentum the Manning equation can be used for flow resistance (Julien et al. 1995; Julien, 2002):

$$Q = \frac{1}{n} A_c \, R_h^{2/3} \, S_f^{1/2} \tag{2.15}$$

where: R_h = hydraulic radius of flow = A_c / P_c [L]
P_c = wetted perimeter of channel flow [L]

CHAPTER 3 SITE DESCRIPTION AND EXTREME EVENTS

3.1 DUKSAN CREEK WATERSHED

Gangwon Province is located in the north eastern part of South Korea. Inje County is in the north central part of Gangwon Province and on the western side of the Taebaek Mountains. The latitude and longitude of Inje County are 38°30'N to 37°49'N and 127°58'E to 128°31'E. The area and population of Inje County is 32,175 and 1,645.54 km^2.

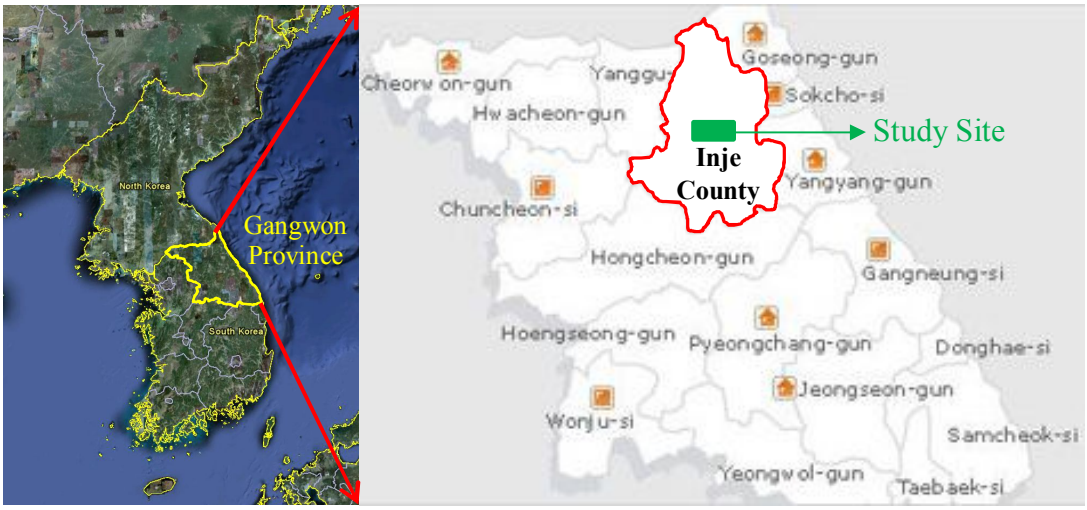

Figure 3.1. Location of study site

3.1.1 Watershed Characteristics

Duksan Creek is located in Inje County in Gangwon Province and at the following latitude and longitude: 38°02'80"N ~ 38°05'68"N, 128°10'25"E ~ 128°7'16"E. The study site has a drainage area of 33.1 km^2, a channel length of 12 km long, and the average width of 2.78 km. Duksan Creek is one of the tributaries of Inbuk Stream and it flows from east to west. The watershed map is shown in Figure 3.2.

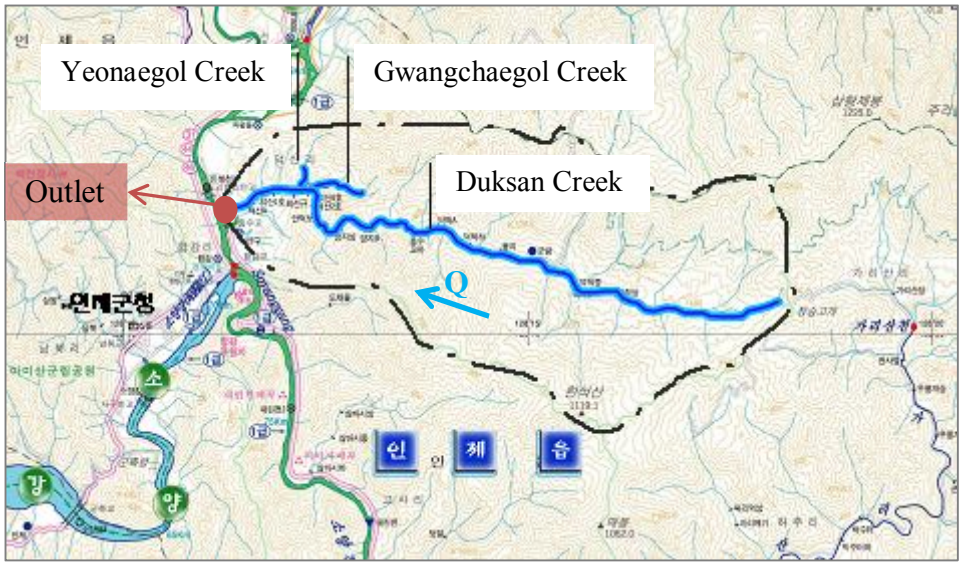

Figure 3.2. Duksan Creek watershed

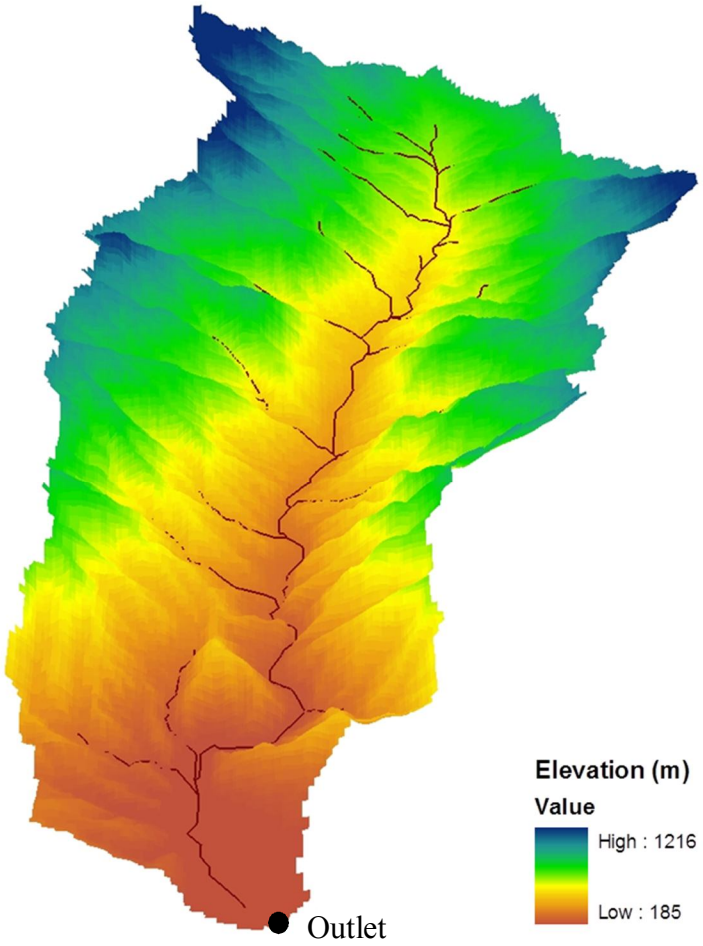

Figure 3.3. Elevation within Duksan Creek watershed

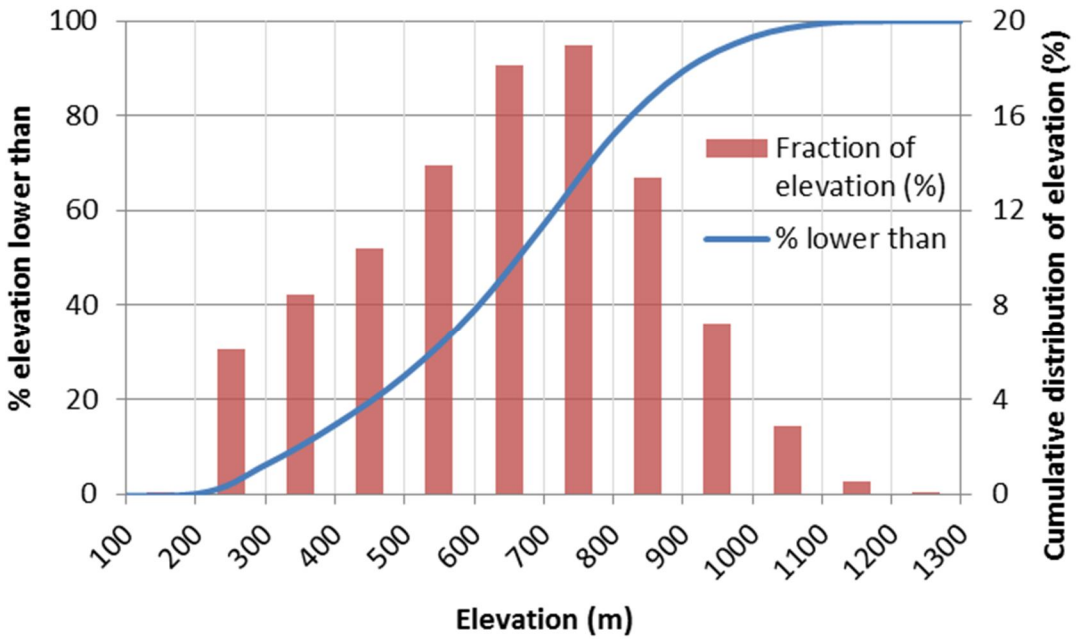

Figure 3.4. Frequency and cumulative distribution of elevation

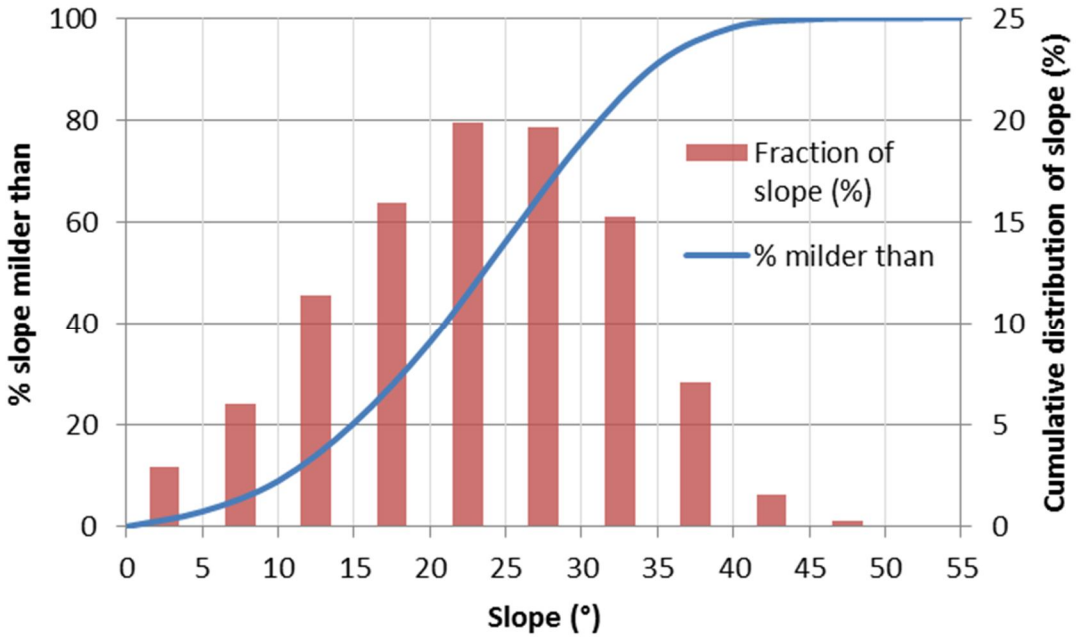

Figure 3.5. Frequency and cumulative distribution of slope

In Figure 3.3, Duksan Creek has a bed slope of approximately 0.04 m/m and the study site is a very steep mountainous watershed. The highest and lowest elevations of this watershed are 1216 m and 185 m respectively. 37 % of the area is between 600 and 800 m of elevation. In Figure 3.5, the slope ranging from 20° to 30° is dominant in total slope distribution. Due to steep average watershed slope and bed slope, flows from rainfall drain very rapidly.

3.1.2 Geology

Rock types are classified as igneous rock, metamorphic rock, and sedimentary rock. Igneous rocks were molten from magma and they are mostly crystalline. Granite is composed of orthoclase feldspar, quartz, plagioclase feldspar, muscovite, biotite mica, and amphibole.

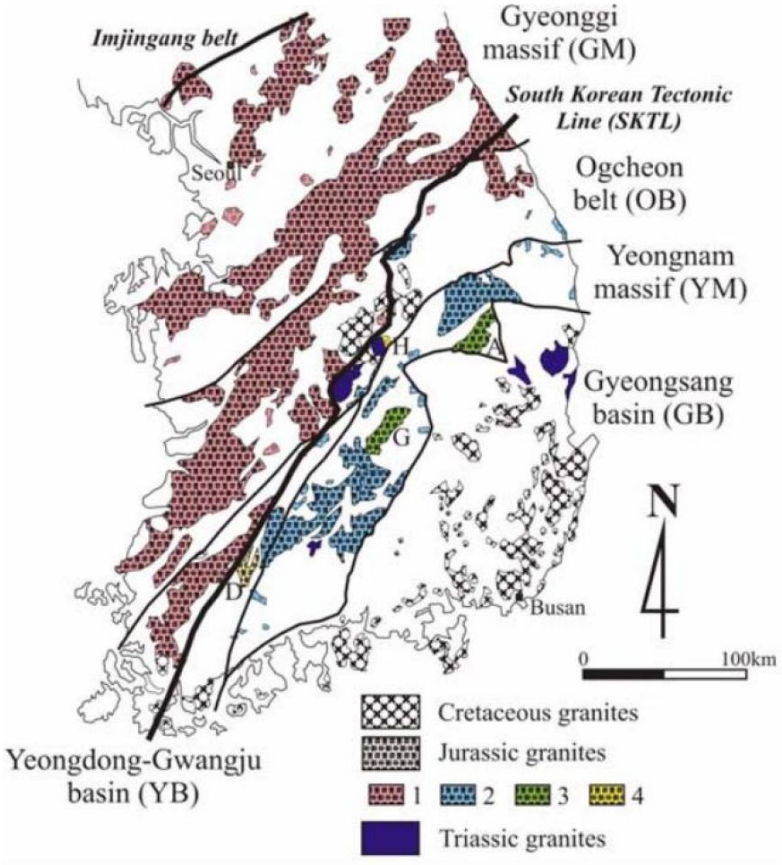

(a)

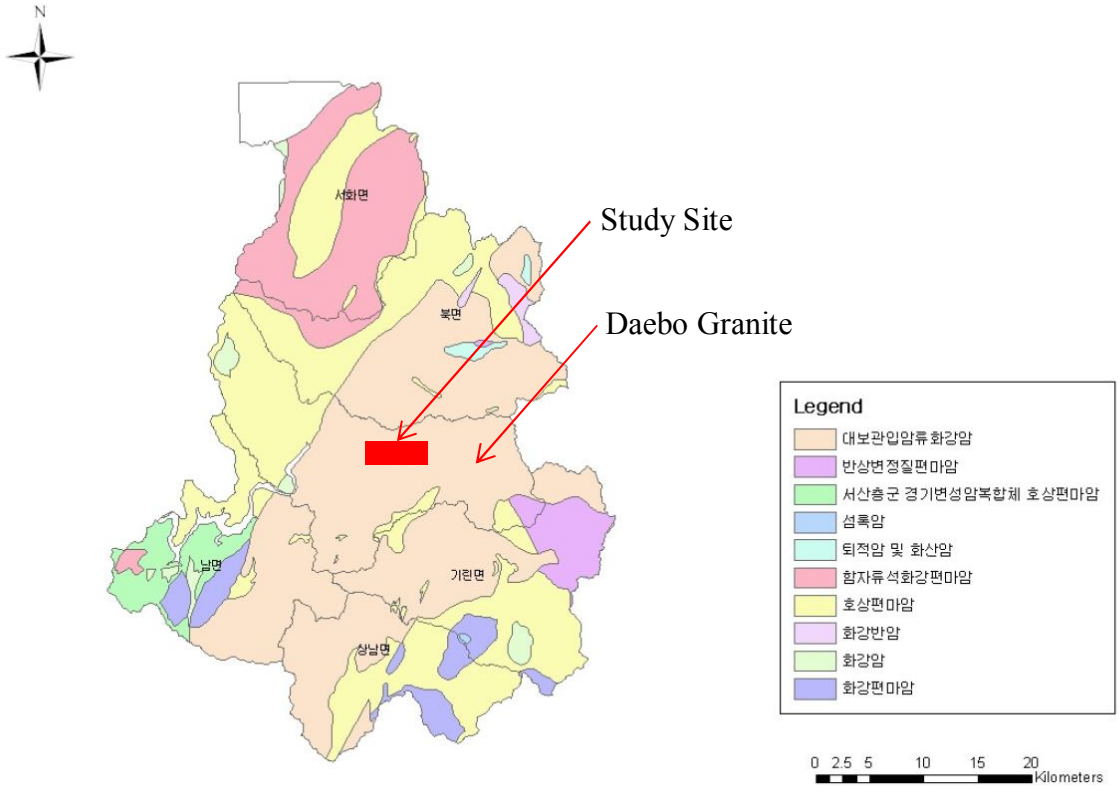

(b)

Figure 3.6. The geology map in South Korea (a) and Inje County (b) (Park et al., 2010)

Most bedrock in South Korea is granite and one quarter of South Korea is composed of the Jurassic and the Cretaceous granites in the Mesozoic era (Jin, 1980). The geology map in South Korea and Inje County is shown in Figure 3.6. The granite type in Inje County in Gangwon Province is Daebo granite by Daebo orogeny. This Daebo granite includes biotite granite and porphyritic granite and the biotite granite is distributed in the Duksan Creek watershed.

When it comes to landslides with respect to geochemical properties of soil minerals, Kim et al. (2005) analyzed micro texture, particle size distribution, X-ray diffraction, scanning electron microscope, and energy dispersive spectrum on soils sampled from landslide slopes of gneiss, granite, and sedimentary rock areas. The results of this analysis were that granite at no landslide area was less weathered and had little clay minerals, but granite at landslide areas was largely weathered and had much clay minerals. Therefore, it was concluded that the degree of weather and the content of clay mineral in soils can affect the occurrence of landslides. Kim et al. (2006) investigated landslide areas with different geology condition in South Korea. The frequency of landslides occurrence was high in Sangju areas where granite bedrock was distributed and most failure depth was below 1 m. Cho (2006) examined landslide characteristics and tried to predict landslide map using statistical method in Gangneung area with granite bedrock. The failure depth in this study site was mostly below 1 m. Therefore, the failure depth in granite areas was considered to be as shallow as 1 m.

3.1.3 Soil Types

The U.S. Department of Agriculture (USDA) has classified soils based on relative proportions of sand, silt, and clay. Based on this classification, there are five soil types within Duksan Creek watershed as shown in Figure 3.7.

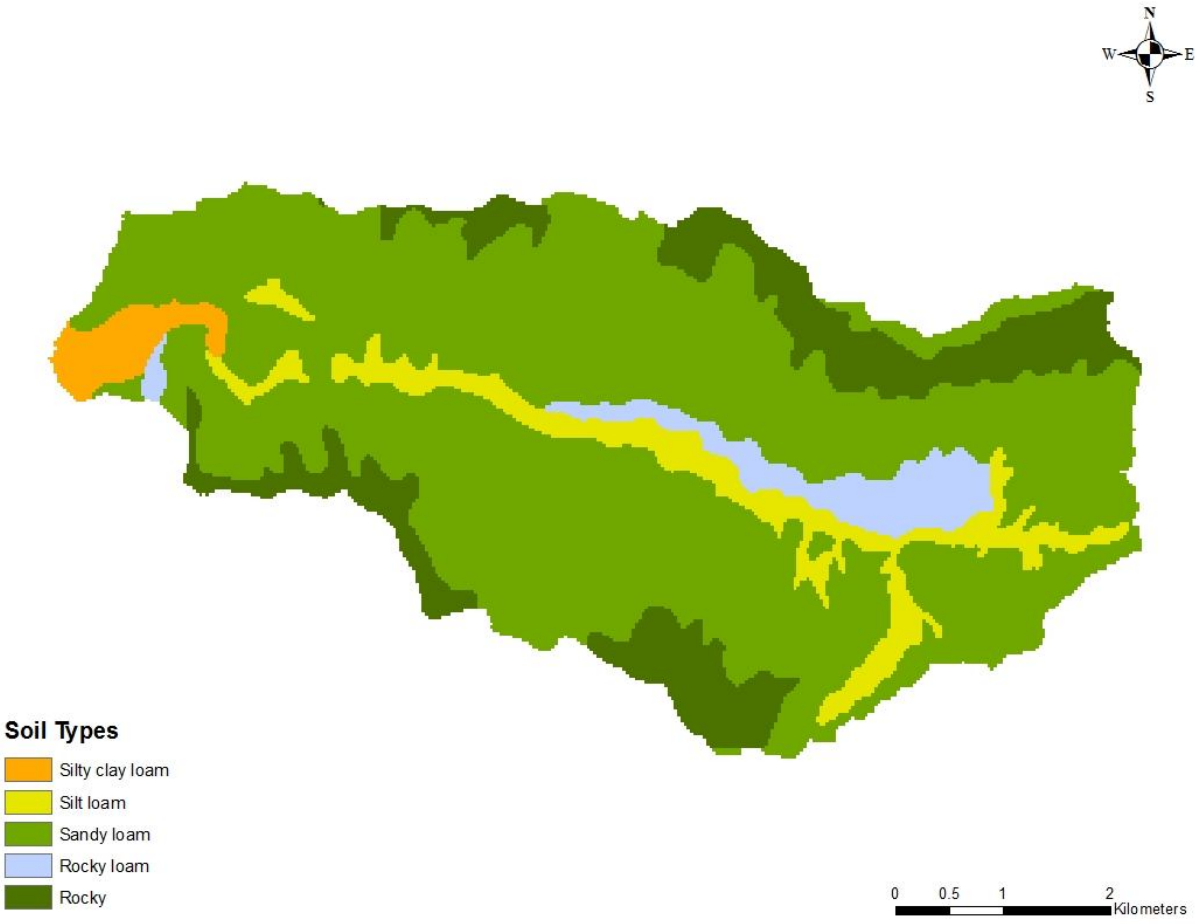

Figure 3.7. Soil types within Duksan Creek watershed

Most soil types at the study site are sandy loam, which is composed of forest soils. The soil type downstream is silt clay loam, and this area is crop land. The northern and southern edges of the watershed are rocky, and this is due to high elevation.

The most common soil classification in geotechnical engineering is the Unified Soil Classification System (USCS). The USCS divides soils to three major soil groups such as coarse grained soils, fine grained soils, and highly organic soils. This is shown in Table 3.1.

Table 3.1. Unified soil classification system

	Major divisions		Group symbol	Group name
Coarse grained soils More than 50% retained on No.200 (0.075 mm) sieve	**Gravel** >50% of coarse fraction retained on No.4 (4.75 mm) sieve	Clean gravel <5% smaller than #200 Sieve	GW	Well-graded gravel, fine to coarse gravel
			GP	Poorly graded gravel
		Gravel with >12% fines	GM	Silty gravel
			GC	Clayey gravel
	Sand >=50% of coarse grain fraction passes No. 4 sieve	Clean sand	SW	Well-graded sand, fine to coarse sand
			SP	Poorly graded sand
		Sand with >12% fine	SM	Silty sand
			SC	Clayey sand
Fine grained soils More than 50% passes No.200 sieve	**Silt and Clay** Liquid limit <50	Inorganic	ML	Silt
			CL	Clay
		Organic	OL	Organic silt, organic clay
	Silt and Clay Liquid limit >=50	Inorganic	MH	Silt of high plasticity, elastic silt
			CH	Clay of high plasticity, fat clay
		Organic	OH	Organic clay, organic silt
Highly organic soils			Pt	Peat

Kim et al. (2011) analyzed weathered granite soils in three regions including Inje County in South Korea. Soil in the Inje County area was classified as SW, sand fraction was 88.6 %, and silt and clay fraction was 2.8 %.

3.1.4 Land use

Inje County is located on the west side of the Taebak Mountains in South Korea and most land use in this area is forest. The area of land category in Inje County has 88.2% of forest and 4.6 % of paddy field. There are three types of land use in the Duksan Creek watershed. They are shown in Figure 3.8.

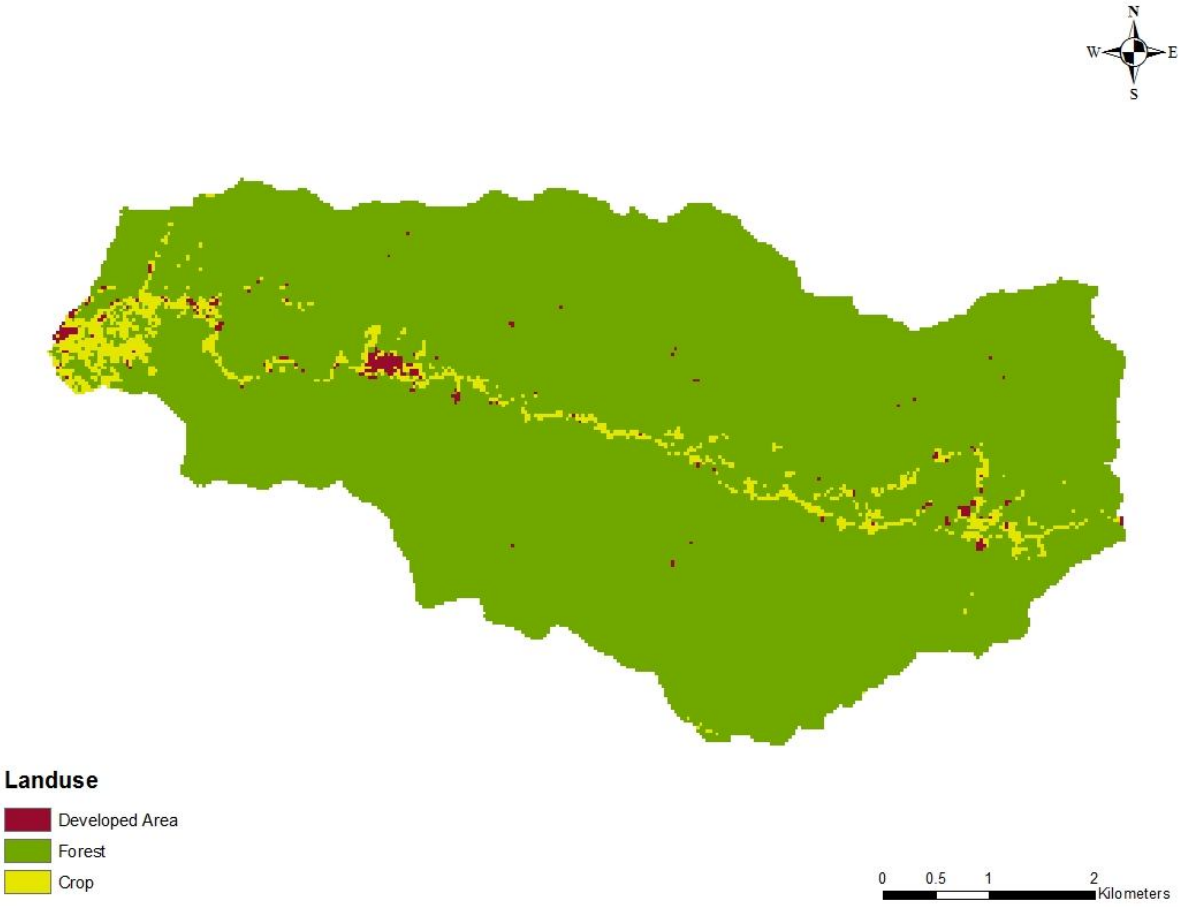

Figure 3.8. Land use within Duksan Creek watershed

Land use at the study site is composed of 95.5 % forest and 3.8 % crop area. The crop lands are located near a main channel area upstream and in the middle of a watershed. Most crop lands and residential areas are placed in a downstream area.

3.1.5 Forest Types

Total forest area in Inje County is 157,581 ha and can be classified as conifer forest, broadleaved forest, and mixed forest. The ratio of each forest is 20 %, 43 %, and 37 %, respectively. There are four main forest types within Duksan Creek watershed and they are shown in Figure 3.9.

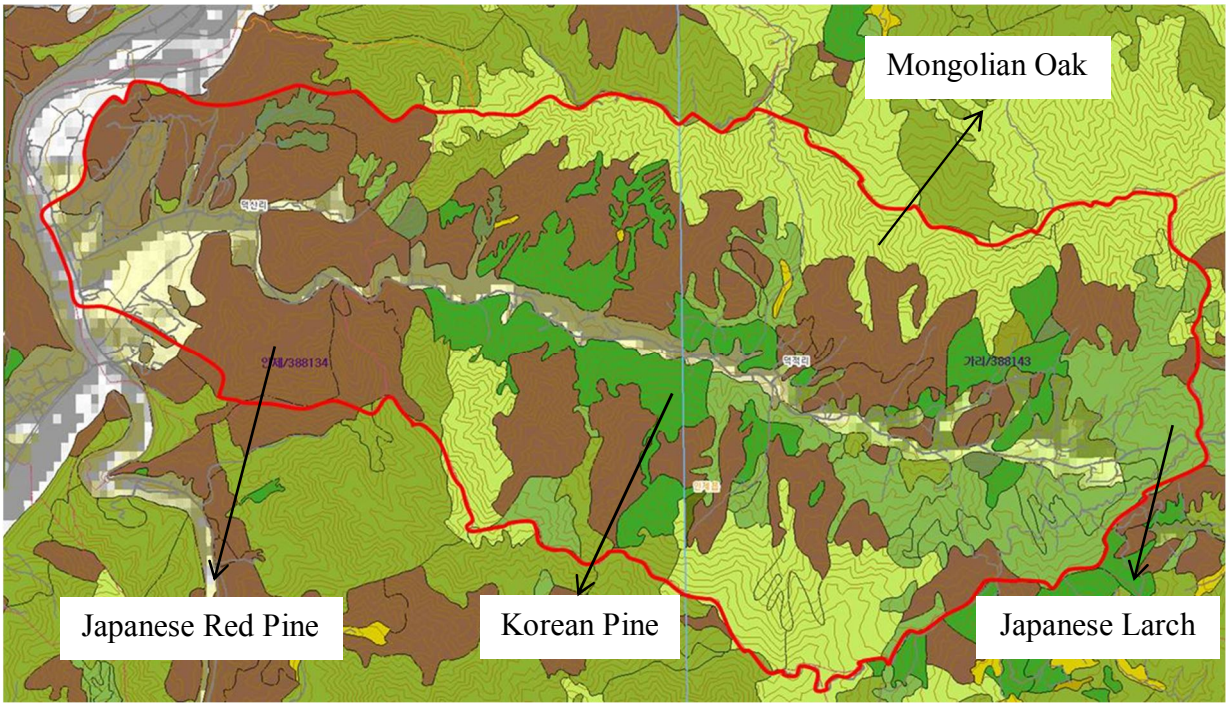

Figure 3.9. Forest types in Duksan Creek watershed

Forest types in Duksan Creek are broadleaved forest (mostly Mongolian Oak), mixed forest, larch, red pine, Korean pine, pine plantation forest, broadleaved plantation forest, and poplar forest. Four main forest types occupy 88.2 % of the Duksan Creek surface. These forests are Japanese red pine (35.3 %), Mongolian oak (21.6 %), Japanese larch (14.8 %), and Korean pine (10.9 %). Table 3.2 to Table 3.5 show the main characteristics of each forest type including Diameter of Breast Height (DBH) class, age class, and crown density.

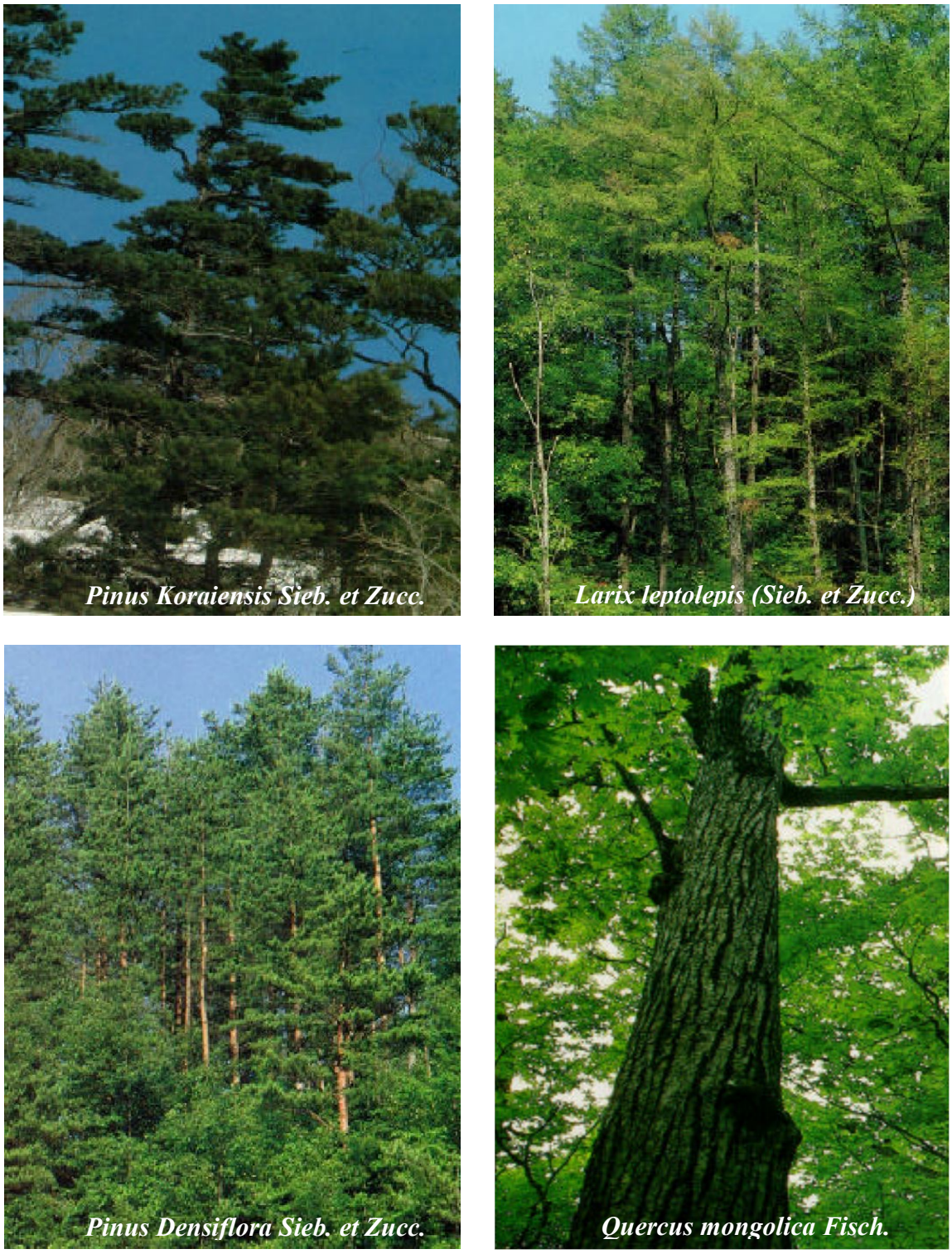

Figure 3.10. The main species within Duksan Creek watershed

Table 3.2. Forest types

Forest types	Symbol	Description
Broadleaved forest	H	Crown occupation area or number of trees, >75 %
Mixed forest	M	25 % < Conifer and Broadleaved forest <75%
Korean pine forest	PK	Crown occupation area or number of trees, >75 %
Larch forest	PL	Crown occupation area or number of trees, >75 %
Red pine forest	D	Crown occupation area or number of trees, >75 %

Table 3.3. DBH class

Class	Symbol	Description
Young growth reproduction	0	DBH < 6 cm Crown occupation area > 50 %
Small	1	6 cm < DBH < 16 cm Crown occupation area > 50 %
Medium	2	18 cm < DBH < 28 cm Crown occupation area > 50 %
Large	3	DBH > 30 cmCrown occupation area > 50 %

Table 3.4. Age class

Class	Symbol	Description
1	I	Age 1 – 10, Crown occupation area > 50 %
2	II	Age 11 – 20, Crown occupation area > 50 %
3	III	Age 21 – 30, Crown occupation area > 50 %
4	IV	Age 31 – 40, Crown occupation area > 50 %
5	V	Age 41 – 50, Crown occupation area > 50 %
6	VI	Age > 51, Crown occupation area > 50 %

Table 3.5. Crown density

Class	Symbol	Description
Low	A	Trees, Crown occupation area < 50 %
Medium	B	Trees, 51 % < Crown occupation area < 70 %
High	C	Trees, Crown occupation area > 71 %

The forest types in Inje County consist of coniferous forest (24%), broadleaved forest (39%), and mixed forest (38%). However, at the study site the forest is composed of 63 % coniferous forest, 22 % broadleaved forest, and 4 % mixed forest. The main species of coniferous at the study site are Korean pine (Pinus Koraiensis Sieb. et Zucc.), Japanese larch (Larix leptolepis (Sieb. et Zucc.) Gordon), and Japanese red pine (Pinus Densiflora Sieb. et Zucc.). The main species of the broadleaved forest at the study site are sawtooth oak (Quercus mongolica Fisch.).

Forest types, diameter of breast height (DBH) class, age class, and crown density for four main forest types were investigated and are summarized in Table 3.6.

Table 3.6. Field investigation for forest in Duksan Creek watershed

Forest types	DBH class	Age class	Crown density
PK	1	I	C
PL	1	III	C
D	2	V	B
H	2	V	B

3.2 EXTREME PRECIPITATION

3.2.1 Weather Conditions

Temperature and relative humidity for the past 20 years was analyzed to recognize general conditions at the Inje County area. The average temperature in Inje County was 10.2°C, and the monthly maximum and minimum temperature were 26.2°C and -7.9°C, respectively. The average relative humidity was 69 %, and the monthly maximum and minimum relative humidity were 88 % and 40 %, respectively. The monthly maximum temperature and relative humidity records occurred in July and August. Both high temperature and relative humidity happened in the summer season.

Rainfall data in Inje County for the past 10 years was investigated to identify a rainfall pattern. Annual precipitation from 2001 to 2010 is shown in Figure 3.11, and the mean annual precipitation is 1317 mm.

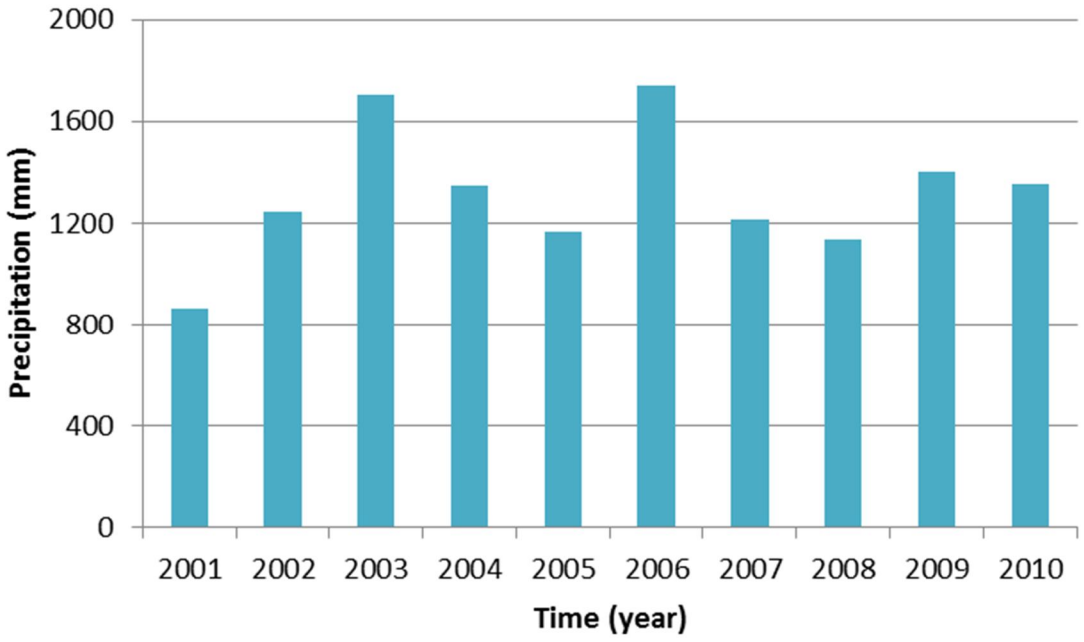

Figure 3.11. Annual precipitation in Inje County from 2001 to 2010

The two typhoons, Rusa in 2002 and Maemi in 2003, went through the Korean peninsula, but they did not cause much rainfall in Inje County. The annual rainfall of 1701 mm in 2003 came from heavy rainfall, not the typhoon. On the contrary, the annual rainfall of 1740 mm in 2006 resulted from heavy rainfall in Inje County. The duration of rainfall was short, and rainfall intensity was a high of 62 mm/hr on July 15, 2006.

The monthly rainfall for the 10 past years was also examined to understand a rainfall pattern in Inje County, and this is plotted in Figure 3.12.

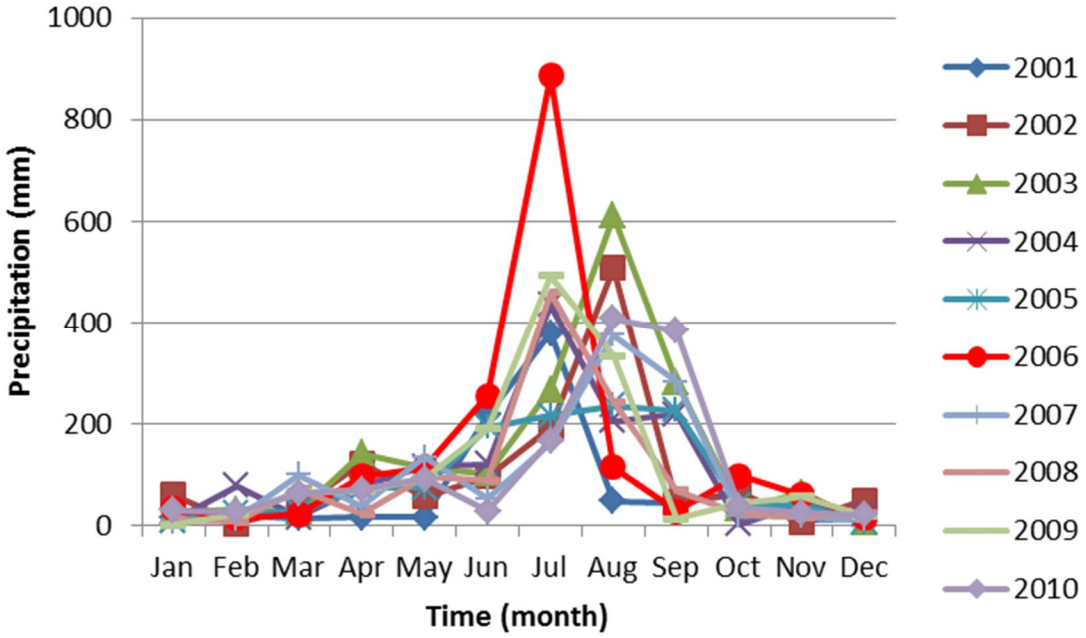

Figure 3.12. Monthly rainfall in Inje County

The maximum monthly rainfall of 886 mm occurred in July 2006 as compared to just 611 mm in August 2006. The high rainfall in 2006 came from heavy rainfall with short duration, not the typhoon. This rainfall caused a lot of damage in mountainous areas, such as debris flow and landslides.

3.2.2 Extreme Precipitation Analysis

Extreme rainfall occurred in Duksan Creek on July 14 to 17 in 2006. This rainfall was caused by two effects. The first one was a rain front from North Korea and the second one was vapors developed in China due to typhoon Bilis. The satellite images on July 15 in 2006 are shown in Figure 3.14. On July 14, 21:33 PM, rain clouds were located in North Korea, but most rain clouds were focused on the Inje County area after on July 15 06:00. From July 15, 08:00 AM to 11:00 AM, rain clouds stayed in Inje County and brought 168 mm of rainfall. On July 15 15:33 PM, most rain clouds were moved to the eastern part of South Korea. Bae (2007) investigated rain cloud routes with satellite images and compared them with elevation data in the cross section near the Inje County area. This is shown in Figure 3.13.

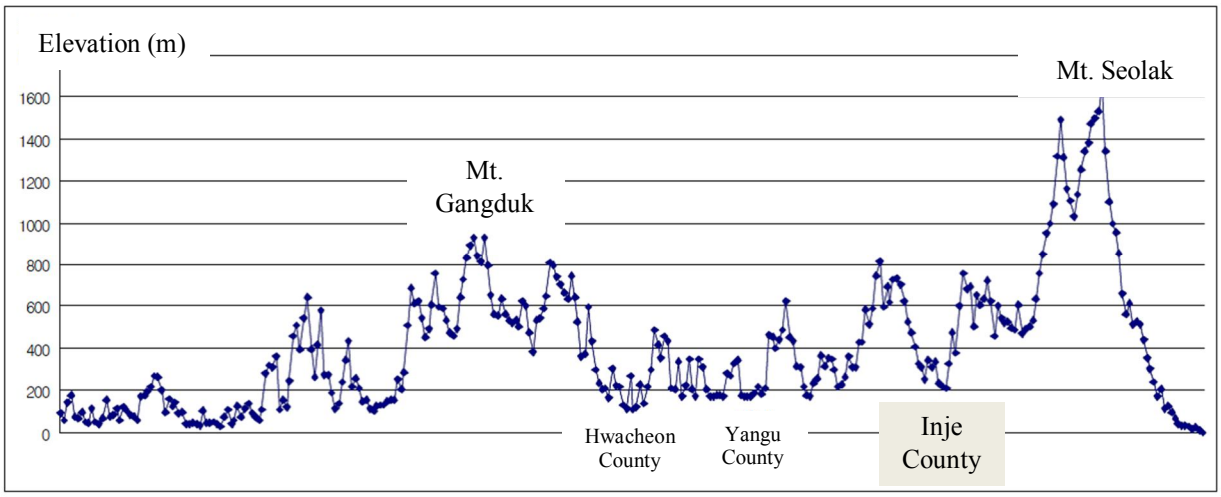

Figure 3.13. A cross section near Inje County

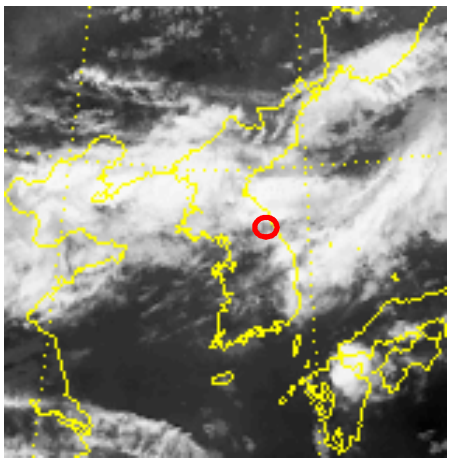

(a)7/14/2006 21:33 PM

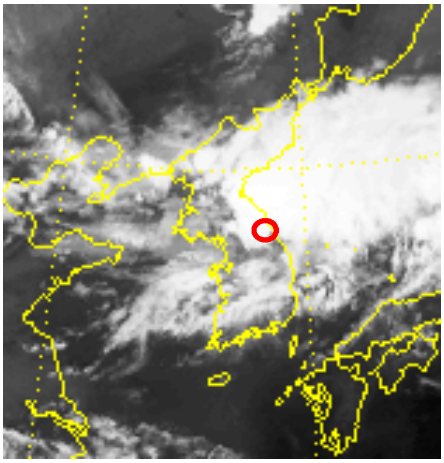

(b) 7/15/2006 06:00 AM

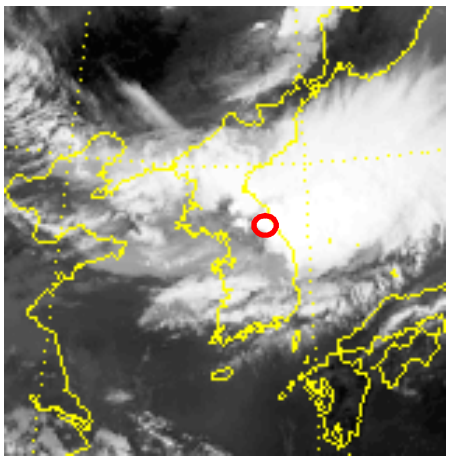

(c)7/15/2006 08:33 AM

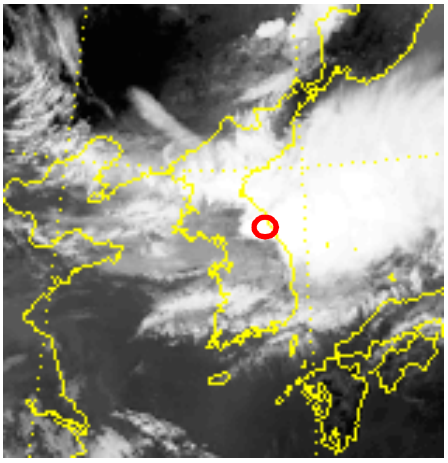

(d) 7/15/2006 09:33 AM

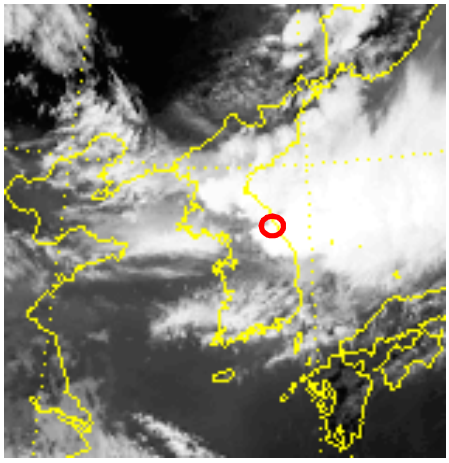

(e) 7/15/2006 11:33 AM

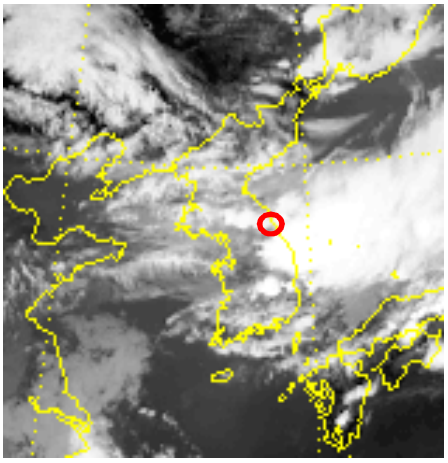

(f) 7/15/2006 15:33 AM

Figure 3.14. Satellite images on July 15, 2006

When rain clouds arrived in Inje County, they were stuck due to the high elevation of Mt. Seolak in Figure 3.14. Because of the effect of rain clouds routes and topography, the damages from the small mountain stream and steep slope area had been accelerated in Inje County.

The three days of rainfall from July 14 to July 17 are shown in Figure 3.15.

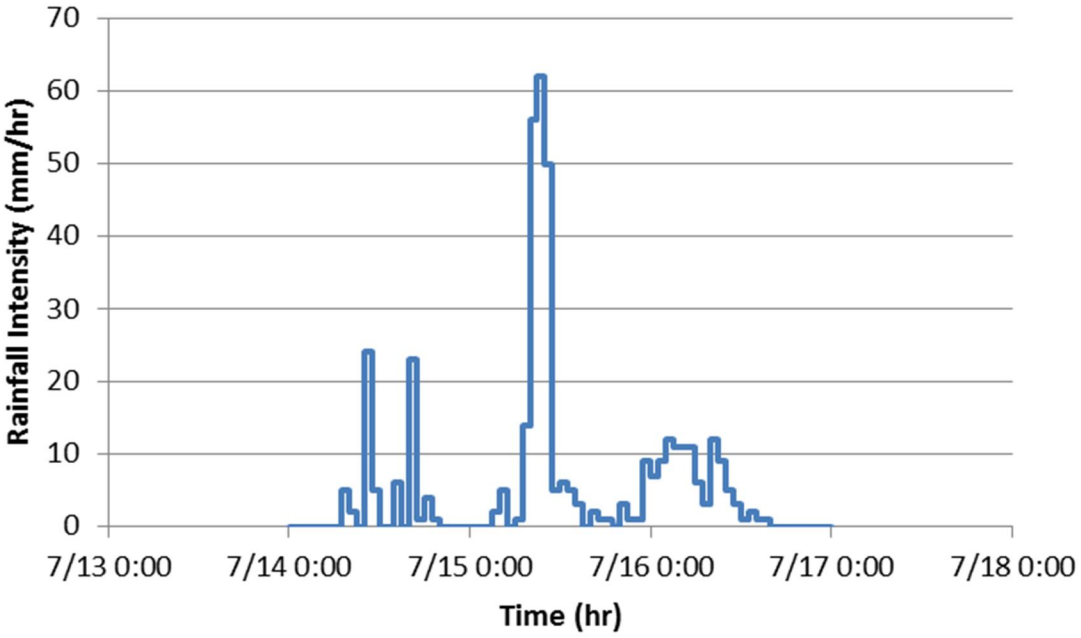

Figure 3.15. Rainfall Event in July 2006

The total rainfall from July 14 to July 16 in 2006 was 402 mm. The maximum rainfall occurred 227 mm on July 15 in 2006. The highest rainfall intensity focused on 8 am to 11am and that three hour rainfall was to 168 mm. The maximum hourly rainfall intensity on July 15 in 2006 was 62 mm/hr.

The magnitude of this event was compared with three different precipitation events including the world's greatest rainfall event, PMP values in the vicinity of the Inje area, and 100 years of return period values. This is shown in Figure 3.16. The two hour rainfall, the three hour rainfall, and the four hour rainfall in Inje County were 118 mm, 168 mm, and 182 mm, respectively.

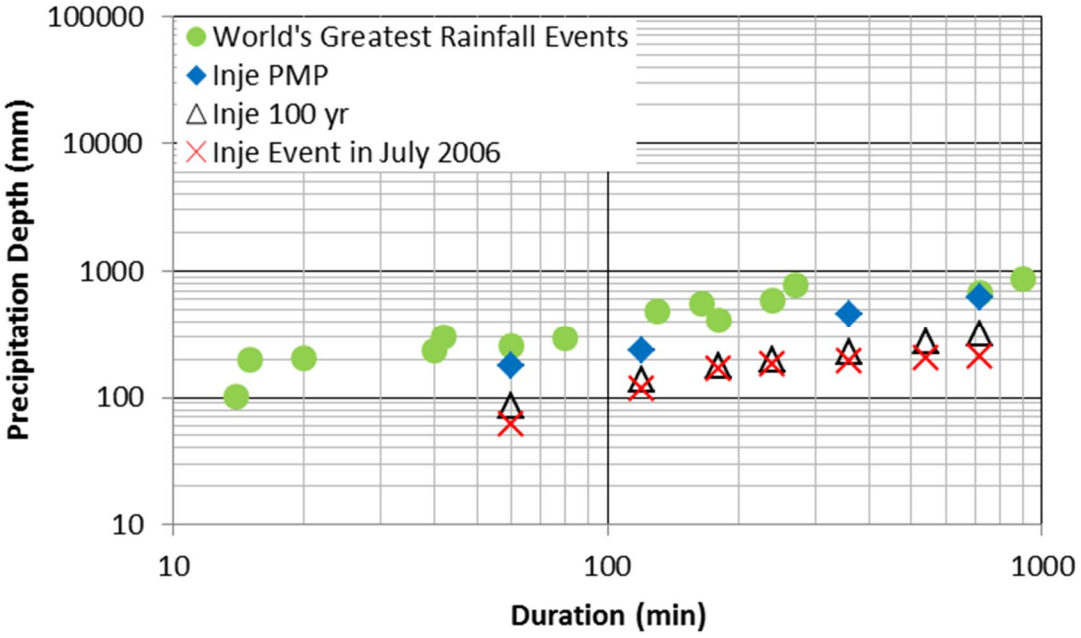

Figure 3.16. The comparison between different magnitudes of precipitation

To describe this rainfall in detail, an IDF curve was introduced and this is shown in Figure 3.17.

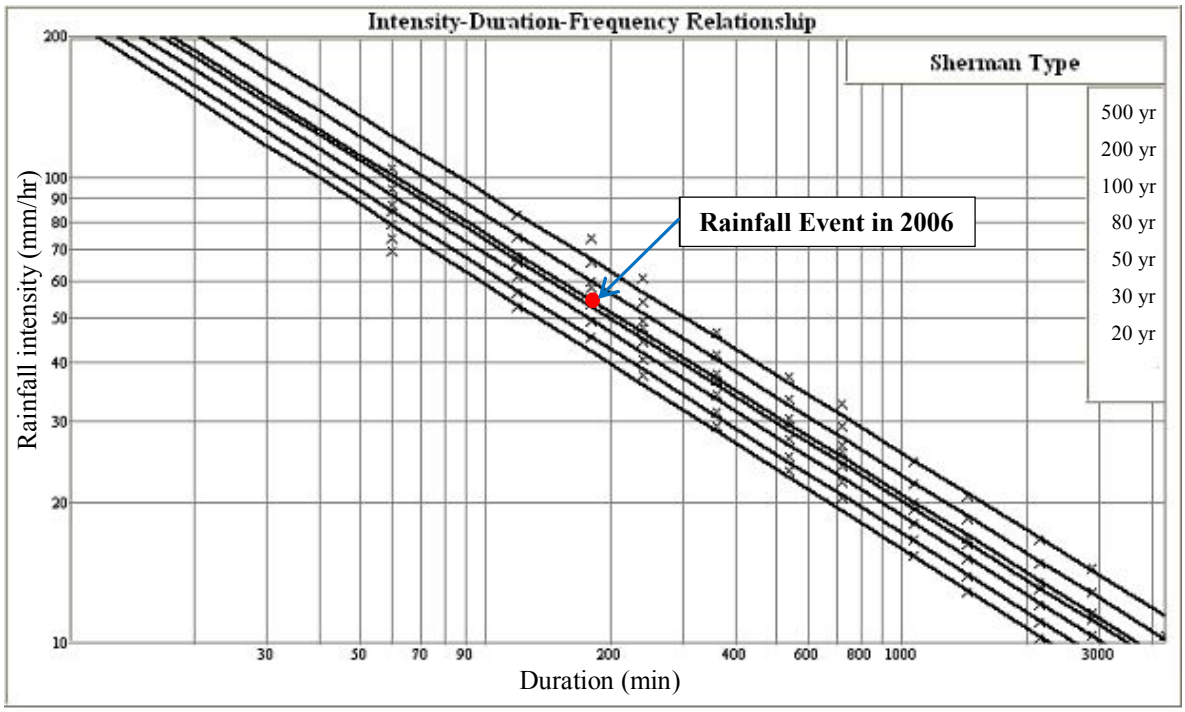

Figure 3.17. Intensity-Duration-Frequency Curve in Duksan Creek Watershed (Inje County, 2008)

IDF curves using Talbot type, Sherman type, and Japanese type are generally used in South Korea for their easy estimation of parameters, and the Sherman type was selected for its maximum parameters. The x mark in Figure 3.17 represents probability analysis of rainfall using Gumbel distribution and the return periods are 20 year, 30 year, 50 year, 80 year, 100 year, and 200 year. The three hour rainfall on July 15 is indicated as a red point in Figure 3.17, or about a 100 year event. The characteristics of extreme rainfall compared with the typhoon needs to be investigated, and it was analyzed using TREX.

CHAPTER 4 TREX MODEL APPLICATION

TREX was applied with a preprocessed input file using GIS. TREX was run with two main conditions that are impervious condition and infiltration condition, to check model performance before starting the simulation in the Duksan Creek watershed.

4.1 INPUT DATA

The TREX model needs three basic input data that are: DEM, soil type, and land use. These files should be processed with GIS. The procedures for input file generation in GIS are mainly composed of 11 steps: resampling, fill, flow direction, flow accumulation, pour points, watershed delineating, flow length, stream network, clip, reclassification, and converting to an ASC file. TREX input files can be divided into two main categories: hydrology and sediment. For the hydrology part, seven files can be generated from the original data of DEM: mask, elevation, link, node, storage depth, overland flow, and initial water in soil. Two more files are needed for the hydrology part and those are channel properties files. The channel properties include channel width, side slope, bank height, Manning roughness, sinuosity, and dead storage depth. For the sediment part, two file can be created: soil and land use.

4.2 TREX MODEL TESTING

The TREX simulation was tested in impervious condition and pervious condition to verify time to equilibrium at the watershed. For small watershed, the system responses very quickly for rainfall and time variability in hyetograph is more important. For large watershed, the system responses slow for rainfall and spatial variability is more important. The area of the Duksan Creek watershed is 33.1 km^2 and this is relatively small watershed. Thus, time to equilibrium with respect to rainfall intensity needs to be checked.

4.2.1 Impervious Condition

Impervious condition means that there is no infiltration in the watershed. When some amount of rain fall into the watershed, all water from the rainfall should flow out to an outlet in the watershed. To satisfy this condition above, the saturated hydraulic conductivity values of all soils were set to zero.

The total running time was set to 5 hours, the duration of rainfall was 3 hours, and the time step was 0.05 second. The rainfall intensity depends on different extreme condition. The highest rainfall intensity was assumed to be 100 mm/hr to test whether TREX can run at an extremely high condition. The intensity of 50 mm/hr was selected because this intensity was similar to that of July 15 in 2006. For low rainfall intensity, 20 mm/hr and 10 mm/hr of rainfall intensity were chosen. The SI unit in this research was performed for all analysis and the results are shown in Figure 4.1.

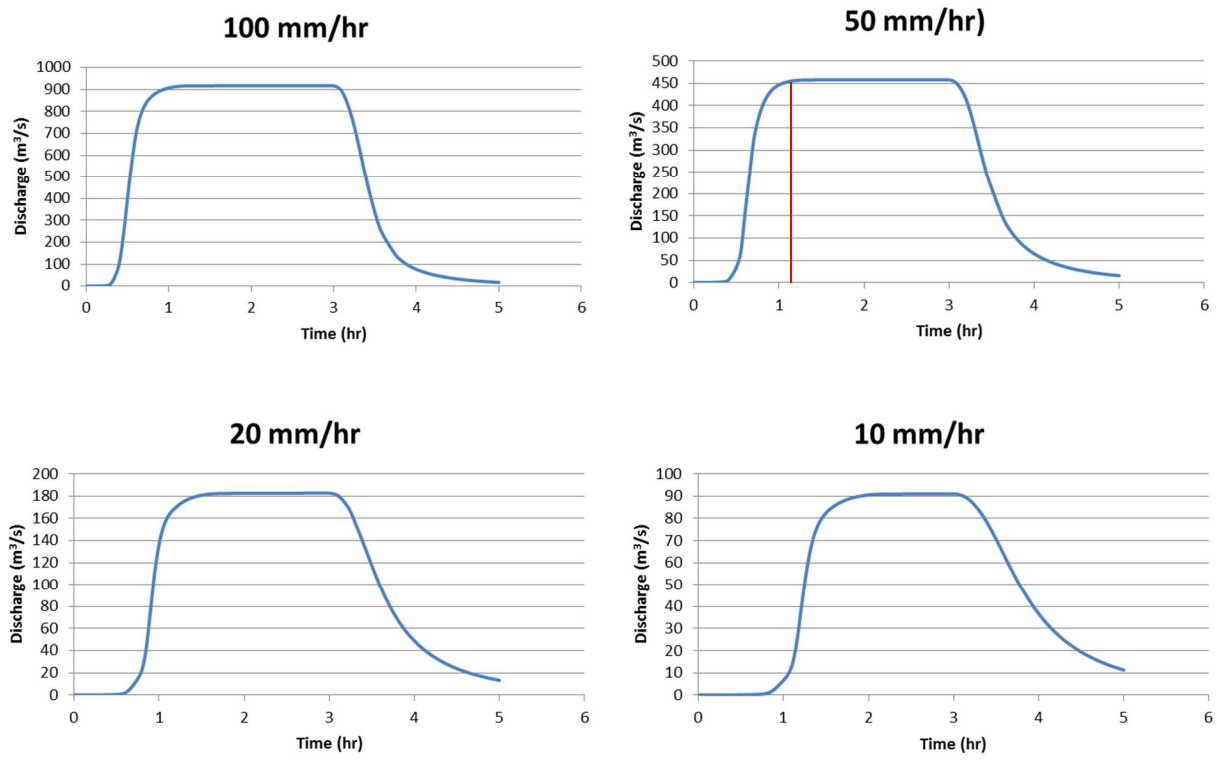

Figure 4.1. The results of impervious condition

The shape of the four graphs shows the same pattern. The rainfall was started from 0 hour and the runoff began suddenly between 0 and 1 hour. When the runoff reached its peak, it passed constantly for 3 hours, that is the end point of rainfall, and then it went down relatively slowly compared with rising limb. Runoff occurred around 30 minutes from the beginning point in the high rainfall intensity, including 100 mm/hr and 50 mm/hr, whereas in the low rainfall intensity involving 20 mm/hr and 10 mm/hr, runoff rose close to 1 hour from starting point. The reason for the different times of concentration is due to the entire rainfall by different rainfall intensities within the watershed. The three hour rainfall in July 15, 2006 was 168 mm and the hourly rainfall from this event was 56 mm/hr. From Figure 4.1, when rainfall intensity was 50 mm/hr, time to equilibrium was around 1 hour. Since the duration of extreme event is longer

than the time to equilibrium with the rainfall intensity of 50 mm/hr, the Duksan Creek watershed is considered to be affected by rainfall intensity.

The simulated result was compared with theoretical values from the rational method. The equation for theoretical value is expressed as below.

$$Q = C\, i\, A \tag{4.1}$$

where: Q = peak discharge [m^3/s]
C = runoff coefficient (Impervious, $C = 1$)
i = rainfall intensity [mm/hr]
A = drainage area [km^2]

Runoff coefficient is assumed to be 1 because the initial condition was set to impervious. For impervious conditions, the saturated hydraulic conductivity values of five soils types were set to zero. Thus, the peak discharge can be obtained by the multiplication of rainfall intensity and drainage area of 33.1 km^2. These results are summarized in Table 4.1 below.

Table 4.1. The comparison between theoretical and simulated value

Rainfall Intensity (mm/hr)	Theoretical Value (m^3/s)	Simulated Value (m^3/s)	Relative percent difference (%)
100	928	917	-1.19
50	464	458	-1.29
20	186	183	-1.61
10	93	91	-2.15

Relative percent difference from all simulated values was within 2 %. This means that 98 % of simulated peak discharge value was matched with theoretical peak discharge value.

4.2.2 Pervious Condition

Pervious condition means that there is infiltration in the watershed. When some amount of rainfall drops into the watershed specific amounts of water from rainfall infiltrate into ground and peak flow would be reduced at the outlet of the watershed. To satisfy this condition above, the saturated hydraulic conductivity values with respect to soil type should be set and are summarized in Table 4.2.

Table 4.2. Saturated hydraulic conductivity

Soil Type	Saturated Hydraulic Conductivity (m/s)
Silt clay loam	5.5556E-07
Sandy loam	6.0556E-06
Loam	3.6667E-06
Clay loam	5.5556E-07
Impervious	0.0000E+00

The total running time was set to 5 hours, the duration of rainfall was 3 hours, and the time step was 0.05 second. For pervious conditions, rainfall intensity was determined to 100 mm/hr, and 50 mm/hr, because this simulation is based on flood conditions. The simulation results are shown in

Figure 4.2.

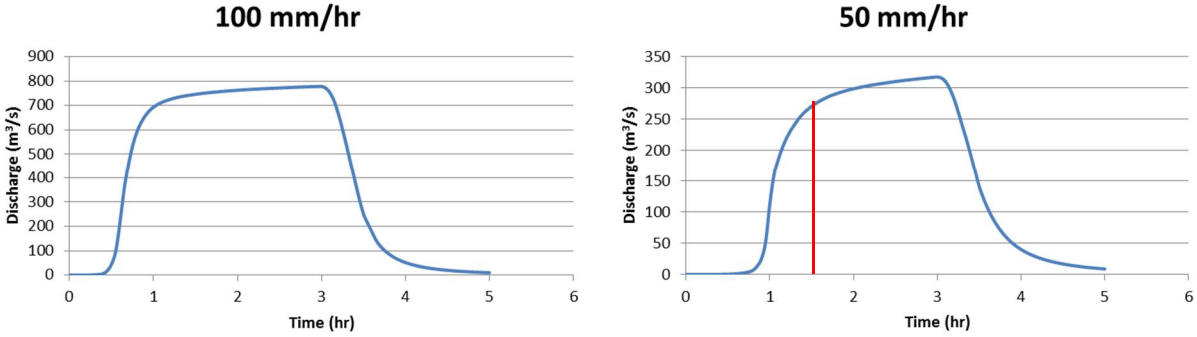

Figure 4.2. The result of pervious conditions

The two graph patterns were similar, and the peak flow showed in 3 hours from beginning. When the rainfall intensity is 100 mm/hr, the runoff started to rise around 30 minutes, however, in the rainfall intensity of 50 mm/hr, the runoff began to increase around 1 hour from beginning. From Figure 4.2, the time to equilibrium with rainfall intensity of 50 mm/hr was 1.5 hour. The duration of extreme event in July 15, 2006 is also longer than the time to equilibrium in pervious condition with rainfall intensity of 50 mm/hr. Thus, it is concluded that the Duksan Creek watershed response very quickly for rainfall and time variability in hyetograph is more important.

The pervious simulated result was also compared with theoretical values from the rational method above. In the equation of 3.1, the runoff coefficient is very important to validate the simulated result. This value can be computed from a theoretical value and a simulated value, and the calculated runoff coefficient is summarized in Table 4.3.

Table 4.3. The simulation results and runoff coefficient calculation

Rainfall Intensity (mm/hr)	Drainage area (km^2)	Simulated value (m^3/s)	Runoff Coefficient
100	33.1	779	0.84
50	33.1	318	0.69

In general, the runoff coefficient is low in urban areas but this area is a steep mountainous site. KWRA (2009) suggested that the large coefficient can be used for a small watershed area and the runoff coefficient on the steep mountain is 0.40 to 0.80. They also provided revised runoff coefficient with respect to topography and geology. In case of forest area, if the return period is large than 50 yr or the mean annual precipitation is bigger than 900

mm, the runoff coefficient is revised to increase as 0.05 and 0.03 respectively. Yun (2003) also represented a runoff coefficient as 0.75 to 0.90 in a steep mountainous area. Thus, the runoff coefficient from Table 4.3 belongs to the range of two references.

4.3 TREX MODEL CALIBRATION

The Duksan Creek watershed had no gaging station of water level or flow discharge. Thus, the Naerin Stream, that is adjacent of the Duksan Creek, and the Naesung Stream were selected for the calibration of the TREX model.

4.3.1 Naerin Stream watershed

The Naerin Stream watershed is on the south eastern part of the Duksan Creek. The watershed area covers 1,039 km^2 and the elevation ranges from 240 m to 1,575 m. The watershed of 96 % is forest and the dominant soil type is sandy loam. Discharge data at the Naerin Stream station was obtained from WAter Management Information System (WAMIS) in South Korea and this data was acquired from a stage-discharge rating curve. The hydrologic parameters for model calibration are the effective hydraulic conductivity, Manning's roughness coefficients for overland and channels, and soil moisture deficit. The effective hydraulic conductivity influences the total volume of runoff. The resistance of flow affects the timing of peak flow. Soil moisture conditions also change runoff volume and the time of peak flow.

The TREX model was calibrated by simulating rainfall and runoff on July 15 to July 17 in 2006. This time period corresponds to the extreme rainfall event time as Duksan Creek. The comparison between measured data and simulation results is shown on Figure 4.3.

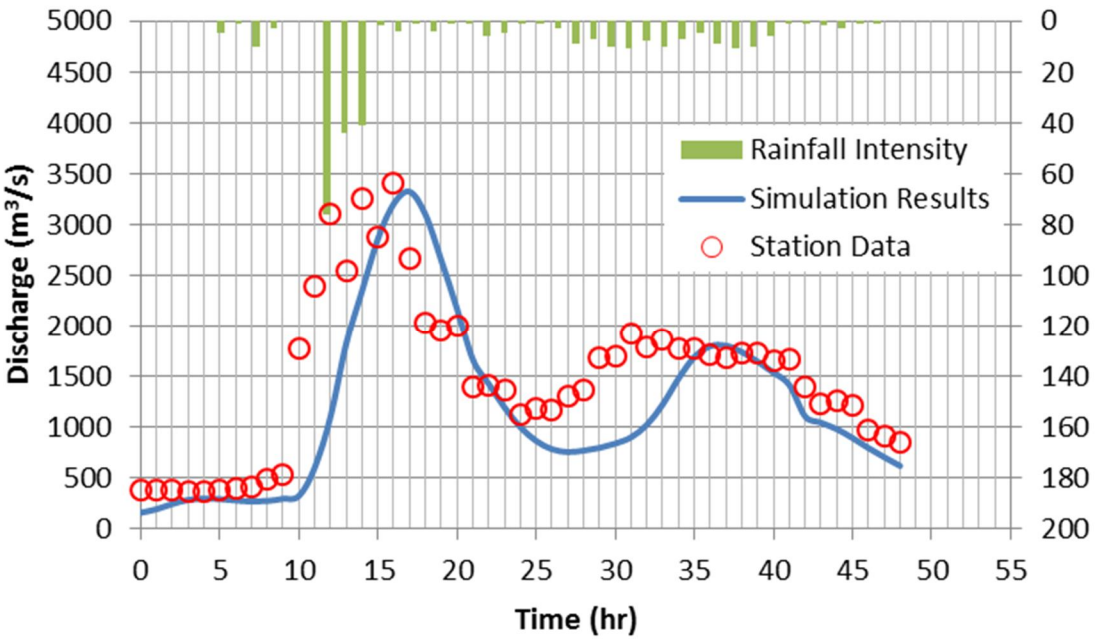

Figure 4.3. TREX model calibration at the Naerin Stream station

Relative percent difference (RPD) for time to peak and peak discharge was obtained from this result and is summarized in Table 4.4.

Table 4.4. The model evaluation using RPD in the Naerin Stream

	Measured Data	Simulation Result	RPD (%)
Time to peak (hr)	16	17	6.25
Peak discharge (m^3/s)	3410	3322	-2.58

Measured data and simulation result on time to peak and peak discharge had a 1 hour difference and 88 m^3/s, respectively. The performance of this model has generally good agreement.

4.3.2 Naesung Stream watershed

The second calibration was carried out in the Naesung Stream. The Naesung Stream is located in the northern part of Gyeongsangbuk Province, South Korea. The watershed area is 1,815 km^2 and elevation ranges from 54 m to 1,420 m. Land use consists of forest, crop, and paddy, and the dominant soil types are rocky loam and sandy loam. Discharge data at Hyangseok Station was obtained from a stage-discharge rating curve. The hydrologic parameters for calibration are the same as those of Naerin Stream. This model was calibrated by simulating runoff and rainfall on July 24 to 26 in 2008. The simulation result is shown in Figure 4.4.

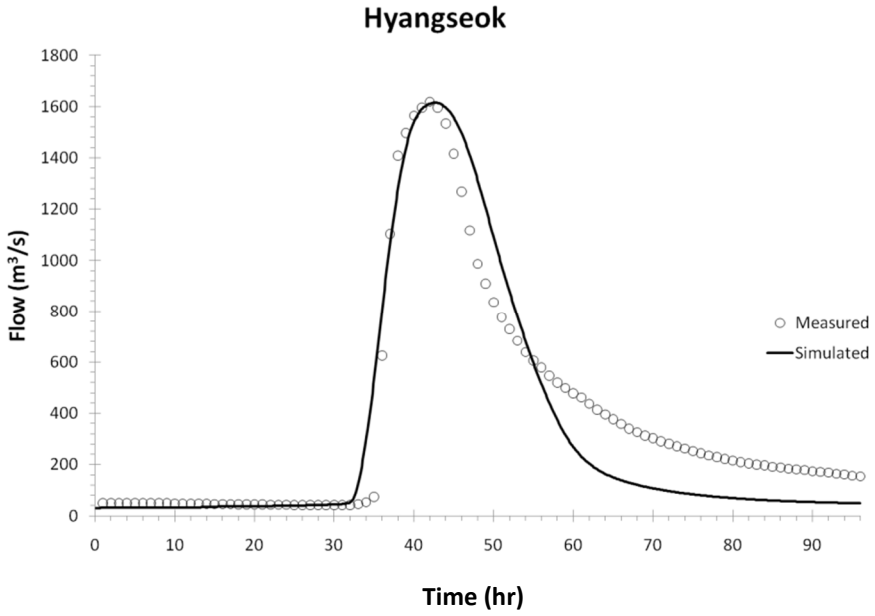

Figure 4.4. TREX model calibration at the Hyangseok Stream station (Velleux et al., 2012)

Relative percent difference (RPD) for time to peak and peak discharge was obtained from this result and is summarized in Table 4.5.

Table 4.5. The model evaluation using RPD in the Naesung Stream

	Measured Data	Simulation Result	RPD (%)
Time to peak (hr)	42.0	42.8	1.90
Peak discharge (m^3/s)	1619	1615	-0.25

The difference between measured data and simulation result on time to peak and peak discharge was 0.8 hour and 4 m^3/s, respectively. Overall this model performed well.

The saturated hydraulic conductivity for sandy loam on the Naerin Stream and the Naesung Stream is 3.03E-07 and 4.24E-06, respectively. The soil type in the Naerin Stream is 97 % of sandy loam. However, the soil type in the Naesung Stream is various, and sandy loam and rocky loam are dominant soil type. The Duksan Creek watershed is consists of 76 % of sandy loam. Therefore, the saturated hydraulic conductivity on the Duksan Creek was referred from that of the Naesung Stream.

4.4 TREX MODEL SIMULATION

4.4.1 Considerations for Initial Running

The Duksan Creek watershed had heavy intensive rainfall on July 14th to July 16th in 2006. For three days, total rainfall was 402 mm, and 168 mm occurred from 8 am to 11 am on July 15th in 2006. Rainfall data were obtained from the Gunryang Rainfall Station, which is located in the middle of the Duksan Creek watershed. With this rainfall condition, the TREX model was utilized.

Unlike impervious conditions, the infiltration effect was considered with saturated hydraulic conductivity with respect to soil type. Soil types were determined by soil map, land use map, and field investigation. Based on the soil and land use map, several soil types were decided and the final soil type was selected by a field trip.

Six channel properties including channel width, side slope, bank height, Manning roughness, and sinuosity were also determined by field investigation and reference to the report of Inje County (2008). Manning roughness was assumed to be 0.04 and sinuosity was determined to be 1 within a 30 m cell size.

4.4.2 Watershed Modeling Results

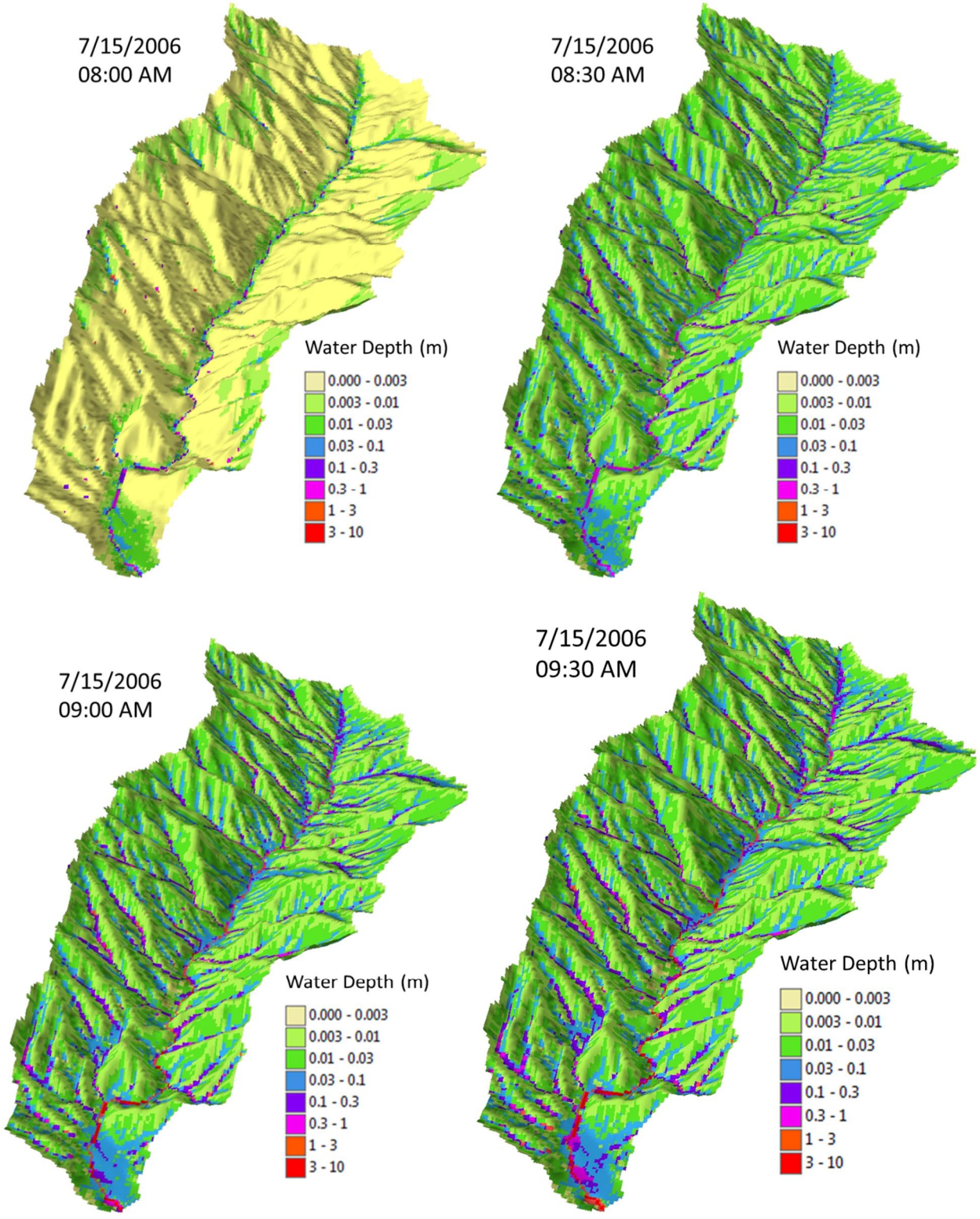

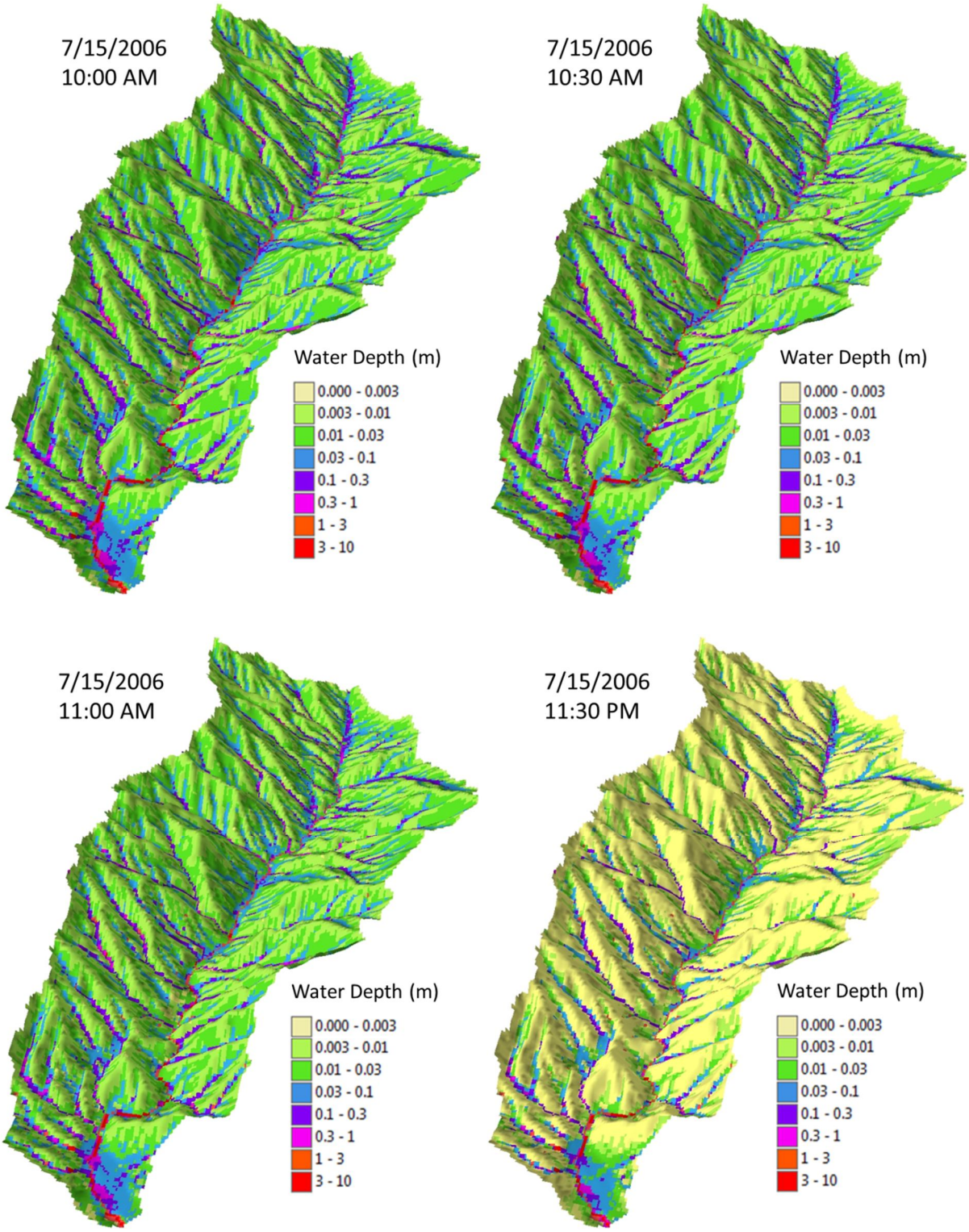

Figure 4.5. Flow depth simulation using TREX on the Duksan Creek watershed on July 15 in 2006

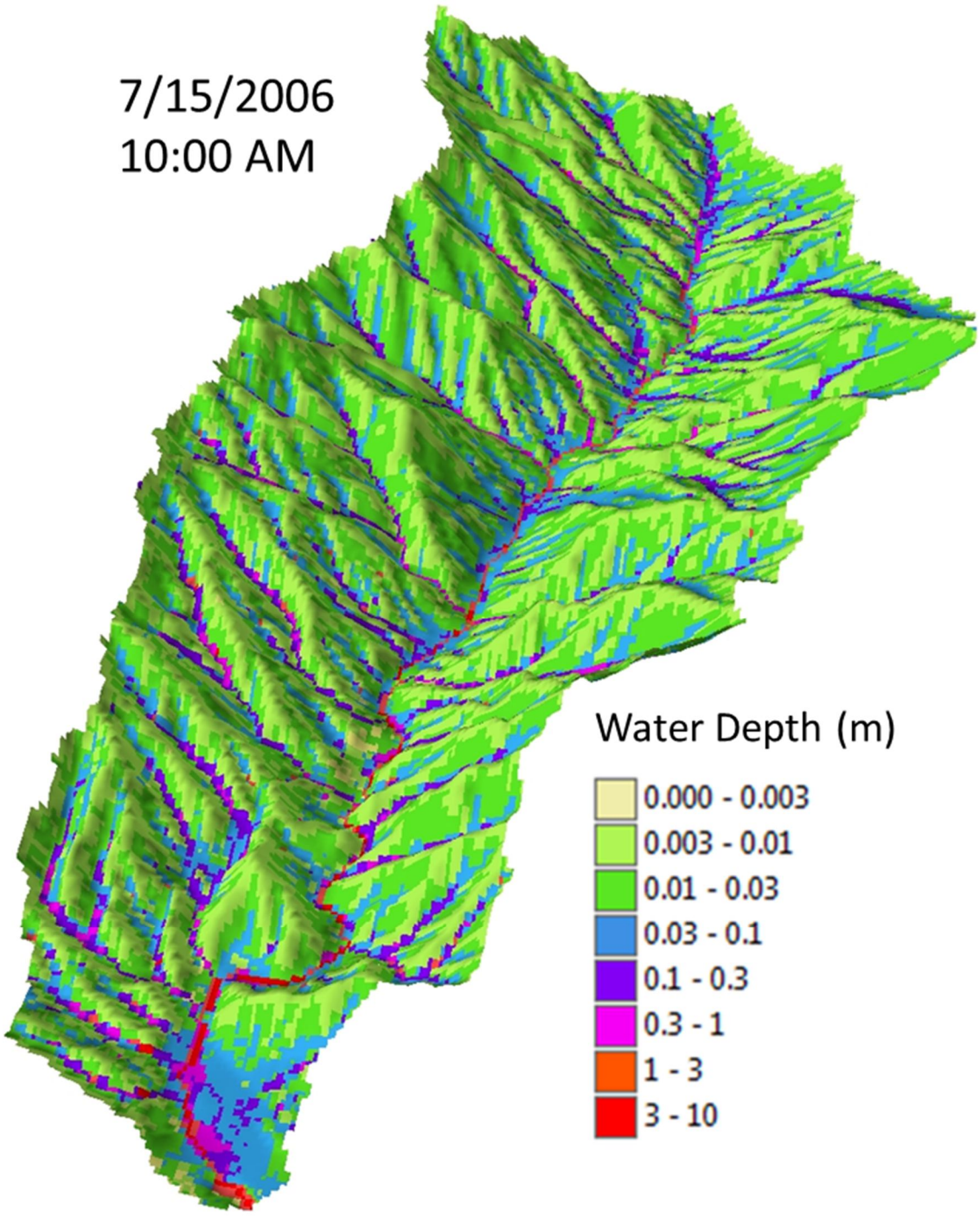

Figure 4.6. Flow depth simulation using TREX at 10:00 AM on July 15 in 2006

The visualization of Duksan Creek watershed modeling is shown in Figure 4.5. These results came from real rainfall data on July 12 and July 19 in 2006. Rainfall intensity at 08:00 AM on July 15 in 2006 was 56 mm/hr, and surface runoff in the main channel can be observed. After 1 hour, the entire watershed was wet and 0.3 m to 1.0 m of water depth occurred in the main channel and tributaries. The crop land near outlet was full of water with a depth of 0.03 m to 1 m. From 09:00 AM to 10:00 AM on July 15 in 2006, rainfall had the maximum intensity of 62 mm/hr. Water depth in the main channel and tributaries increased up to 5.3 m. Flows from tributaries on the left side near downstream accelerated shear stress, upland erosion would occur, and residential areas just below the tributaries would have a lot of damage. After 11 AM on July 15 in 2006, rainfall intensity was reduced to 5 mm/hr, and most water focused on the downstream near outlet compared to the steep mountainous area.

The infiltration depth and the discharge pattern with respect to this rainfall are shown in Figure 4.6 and Figure 4.8. From July 12 to July 14, the infiltration depth at the Duksan Creek watershed was 0.1 to 0.15 m. After two short rainfall events in July 14, the infiltration depth in July 15 increased to 0.2 to 0.25 m. This 24 hour duration showed the time to take the increase of the infiltration depth of 10 cm.

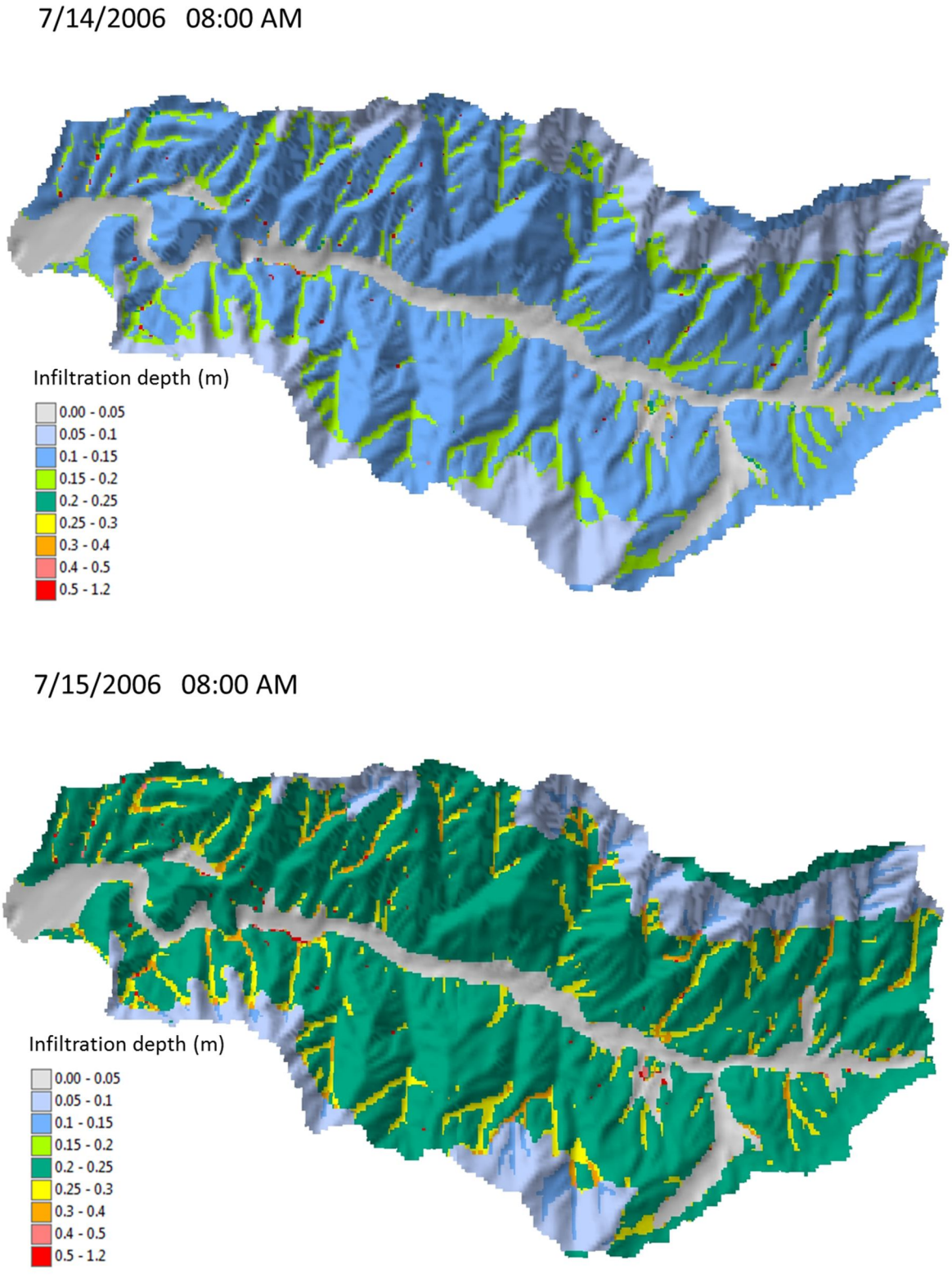

Figure 4.7. Infiltration depth in the Duksan Creek watershed

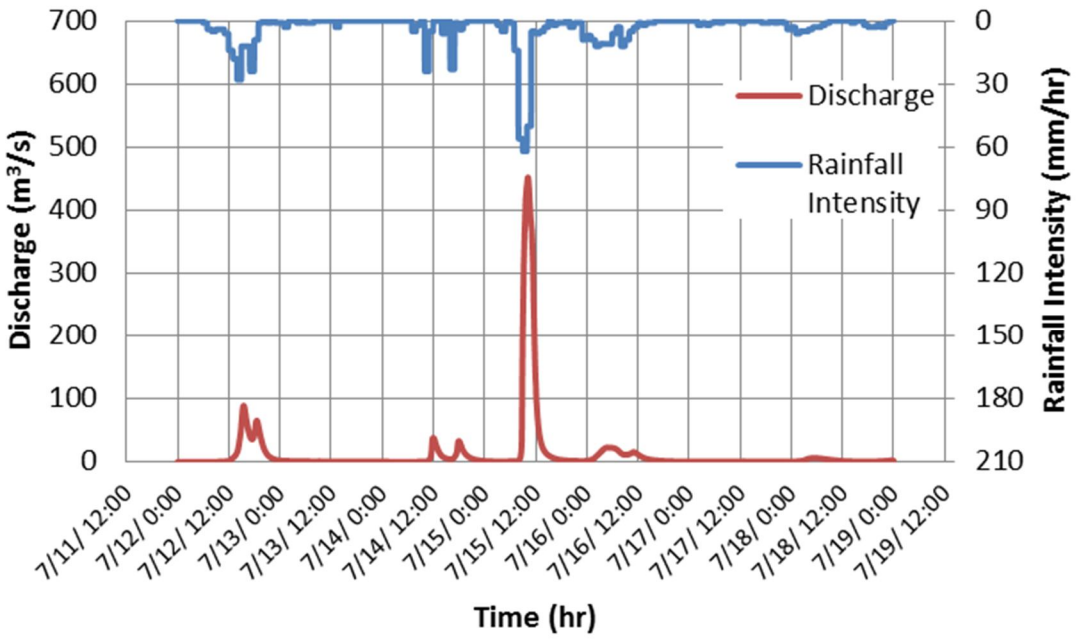

Figure 4.8. Hydrograph in Duksan Creek watershed

High intense rainfall was concentrated for only three hours from 08:00 AM to 11:00 AM on July 15 in 2006. The amount of rainfall was 168 mm, and the peak discharge from this rainfall amount was 452 m^3/s.

4.4.3 Modeling Results Comparison

Duksan Creek watershed has a rainfall station but no water level or discharge station. To validate the peak discharge that was acquired from the simulated result, two approaches were executed.

The first method was the comparison with the peak discharge from Inje County (2008). This report showed four methods to obtain the estimation of flood: Nakayasu and SCS methods by synthetic unit hydrograph and Clark method by flood routing. The peak discharge with respect to each method for 100 years of return period is summarized in Table 4.6.

Table 4.6. The comparison with each peak discharge value

	Peak discharge (m^3/s)	Relative Percent Difference (%)
TREX	452	
SCS	457	-1.1
CLARK	475	-4.8
Nakayasu	369	22.5

The value of the Nakayasu method was the least, and the result of two methods, including SCS and Clark were relatively similar with each other. This report selected the Clark's method because the peak discharge of 475 m^3/s was the maximum value in all the methods, and the maximum value was used to establish a river plan. The result of the SCS method displayed the closest value with the value of the TREX simulation. It is difficult to get the exact value for peak discharge but the TREX simulation result had good agreement with the results of other models.

The second method used the peak specific discharge graph that shows specific-discharge conditions as a function of the drainage area. The data came from America and Canada's rivers and creeks, and is shown in the Figure 4.9.

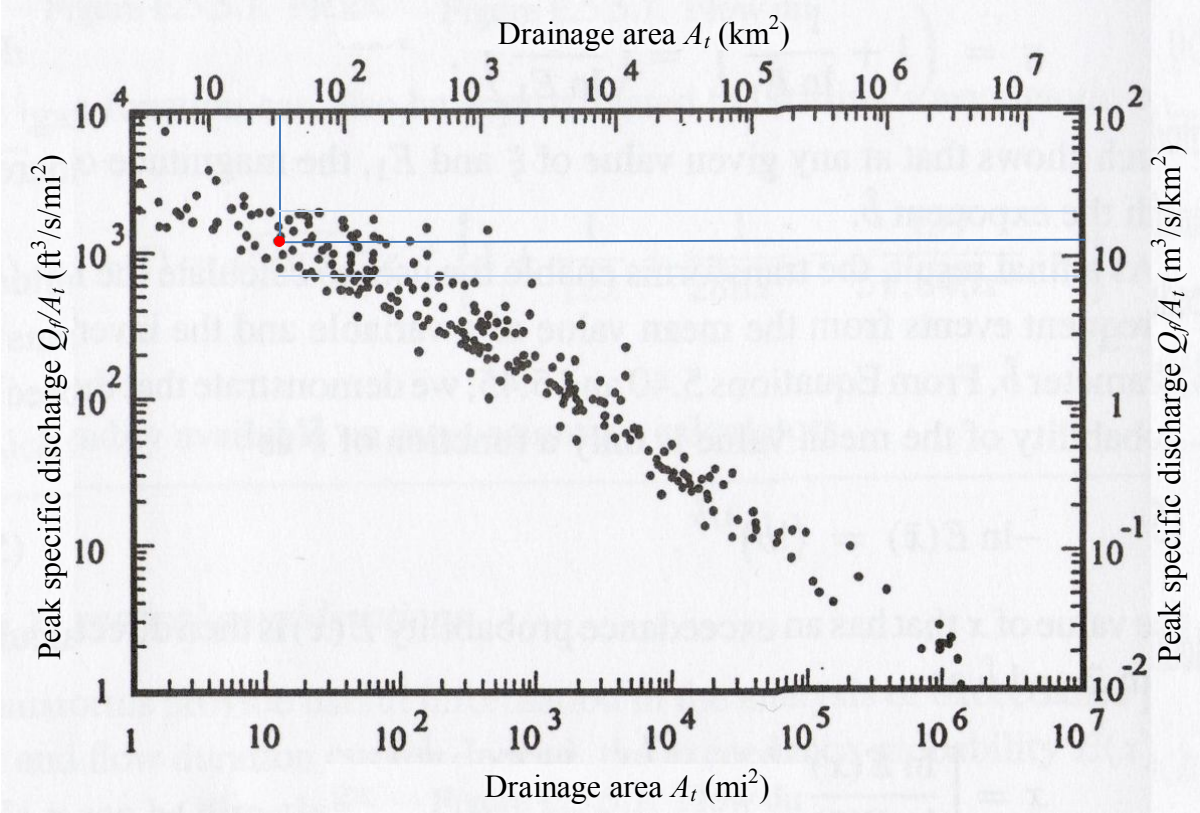

Figure 4.9. Specific discharge vs. drainage area (modified after Creager et al., 1945)

The peak discharge and the drainage area at Duksan Creek watershed are 452 m^3/s and 33.1 km^2, respectively. The peak specific discharge can be calculated to the peak discharge divided by drainage area and it was computed to be 13.7 $m^3/s/km^2$. The peak specific discharge for Duksan Creek watershed was located in the middle point at the same drainage area. The range of peak specific discharge at the same watershed area of 33.1 km^2 is around 8.1 $m^3/s/km^2$ to 21 $m^3/s/km^2$, and these values can be converted to peak discharge as 271 m^3/s to 701.4 m^3/s. The peak specific discharge value for Duksan Creek belongs to the range of the plotted points.

CHAPTER 5 HAZARD AREA MAPPING

5.1 INFINITE SLOPE MODEL

The most common types of landslides in South Korea are translational landslides, and the characteristics of the translational landslides are: the surface of a rupture is a straight line and the depth of landslide is shallow. Therefore, these types of landsides are similar to infinite slope. The infinite slope method is appropriate when the ground surface may be idealized as an infinite plane with potential slip surface parallel to it (Skempton and Delory, 1957). Long natural slopes are good examples to be investigated by the infinite slope method (Salgado, 2006). The saturated depth is important in this method and TREX can calculate infiltration depth in the hydrology modeling. The result of the infiltration depth at each cell within the watershed can be applied to the Infinite slope method to analyze slope stability in the Duksan Creek watershed. The sketch of the infinite slope method is shown in Figure 5.1.

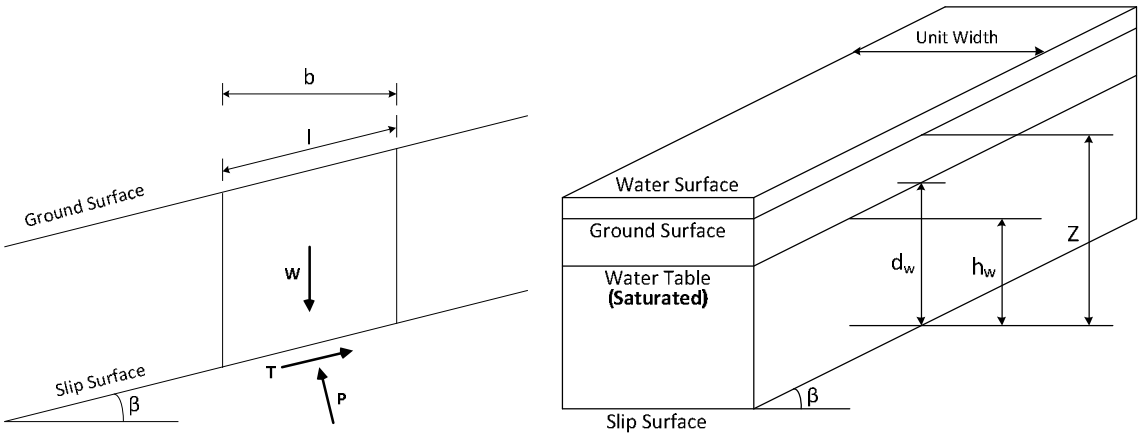

Figure 5.1. Infinite Slope Method

To derive the infinite slope model, free body diagram is used, and this is shown in Figure 5.2.

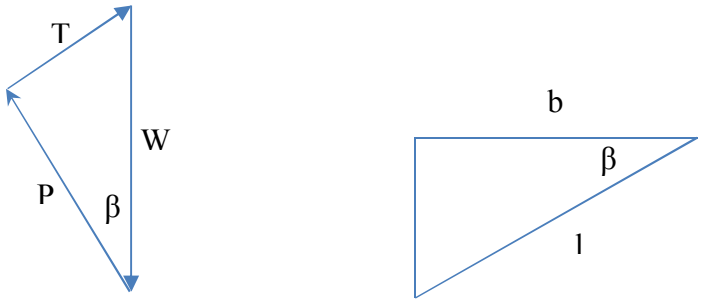

(a) FBD 1 (b) FBD 2

Figure 5.2. Free body diagram for infinite slope model

From Figure 5.2 (a), the tangential force (T) and normal force (P) on the base of the slip surface are given by:

$$\sin\beta = \frac{T}{W}, \quad T = W\sin\beta \quad (N) \tag{5.1}$$

$$\cos\beta = \frac{P}{W}, \quad P = W\cos\beta \quad (N) \tag{5.2}$$

From Figure 5.2 (b), the horizontal length of b can be expressed as:

$$l = \frac{b}{\cos\beta} \quad (m) \tag{5.3}$$

$$b = l\cos\beta \quad (m) \tag{5.4}$$

The weight (W) of soil slice with the equation 5.4 is:

$$W = \gamma_m \, b \, z$$

$$W = \gamma_m \, (l \cos\beta) \, z$$

$$W = \gamma_m \, z \, l \cos\beta \quad (N/m) \tag{5.5}$$

where: γ_m = unit weight of soil [N/m^3]

The unit width of soil slice does not account for this equation. From equation 5.1 and 5.2, forces on the base of the slice are:

$$T = W \sin\beta = \left(\gamma_m \, z \, l \cos\beta \right) \sin\beta = \gamma_m \, z \, l \sin\beta \cos\beta \quad (N/m) \tag{5.6}$$

$$P = W \cos\beta = \left(\gamma_m \, z \, l \cos\beta \right) \cos\beta = \gamma_m \, z \, l \cos^2\beta \quad (N/m) \tag{5.7}$$

When the effect of ground water is considered, the unit weight of soil can be divided by water part and dry part.

$$T = W \sin\beta = \left[\left(\gamma_{sat} - \gamma_w \right) b \, d_w + \gamma_m \, b \left(z - d_w \right) \right] \sin\beta \quad (N/m) \tag{5.8}$$

$$P' = W \cos\beta = \left[\left(\gamma_{sat} - \gamma_w \right) b \, d_w + \gamma_m \, b \left(z - d_w \right) \right] \cos\beta \quad (N/m) \tag{5.9}$$

The seepage force per unit volume of soil and total seepage force acting on slice are:

$$f_s = i\,\gamma_w = \frac{dh}{dl}\,\gamma_w = \sin\beta\,\gamma_w \quad (N/m^3) \tag{5.10}$$

$$F_s = \sin\beta\,\gamma_w\,(b\,d_w) = \gamma_w\,b\,d_w\,\sin\beta \quad (N/m) \tag{5.11}$$

The factor of safety for infinite slope is expressed as the ratio of shear strength of soil to shear stress developed along the potential failure surface, and the equation for the factor of safety is as follows;

$$FS = \frac{\dfrac{c\,b}{\cos\beta} + P'\tan\phi}{T + F_s} \tag{5.12}$$

where: FS = Factor of Safety [dimensionless]
c = cohesion [N/m^2]
b = horizontal length of slice [m]
β = the angle between slip surface and horizontal line [°]
P' = normal effective force [N/m]
ϕ = the angle of friction [°]
T = driving force [N/m]
F_s = total seepage force acting on slice [N/m]

When the equations 5.3, 5.8, 5.9, and 5.11 are substituted for the equation 5.12, the factor of safety is given by:

$$FS = \frac{\dfrac{c}{\left[\left(\gamma_{sat} - \gamma_w\right) d_w + \gamma_m \left(z - d_w\right)\right] \sin\beta \cos\beta} + \dfrac{\tan\phi}{\tan\beta}}{1 + \dfrac{\gamma_w \, d_w}{\left[\left(\gamma_{sat} - \gamma_w\right) d_w + \gamma_m \left(z - d_w\right)\right]}} \tag{5.13}$$

where: γ_{sat} = saturated unit weight of soil [N/m^3]
γ_w = unit weight of water [N/m^3]
d_w = water depth from ground surface to slip surface [m]
γ_m = unit weight of soil [N/m^3]
z = the distance from ground surface to slip surface [m]

If the water table is at ground surface (fully saturated below ground surface), the depth of water (d_w) is equal to the distance from ground surface to slip surface (z). The equation (6.2) can be reduced as below:

$$FS = \frac{\dfrac{c}{\left[\left(\gamma_{sat} - \gamma_w\right) d_w\right] \sin\beta \cos\beta} + \dfrac{\tan\phi}{\tan\beta}}{1 + \dfrac{\gamma_w}{\left(\gamma_{sat} - \gamma_w\right)}} \tag{5.14}$$

The equation 5.3 can be expressed as:

$$FS = \frac{C + \left(\gamma_{sat} - \gamma_w\right) d_w \cos^2\beta \tan\phi}{d_w \, \gamma_{sat} \sin\beta \cos\beta} \tag{5.15}$$

In the equation 5.15, the depth of water (d_w) can be obtained from infiltration depth using TREX simulation. Therefore, the slope stability in the Duksan Creek watershed can be analyzed.

5.2 STABILITY MAPPING USING TREX

5.2.1 Input Parameters

5.2.1.1 Soil Cohesion and Internal Friction Angle

The input parameters in the equation 5.15 for critical slope analysis are soil cohesion, saturated unit weight of water, water depth from ground surface to slip surface, slope angle, and internal friction angle of soil. In the equation 5.15, the most sensitive parameters are soil cohesion and the internal friction angle of soil because these two parameters can be easily affected by unsaturated conditions and saturated conditions. Kim et al. (2011) conducted direct shear test for undisturbed and remolded soils that is shown in Figure 5.3. The results for cohesion reduction ratio (CRR) and friction angle reduction ratio (FRR) are shown in Figure 5.4. For these Figures IJ means the sample taken from the Inje County area.

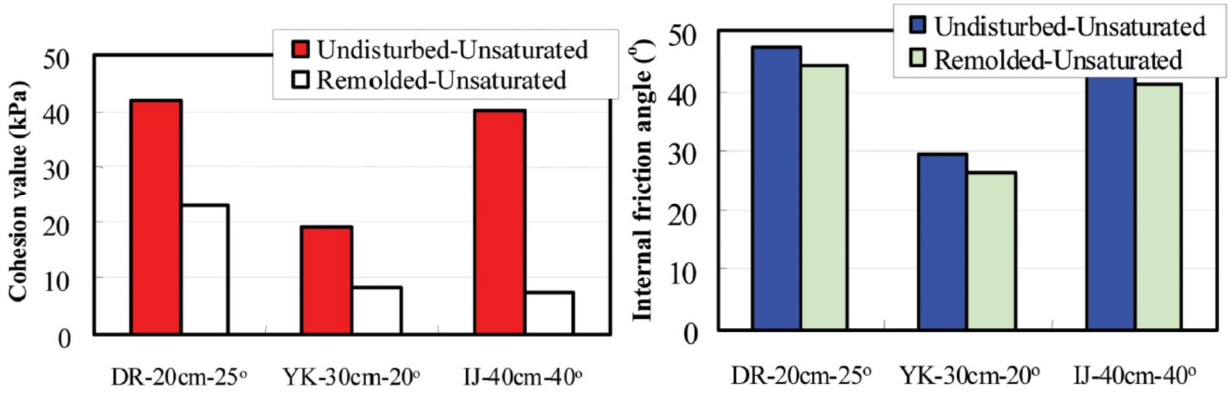

(a) Soil cohesion (b) Internal friction angle

Figure 5.3. Soil cohesion and internal friction angle (Kim et al., 2011)

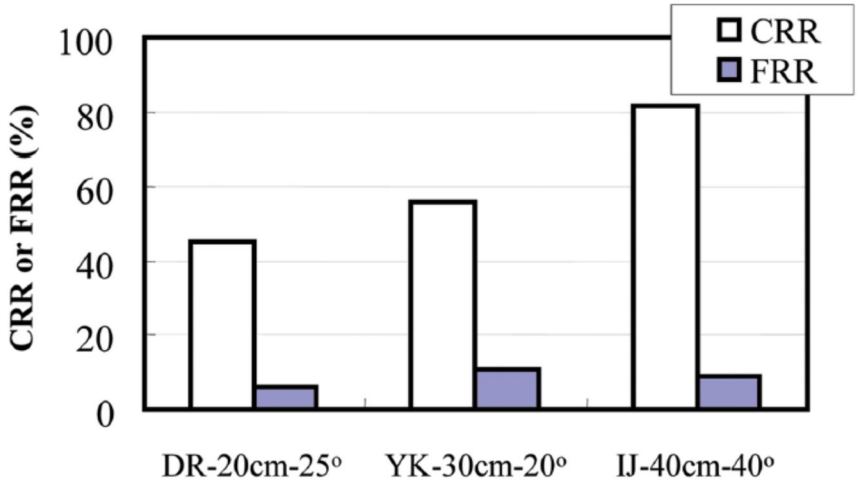

Figure 5.4. CRR and FRR for two types of soils (Kim et al., 2011)

CRR and FRR at the Inje County area was 81.8 % and 9.2 %. These results imply that increased soil weight due to rainfall infiltration induces the modification of soils, and shear strength of soil would be rapidly reduced because of soil cohesion change.

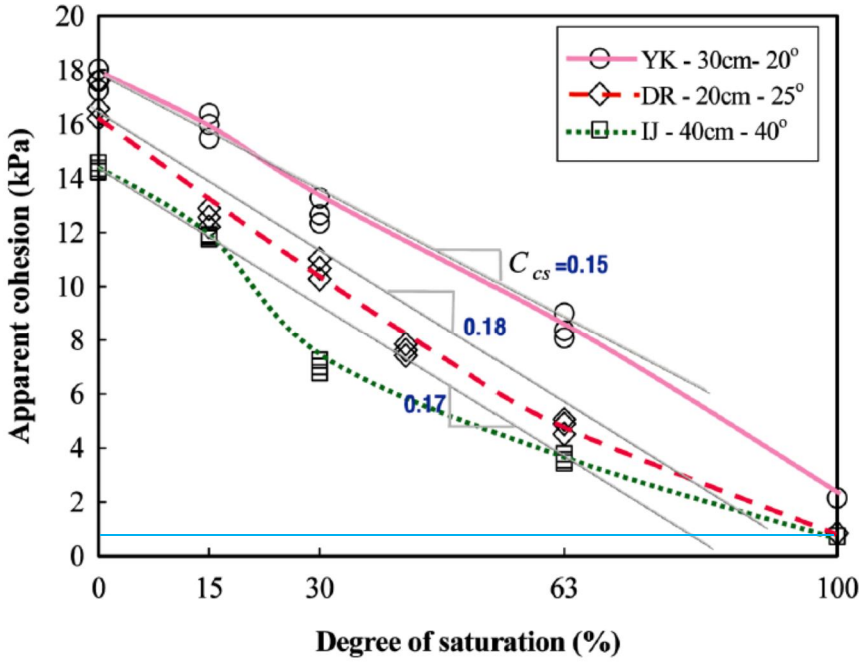

(a) Soil cohesion

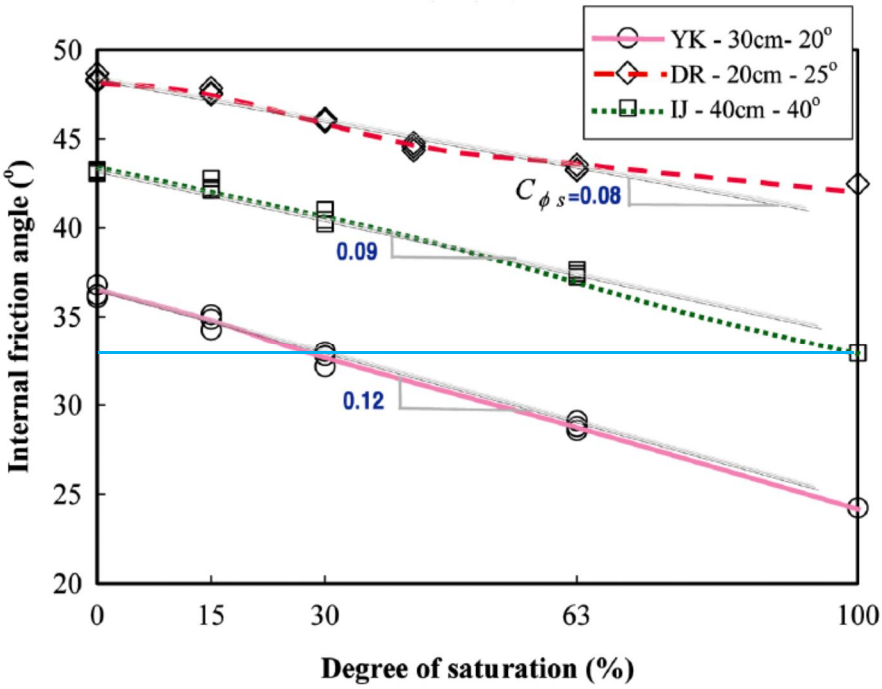

(b) Internal friction angle

Figure 5.5. The soil cohesion and internal friction angle change with respect to the degree of saturation (Kim et al., 2011)

Kim et al. (2011) also performed a shear test with respect to the degree of saturation to understand the change cohesion and internal friction angle. The result is shown in Figure 5.5. In this Figure, IJ means the sample taken from the Inje County area.

When the degree of saturation was changed from 0 % to 100 %, soil cohesion and the internal friction angle were reduced lineally. In Figure 5.5 (b), the blue line indicates soil cohesion and the internal friction angle value when the degree of saturation is 100 %. Therefore, the values of soil cohesion and internal friction angle change are important to interpret the infinite slope model.

5.2.1.2 Infiltration Depth

The next parameter being discussed concerning the infinite slope model is the saturated depth of water. Several methods using wetness index, such as SINMAP, have been studied, but the saturated depth of water is assumed to be the infiltration depth from the TREX simulation in this research. When all infiltration depths within a watershed were set to 0.1 m, 0.2 m, 0.3 m, 0.4 m, 0.5 m, and 1.0 m, the factor of safety using the infinite slope model can be obtained. The results are shown in Figure 5.6.

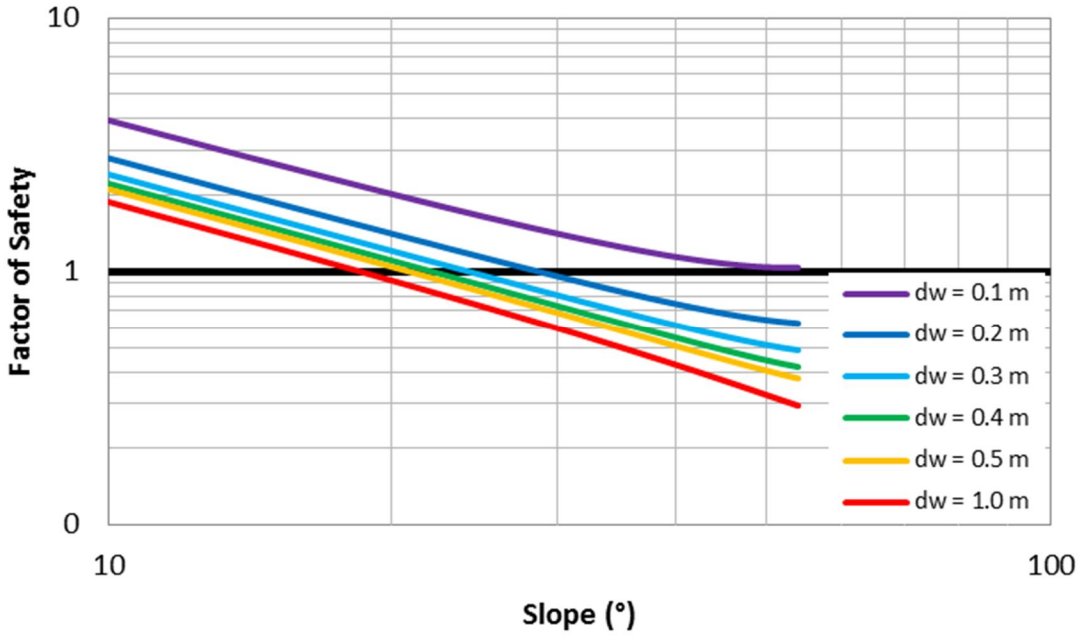

Figure 5.6. Factor of safety and slope angle with respect to infiltration depth

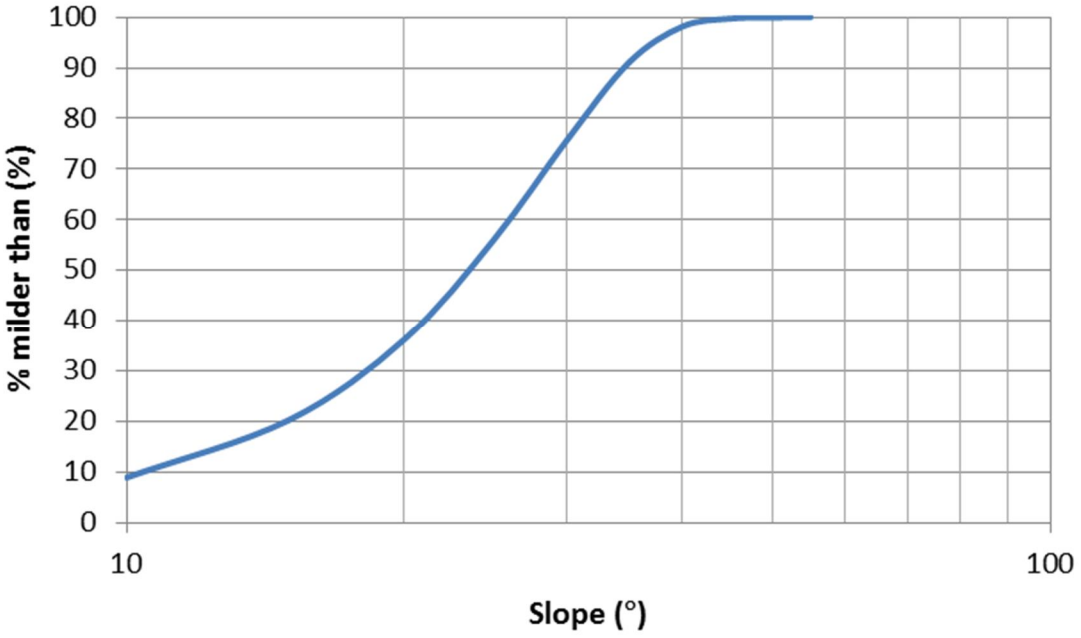

Figure 5.7. Slope distribution in the Duksan Creek watershed

When factor of safety in the slip slide is to 1, the critical slope angle with respect to infiltration depth can be obtained. This angle is summarized in Table 5.1.

Table 5.1. Slope angle with respect to infiltration depth

Infiltration depth (m)	Slope angle (°)
0.2	29
0.3	25
0.4	23
0.5	21
1.0	19

From Figure 5.6 and Table 5.1, the range of the infiltration depth was 0.2 m to 1.0 m and the critical slope angle was 19° to 29°. The range of slope angle corresponded from 35 % to 70 % of slope in the entire watershed in Figure 5.7.

Byun (2010) examined landslide places in Inje County and identified the failure depth of landslides was as shallow as 0.3 m to 0.5 m. Kim (2011) carried out field investigation in Gangwon Province and described failure depth to 0.5 m to 0.8 m. Therefore, an infiltration range of 0.2 m to 1.0 m from the TREX modeling belongs to field investigation result.

Oh et al. (2009) analyzed the landslide characteristics at the Inje County area using 2.5 m resolution of SPOT5 satellite image and GIS. The results showed that the mean slope angle at failure beginning region, debris transport region, and debris accumulation region was 26°, 24°, and 16°. Son et al. (2009) had an analysis of landslides at the Inje County area using aerial photograph taken by 8 million pixels of a camera and GIS. The results showed that the mean slope angle at failure beginning region, debris transport region, and debris accumulation region was 26°, 24°, and 19°. Thus, the slope failure angle of 19° to 29° from critical slope analysis is close to the results of field investigation and aerial photograph analysis.

In Figure 5.6, most infiltration depth in the mountain area was 0.2 m to 0.3m and the critical slope angle with respect to this infiltration depth was 25° to 29°.

Kim (2011) indicated that the most frequent angle of slope failure was 25° through field investigation in Gangwon Province. The results from Oh et al. (2009) and Son et al. (2009) showed that the slope angle on the beginning point of landslide was 26°. Therefore, the critical slope angle of 25° to 29° was very comparable with the slope failure angle of 26°.

5.2.2 Stability Mapping

5.2.2.1 Input Data

From the equation 5.15, input data are: soil cohesion, internal friction angle, saturated unit weight of soil, water depth from ground surface to slip surface, and slope angle. The main two input data are soil cohesion and internal friction angle. From Figure 5.5, when the degree of saturation was 100 %, soil cohesion and internal friction angle were around 0.7 kPa and 33°, respectively.

In case of saturated unit weight soil, this value was obtained from the literature review. Park et al. (2010) performed a direct shear test on weathered granite soil in Inje County, and the result of saturated unit weight of soil was obtained to 17.8 kN/m^3.

Saturated depth would be obtained from infiltration depth in the simulation of the TREX, and this result can be applied to the infinite slope equation. The TREX model can produce infiltration depth at each time step on every cell within the watershed, and this result would be the input value in the infinite slope model. The infiltration depth using the TREX simulation is shown in Figure 5.8.

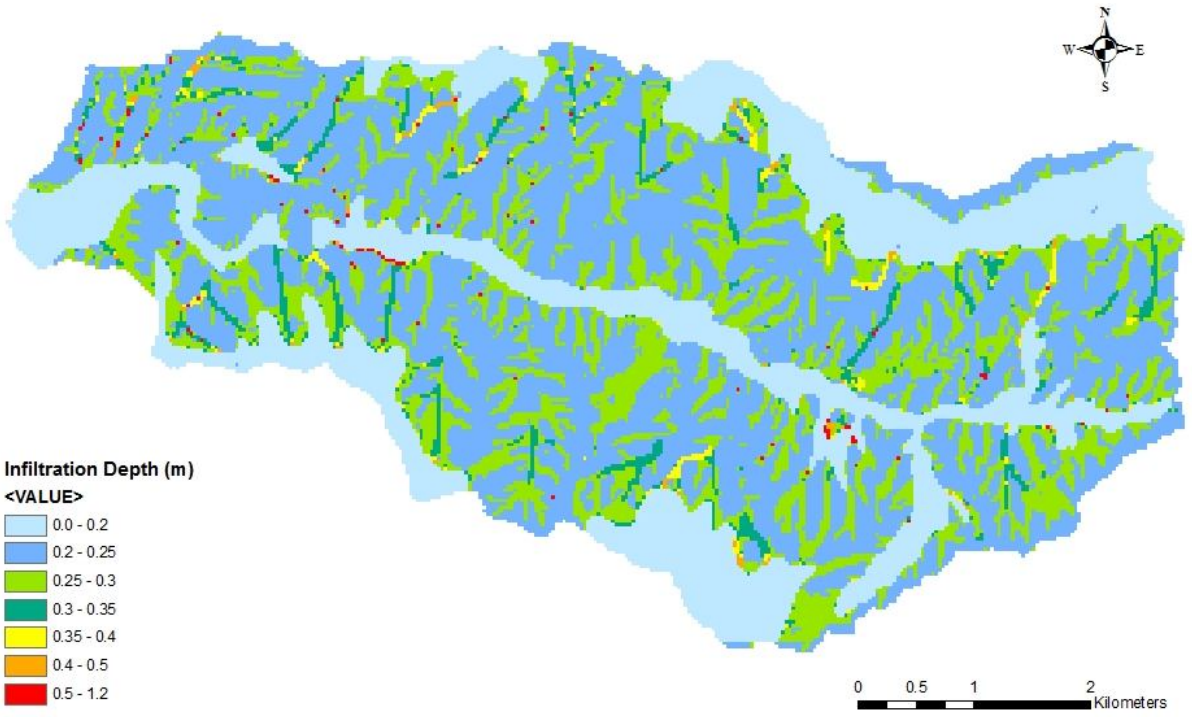

Figure 5.8. The infiltration depth in the study area

The infiltration depth result can be acquired from TREX modeling with respect to each time step and this infiltration depth time is based on July 15, 10:00 AM, because high intense rainfall time was on July 15, 08:00AM to 11:00AM. Landslides and debris flows occurred on July 15 9:00 to 10:00 AM (CJIC, 2006). The maximum infiltration depth was 1.2 m. Low values of infiltration depth were located in the main channel and agricultural area downstream. The infiltration depth range was 0.2 m to 0.25 m and these values were placed in high mountain areas. The infiltration depth from 0.25 m to 0.3 m was adjacent to each tributary. The relatively high infiltration depths were located upstream of each tributary.

The angle between slip surface and horizontal line can be acquired from the slope map in GIS. When all input data are determined, these values were applied to the equation 5.15 and hazard area was obtained.

5.2.2.2 Results

The saturated water depth was assumed to infiltration depth from TREX simulation in this research, and this depth was applied to the infinite slope model. Before factor of safety from the infinite slope model was discussed, the slope angle with respect to the infiltration depth was compared with field investigation data in terms of slope failure depth and slope angle. After discussing failure slope angle and depth, the factor of safety was obtained from the infinite slope model and this is shown in Figure 5.9.

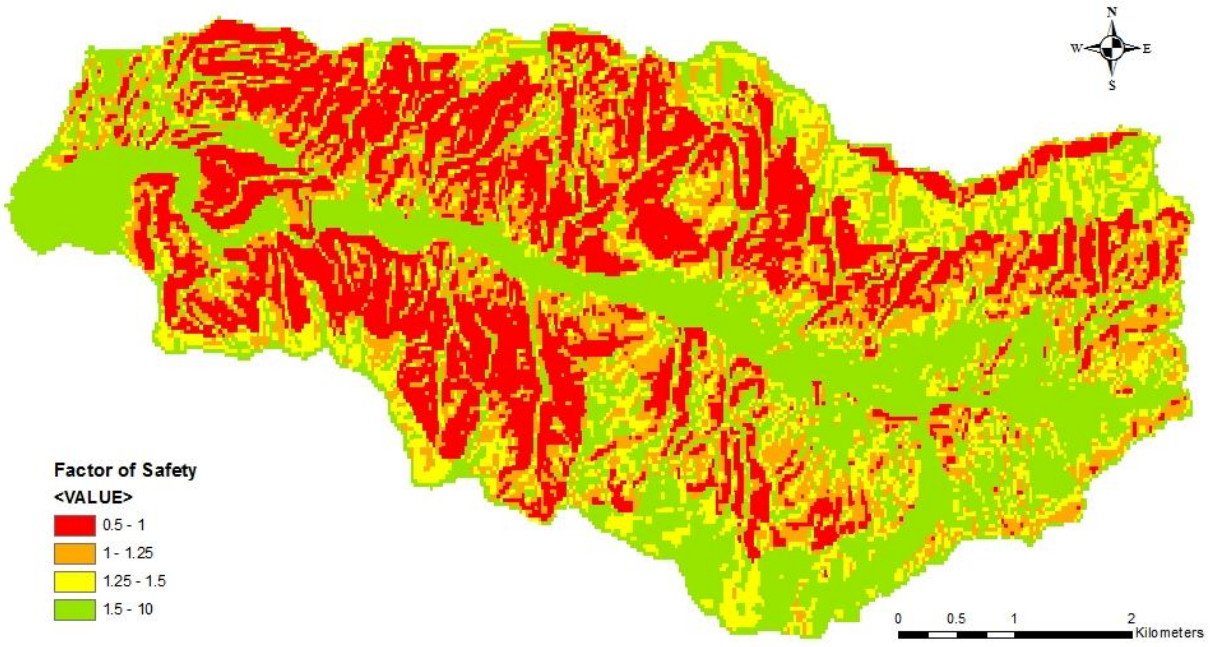

Figure 5.9. Factor of safety using the TREX simulation

In terms of the range for factor of safety, Kim (2010) introduced the minimum factor of safety of South Korea, Japan, and the U.S.A. Each country has different values with respect to the criteria from their government department, but most values were under 1.3 to 1.5. Thus, criterion of factor of safety in this research can be classified as 1.0 for high susceptible and 1.5 low susceptible for landslides. Factor of safety in most mountainous areas was below 1. The red and orange colors were located upstream of each tributary or close to each tributary. Landslides in the Duksan Creek would occur near tributary, and wood and soil debris directly would move to the main channel. These would make a riverbed to increase and bring the secondary damage like floods.

5.3 LANDSLIDE HAZARD MAP IN SOUTH KOREA

5.3.1 Methods

The Korea Forest Research Institute (KFRI) completed a Landslide Hazard Map over South Korea in 2005. The most important factors were categorized as three main components including topographic factors, forest factors, and geologic factors. Topographic factors are slope degree, slope length, slope position, and slope form. Forest factors are forest type and soil depth. The geologic factor is bedrock. These factors can be acquired from digital topographic map, digital forest type map, digital forest site map, and digital geologic map. Each factor has its own weight with respect to the weighted category. The table for landslide hazard score with respect to each factor is summarized in Table 5.2. Using this below, the landslide hazard criteria was determined by the sum of weighted scores. This is presented in Table 5.3.

Table 5.2. Landslide hazard score (KFS, http://sansatai.forest.go.kr/dg_005.do)

Table 1. Score table for prediction of landslide-susceptible area.

Factor	Category				
	1	2	3	4	5
slope length (m)	below 50 0	51-100 19	101-200 36	over 201 74	
bedrock	Sedimentary (mud stone, lime stone, shale, sand stone etc.) 0	Igneous 5	Metamorphic (phyllite, slate) 12	Metamorphic (gneiss, schist) 19	Igneous (porphyry, andesite) 56
slope position	0-4/10 0	5-6/10 9	7-10/10 26		
forest type	· Coniferales Forest (young tree forest, small pole forest) 18	· Coniferales Forest (middle pole forest, large pole forest) · Decideous Forest, Mixed Forest (young tree forest) 26	· Decideous Forest, Mixed Forest (small· middle· large pole forest) 0		
slope form	rising slope 0	equilibrium slope 5	descent slope 12	complex slope 23	
soil depth (cm)	under 20 0	20-100 7	over 101 21		
slope (o)	under 25 16	26-40 9	over 41 0		

Table 5.3. Landslide hazard criteria (KFS, http://sansatai.forest.go.kr/dg_005.do)

Class	Total Score Range	Degree of Hazard
1	> 181	Area with severe susceptibility to landslide
2	121~180	Area with moderate susceptibility to landslide
3	61~120	Area with little susceptibility to landslide
4	< 60	Stable Area

5.3.2 Results

This landslide hazard criterion was applied to all of South Korea, and the landslide hazard map for the study area is shown in Figure 5.10.

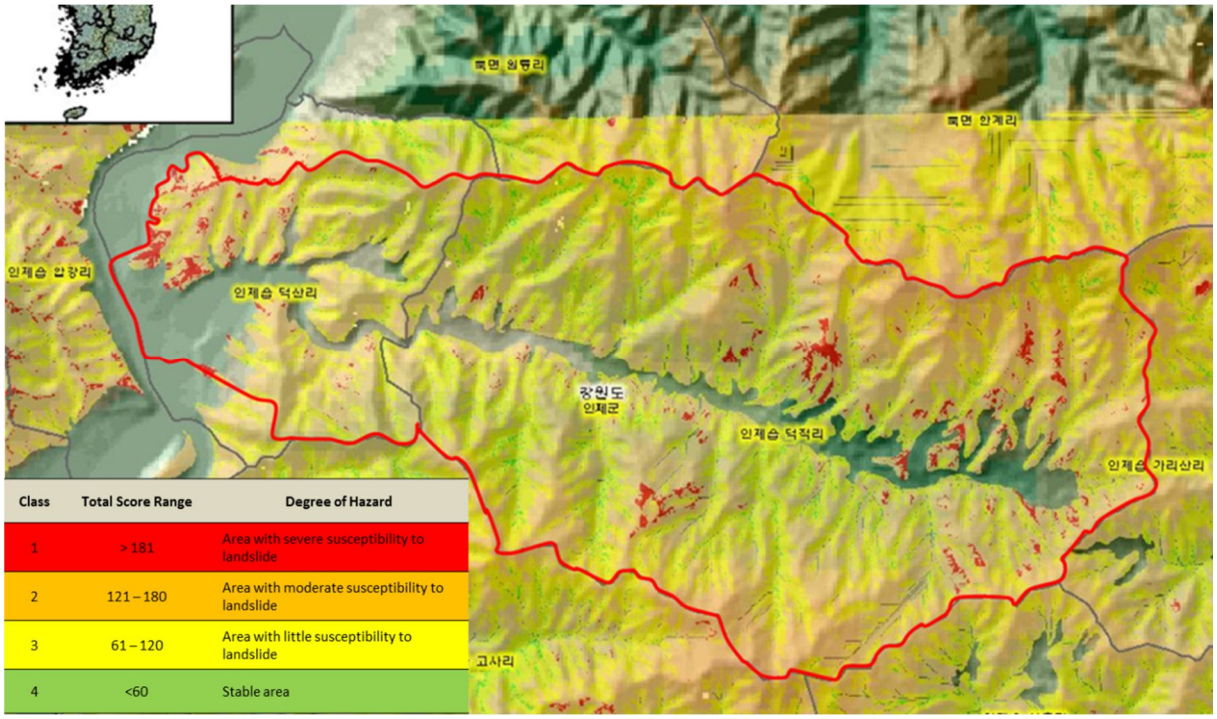

Figure 5.10. Landslide hazard map in the Duksan Creek watershed (http://sansatai.forest.go.kr)

The colors for each class from 1 to 4 are red, orange, yellow and green. The red color is mainly distributed in upstream areas and some mountain regions in the upstream areas. Each tributary was decided to class 3, and the main channel was determined to class 4. This map shows the main channel area is stable.

5.4 STABILITY INDEX MAP (SINMAP)

5.4.1 Methods

SINMAP was selected among landslide models, because the results from SINMAP can be compared with the results of stability mapping using TREX in that both methods provide factor of safety to evaluate slope stability.

SINMAP combines the hydrology model and infinite slope model. The infinite slope model is given by the following equation.

$$FS = \frac{C_r + C_s + \cos^2\theta \left[\rho_s\, g\, (D - D_W) + (\rho_s\, g - \rho_W\, g)\, D_W\right] \tan\phi}{D\, \rho_s\, g \sin\theta \cos\theta} \tag{5.16}$$

where: C_r = root cohesion [N/m^2]
C_s = soil cohesion [N/m^2]
θ = slope angle [°]
ρ_s = wet soil density [kg/m^3]
g = gravitational acceleration [9.81 m/s^2]
D = the vertical soil depth [m]
D_W = the vertical height of the water tble within the soil layer [m]
d_w = water depth from ground surface to slip surface [m]
ϕ = the internal friction angle of the soil [°]

The geometry which is assumed in the equation 5.16 is shown in Figure 5.11.

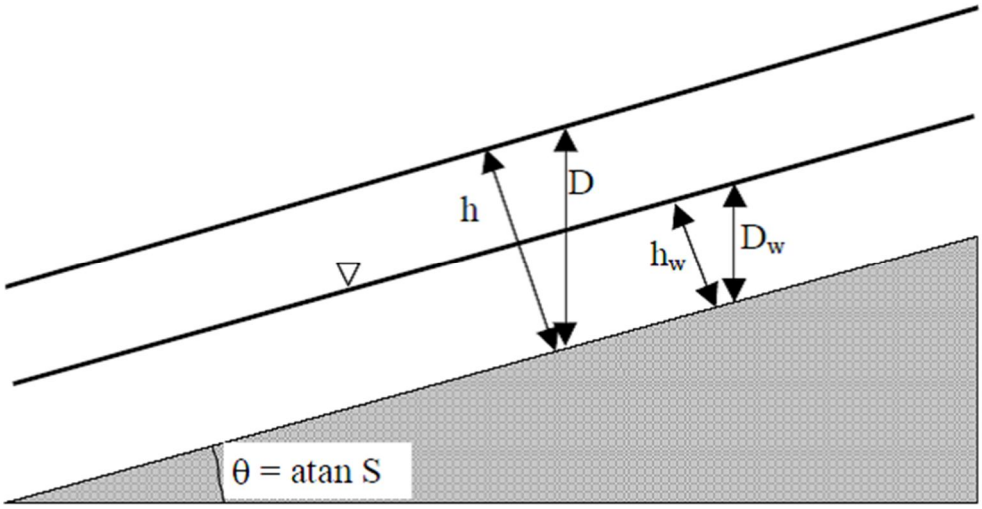

Figure 5.11. Infinite slope stability model schematic (Pack et al., 2005)

Soil thickness in this approach is perpendicular to the slope instead of in a vertical direction. Thus, the soil thickness can be expressed as:

$$h = D\cos\theta \tag{5.17}$$

The soil thickness in this model is assumed by the model user. When the equation 5.17 was applied to the equation 5.16, the factor of safety reduces to the equation 5.18:

$$FS = \frac{C + \cos\theta\left[1 - wr\right]\tan\phi}{\sin\theta} \tag{5.18}$$

where: C = combined cohesion, $C = \left(C_r + C_s\right) / \left(h\,\rho_s\,g\right)$ [dimensionless]

w = relative wetness $w = D_w / D = h_w / h$ [dimensionless]

r = the water to soil density ratio $r = \rho_w / \rho$ [dimensionless]

The relative wetness can be variable because the soil thickness can be changed by the user. Thus, the factor of safety is strongly relying on the value of the soil thickness. Based on the SINMAP model, the stability index can be defined as the following equation:

$$FS = \frac{C + \cos\theta \left[1 - \min\left(\frac{R}{T} \frac{a}{\sin\theta}, 1 \right) r \right] \tan\phi}{\sin\theta} \tag{5.19}$$

where: a = specific catchment area
θ = specific catchment slope
R/T = recharge divided by transmissivity

Once SINMAP is used to obtain the stability index at the target area, this model provides stability class with respect to stability index conditions, and this is summarized in Table 5.4.

Table 5.4. Stability class definitions (Pack et al., 2005)

Condition	Class	Predicted State	Parameter Range	Possible Influence of Factors Not Modeled
SI > 1.5	1	Stable slope zone	Range cannot model instability	Significant destabilizing factors are required for instability
1.5 > SI > 1.25	2	Moderately stable zone	Range cannot model instability	Moderate destabilizing factors are required for instability
1.25 > SI > 1.0	3	Quasi-stable slope zone	Range cannot model instability	Minor destabilizing factors could lead to instability
1.0 > SI >0.5	4	Lower threshold slope zone	Pessimistic half of range required for instability	Destabilizing factors are not required for instability
0.5 > SI > 0.0	5	Upper threshold slope zone	Optimistic half of range require for stability	Stabilizing factors may be responsible for stability
0.0 > SI	6	Defended slope zone	Range cannot model stability	Stabilizing factors are required for stability

The SINMAP program provides lower and upper boundaries of default values including T/R, dimensionless cohesion, internal friction angle, and soil density. These are shown in Figure 5.12.

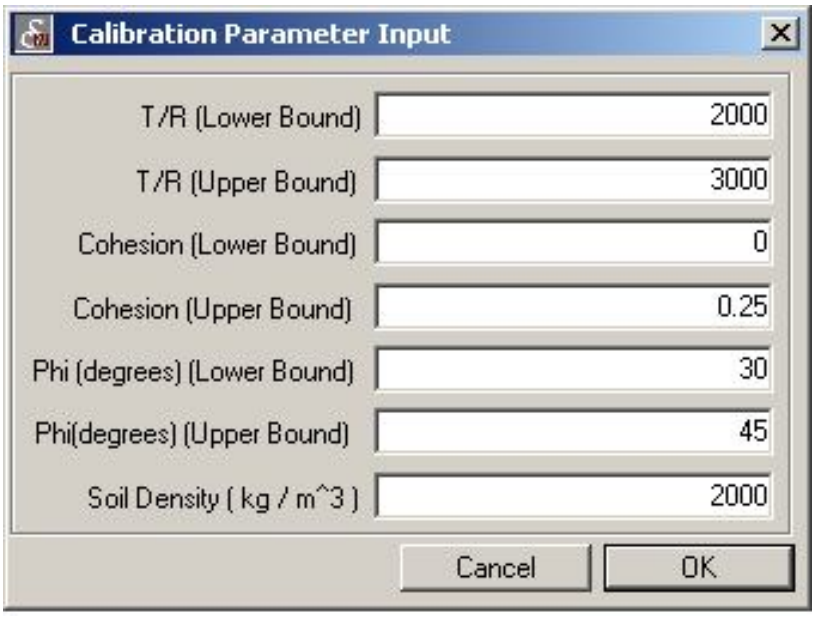

Figure 5.12. The default input parameters in SINMAP (Pack et al., 2005)

From Figure 5.12, T is soil transmissivity and it is hydraulic conductivity times soil thickness which was assumed to 1 m. R is lateral discharge that is in equilibrium with a steady state recharge and daily rainfall on July 15 in 2006 was applied. Cohesion includes root cohesion and soil cohesion, but root cohesion was not considered because it is hard to quantify in the mountainous area. The internal friction angle was taken from Figure 5.5. Soil density was determined to 1,820 kg/m^3 (Park et al., 2010).

Once input parameters for SINMAP were decided, the factor of safety in the Duksan Creek watershed was computed.

5.4.2 Results

Using SINMAP software Duksan Creek watershed was modeled and the stability index was computed. The result is shown in Figure 5.13.

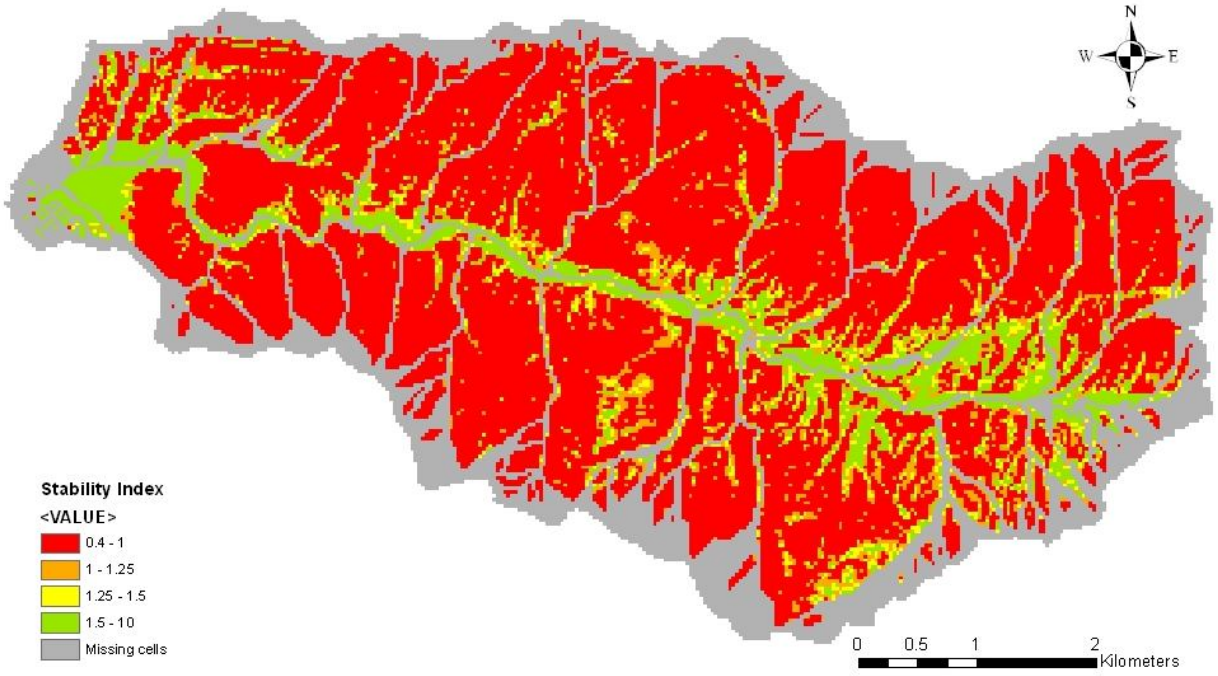

Figure 5.13. Stability index map in the Duksan Creek watershed

The grey color represents the area of missing cells that cover each tributary, the main channel, downstream area, and the edge of the watershed. Most mountainous regions showed upper and lower threshold regions with the stability index of less than 1.0. Flat regions including the main channel areas and the agricultural areas downstream showed safe regions with the stability index of 1.5 to 10.

5.5 MAP COMPARISON

5.5.1 Methods

The three results including stability mapping using TREX simulation, landslide hazard map proved by KFRI, and SINMAP need to be compared with real landslide areas for their accuracy. The real damaged area was obtained from Yeon (2011) by evaluating landslide susceptibility using logistic regression analysis in the Duksan Creek watershed. The real landslide places were provided as a result, and these are shown in Figure 5.14.

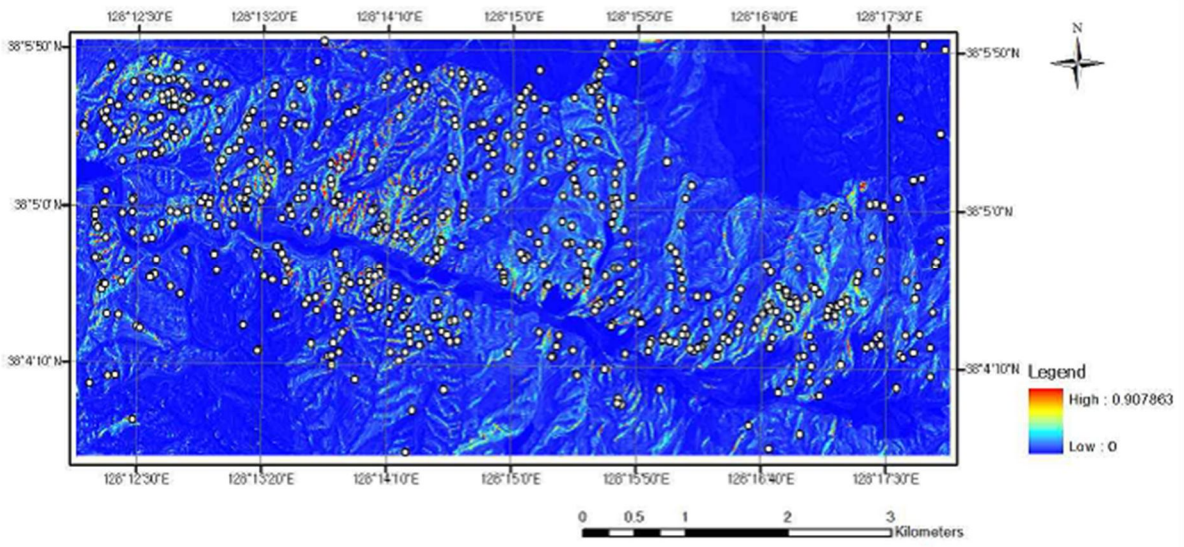

Figure 5.14. Landslide location area (Yeon, 2011)

The white circle represents the places where landslides occurred. This map was matched with aerial images in GIS using georeferencing. Then these white circles were digitized and converted to a shape file in GIS. The color of circles was changed from white to black, and this is shown in Figure 5.15.

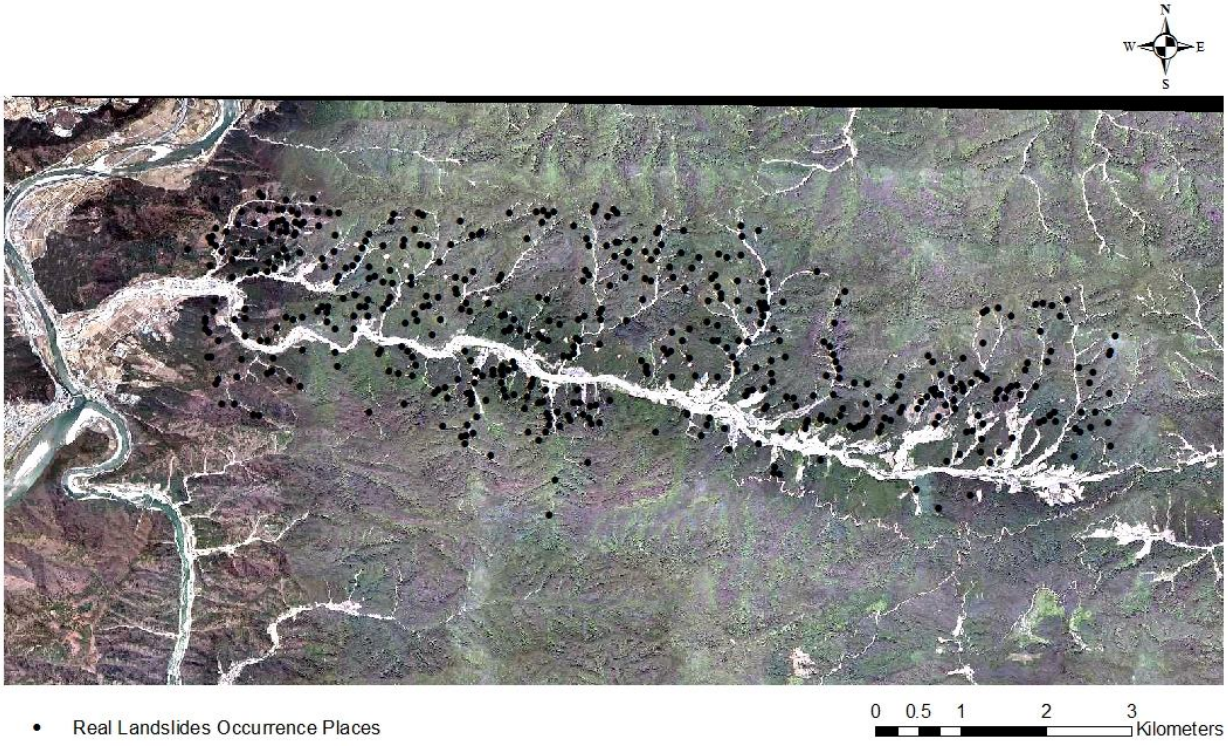

Figure 5.15. The landslides digitized map

After these processes, each map including stability mapping using TREX simulation, landslide hazard map proved by KFRI, and SINMAP was matched with the digitized landslide map to evaluate the accuracy of landslides between real damaged areas and modeling results.

5.5.2 Results

Each comparison between real landslide points and three modeling results was performed, and they are shown in Figure 5.16 to Figure 5.18. The real landslides occurrence places were compared to the area with FS < 1 on each model. The accuracy of each model with respect to real landslide occurrence places is summarized in Table 5.5.

Table 5.5. The comparison of each model with real landslide locations

	Total number of landslides points	Number of points (SI<1)	Predictability (%)
Landslide hazard map (KFRI)	518	18	3.5
SINMAP	518	381	73.6
Stability mapping (TREX)	518	232	44.8

Table 5.6. The area of occupation in SINMAP and TREX results

	SINMAP		TREX	
	Number of cells	Occupancy (%)	Number of cells	Occupancy (%)
SI<1	21,318	58.0	10,405	28.3
1.5 ≤ SI<10	6,900	18.8	26,347	71.7
Missing cells	8,534	23.2	0	0.0
Total	36,752	100.0	36,752	100.0

Table 5.7. Relative predictability between SINAMP and TREX results

	SINMAP	TREX
Number of points (SI<1)	381	232
Number of cells (SI<1)	21,318	10.405
Relative predictability (%)	1.79	2.23
Improvement (%)		24.6

From Table 5.5, the predictability of landslide hazard map from KFRI was 3 % and this result was very low compared to other results. The landslide hazard map was evaluated by landslide hazard score and these criteria were considered to be changed. The predictability of SINMAP was higher than the value of stability mapping using TREX, however, SINMAP produced missing cells and they were 23.2 % at the entire watershed, which is shown in Table 5.6. In addition, the correct landslide location cannot provide in SINMAP when it compared to real landslide locations. To represent the comparison between SINMAP and TREX results, the relative predictability was obtained in Table 5.7. The relative predictability with respect to the area occupancy in SINMAP and TREX was 1.79% and 2.23 %, respectively. This result shows that the result of TREX is improved to 24.6 % compared to the result of SINMAP in terms of the relative predictability.

From Figure 5.16 to Figure 5.18, most damaged areas of the main channel and tributaries still showed a safe area in the Duksan Creek watershed. Thus, the analysis for these areas is still required.

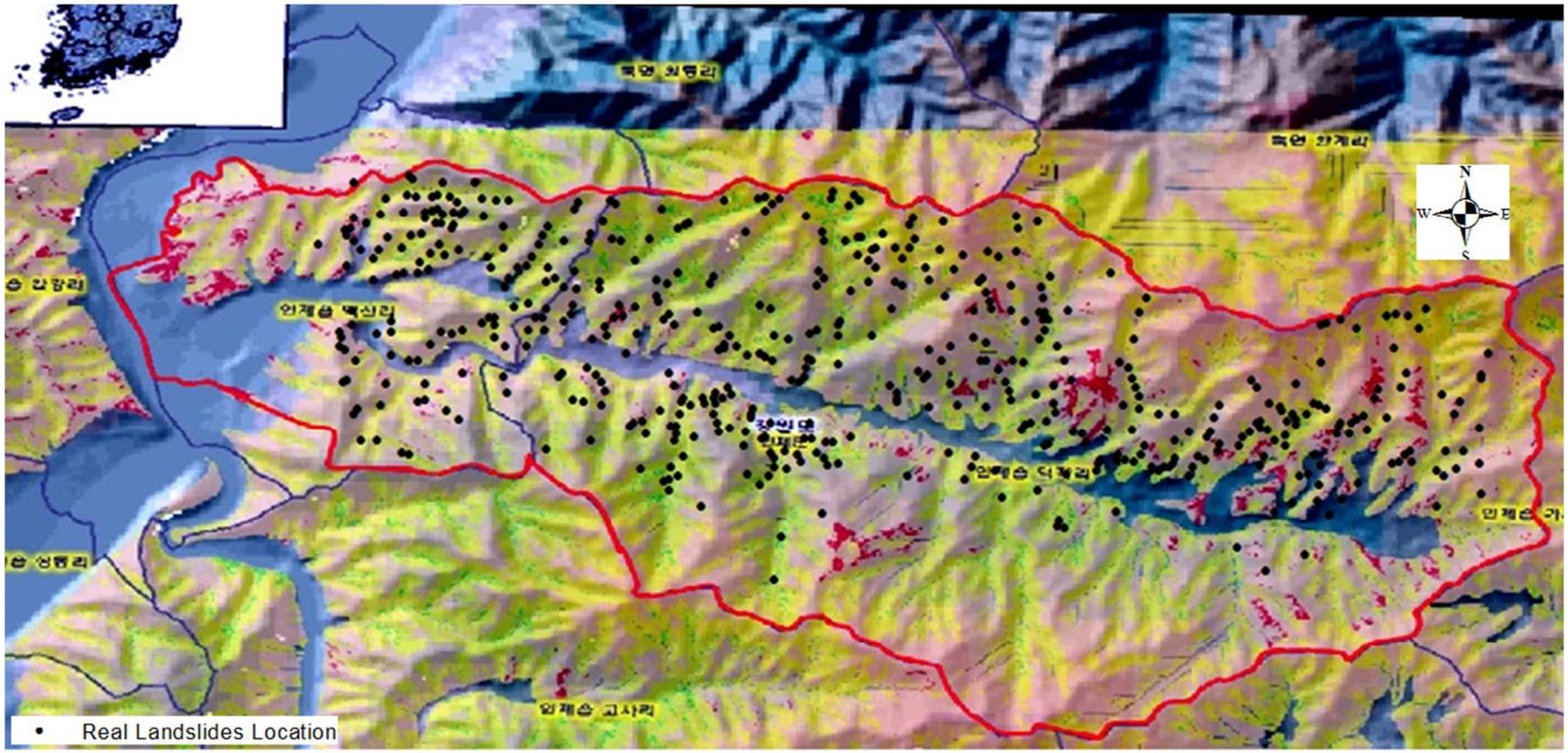

Class	Total Score Range	Degree of Hazard
1	> 181	Area with severe susceptibility to landslide
2	121 – 180	Area with moderate susceptibility to landslide
3	61 – 120	Area with little susceptibility to landslide
4	<60	Stable area

Figure 5.16. Landslide hazard map (KFRI) with real landslide locations

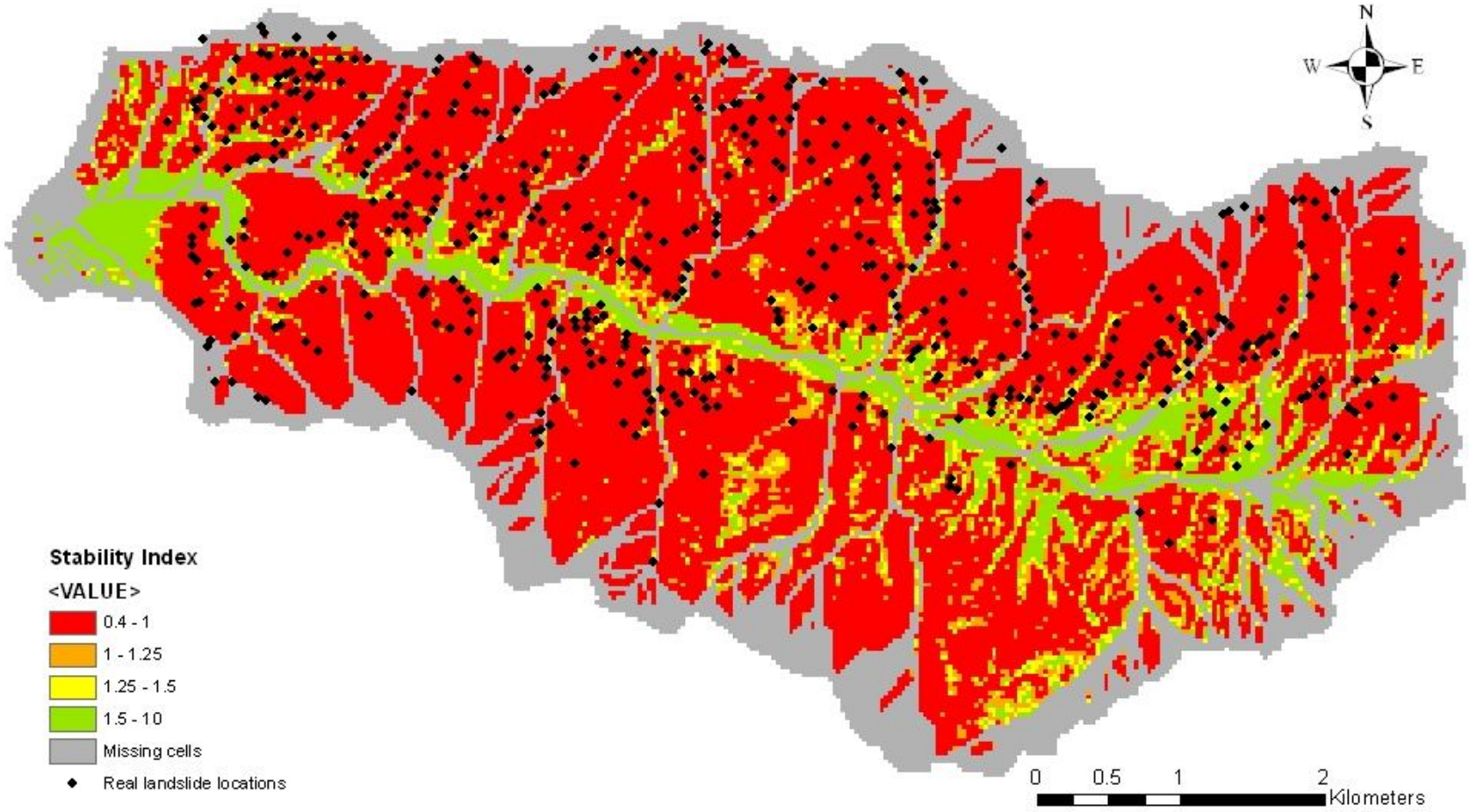

Figure 5.17. SINMAP with real landslide locations

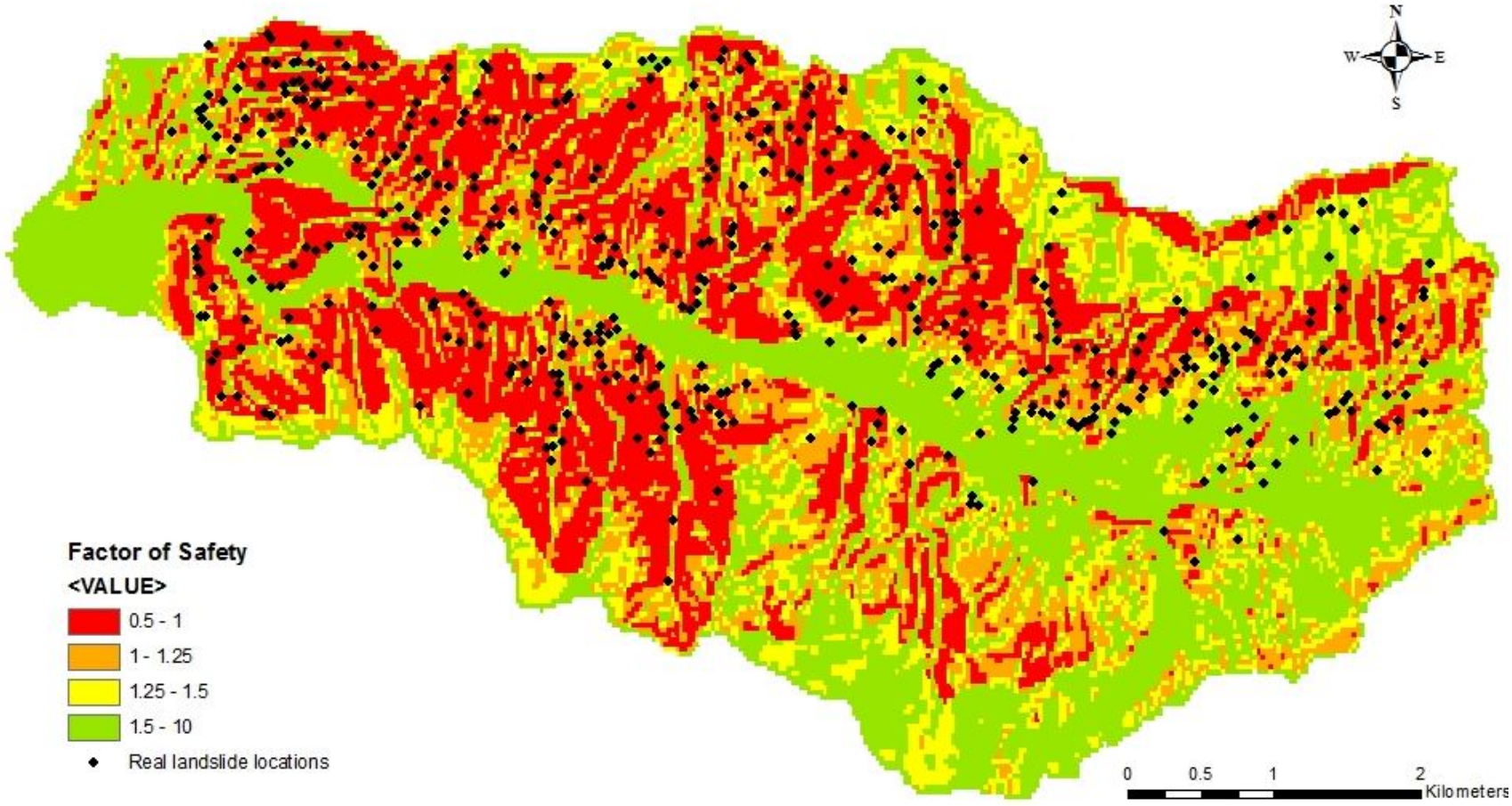

Figure 5.18. Stability mapping using TREX with real landslide locations

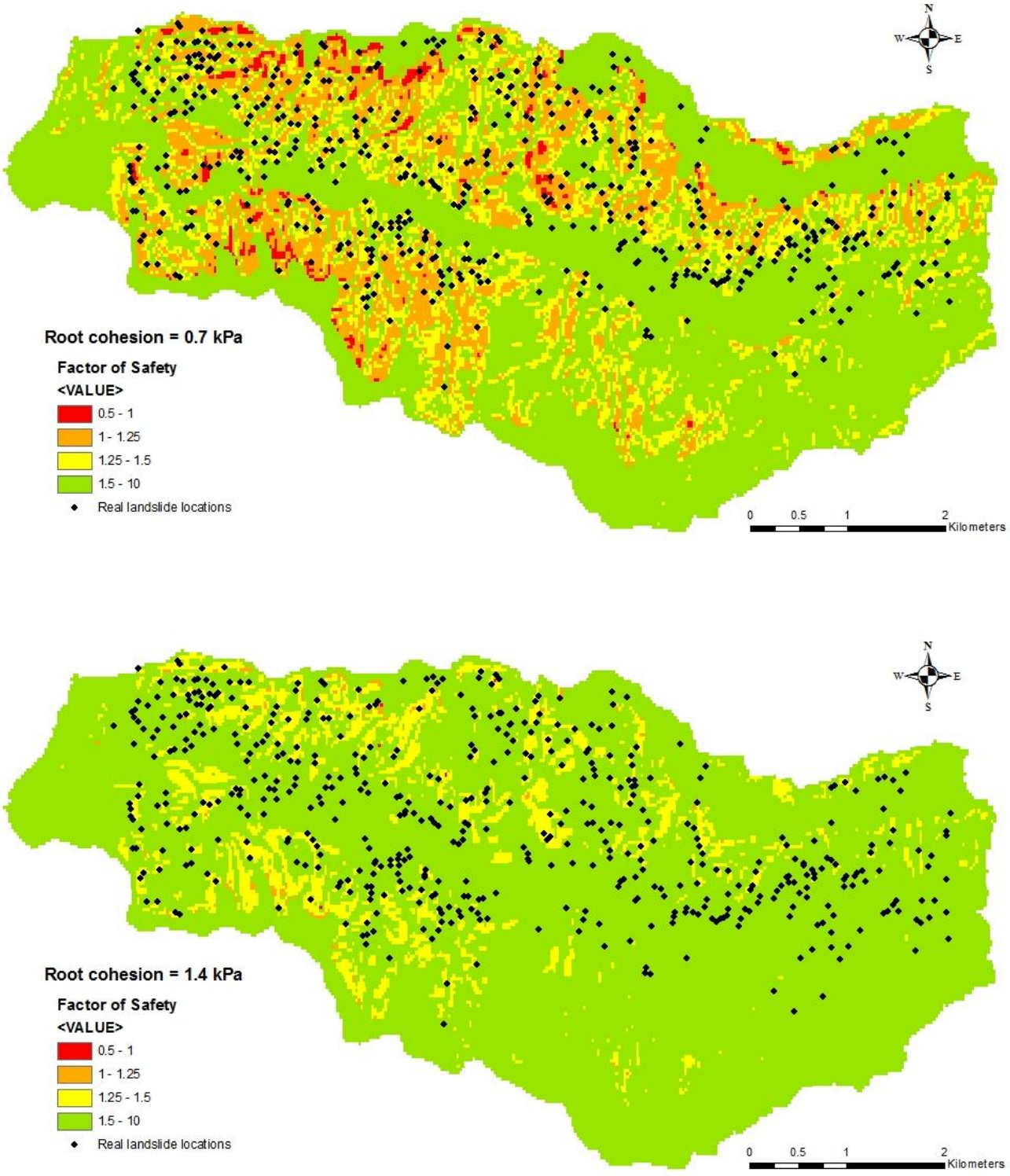

Figure 5.19. The TREX simulation results using root cohesion

Choi (2011) studied to assess the potential landslides in the Naerin Stream using RHESSys (Regional Hydro-Ecologic Simulation System) and stability model. In this research, he estimated root cohesion using leaf area index and the root cohesion was obtained to 0 to 1.4 kPa in the Naerin Stream. The average and the maximum value of this range were 0.7 kPa and 1.4 kPa respectively and these two values were applied to stability mapping using TREX and SINMAP. The results of the TREX simulation are shown in Figure 5.19.

The TREX simulation results showed that the factor of safety was sensitive to the root cohesion. When the root cohesion was 0.7 kPa, the factor of safety in the mountain areas was 1 to 1.25. When the root cohesion was 1.4 kPa, the factor of safety in the mountain area was 1.25 to 1.5 and some landslide locations near the main channel area showed stable with the factor of safety of 1.5 to 10.

The SINMAP simulation results showed that the root cohesion did not affect the factor of safety. When the root cohesion was increased to 1.4 kPa, the factor of safety was the same as that of Figure 5.17. This result indicated that SINMAP was not sensitive to little change of the root cohesion.

5.6 SHEAR STRESS MAP

5.6.1 Methods

Shear stress on the main channel and tributaries is very important to interpret the phenomenon of soil and wood debris delivered from upstream due to landslides. These materials increase the main channel bed, induce flood in the main channel, and bring a lot of damage to people, properties, and agricultural areas. Shear stress of water can be obtained from the following equation:

$$\tau_w = \gamma_w \, h \, \sin\theta \tag{5.20}$$

where: τ_w = shear stress of water [N/m^2]
γ_w = specific weight of water [N/m^3]
h = water depth [m]
$\sin\theta$ = slope

The specific weight of water was assumed to be 9,810 N/m^3 with water a temperature of 10°C. For small bed slopes, $\sin\theta$ can be approximated as $\tan\theta$, which is equal to the bed slope. The both simulation results using $\sin\theta$ and bed slope were very close each other.

The water depth on each cell within the Duksan Creek watershed was obtained from TREX simulation and is shown in Figure 5.20.

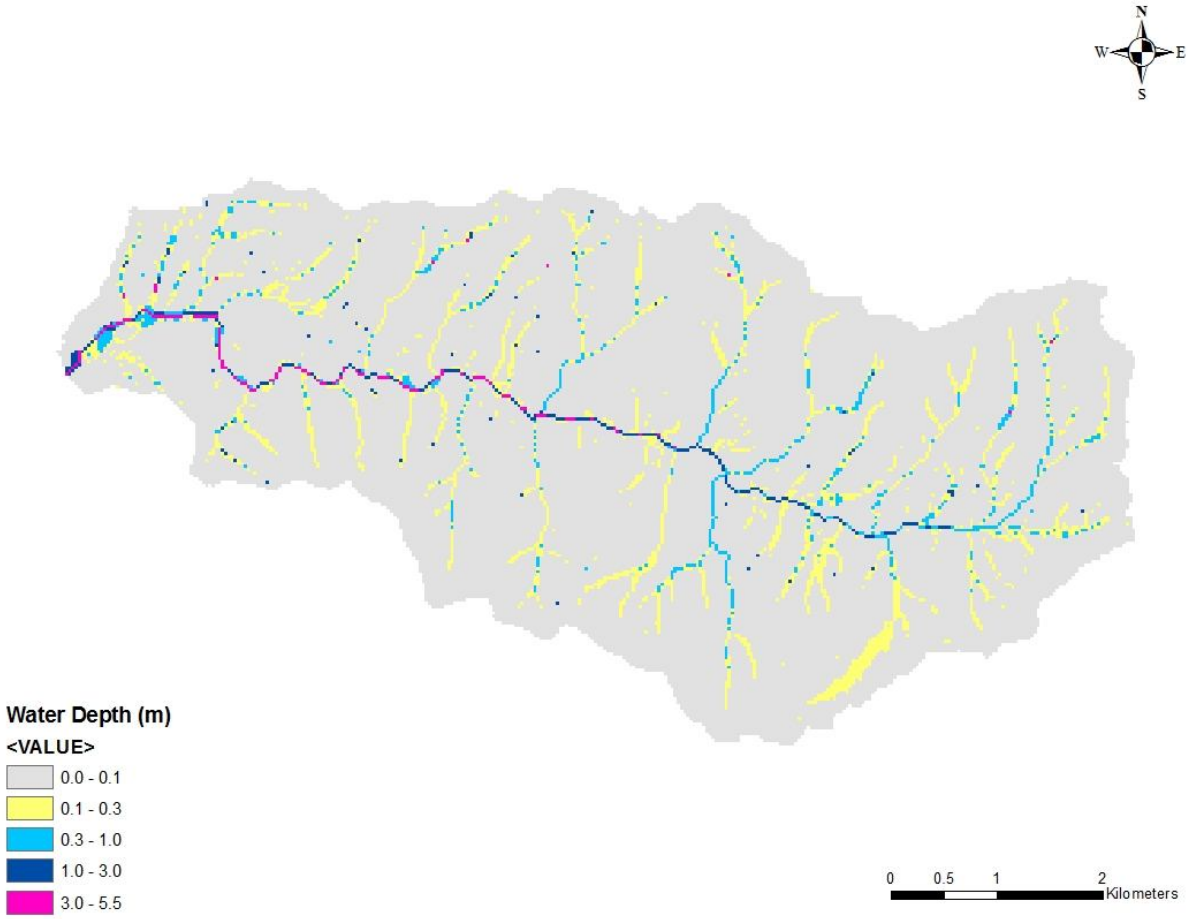

Figure 5.20. Water Depth in the Duksan Creek watershed

The water depth was attained when water depth on July 15, 9:00 to 10:00 AM, because landslides and debris flows occurred at this time (CJIC, 2006). Most areas with grey color showed under 0.1m of water depth. Tributaries of the main channel were expressed up to 1.0 m of water depth. In the downstream area, the water depth was distributed from 3.0 m to 5.5 m.

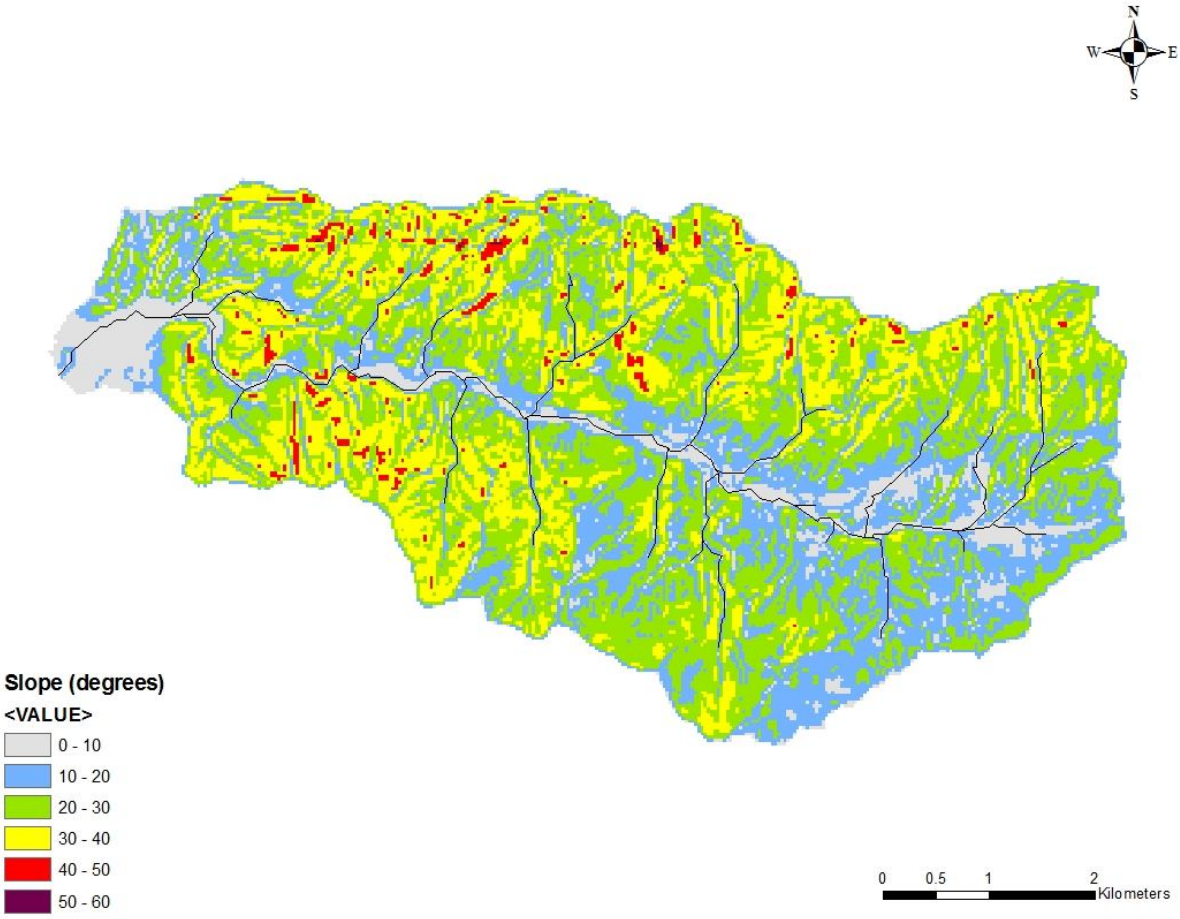

Figure 5.21. Slope in the Duksan Creek watershed

The slope was acquired from DEM and is shown in Figure 5.21. The steep slope was located in downstream area and most of them were displayed in the vicinity of tributaries on the main channel. It was estimated that when the Duksan Creek watershed had much volume of rainfall, debris flow would occur in the tributaries and the main channel.

Once all input parameters were obtained, shear stress was computed using the equation 5.20, and this is shown in Figure 5.22.

5.6.2 Results

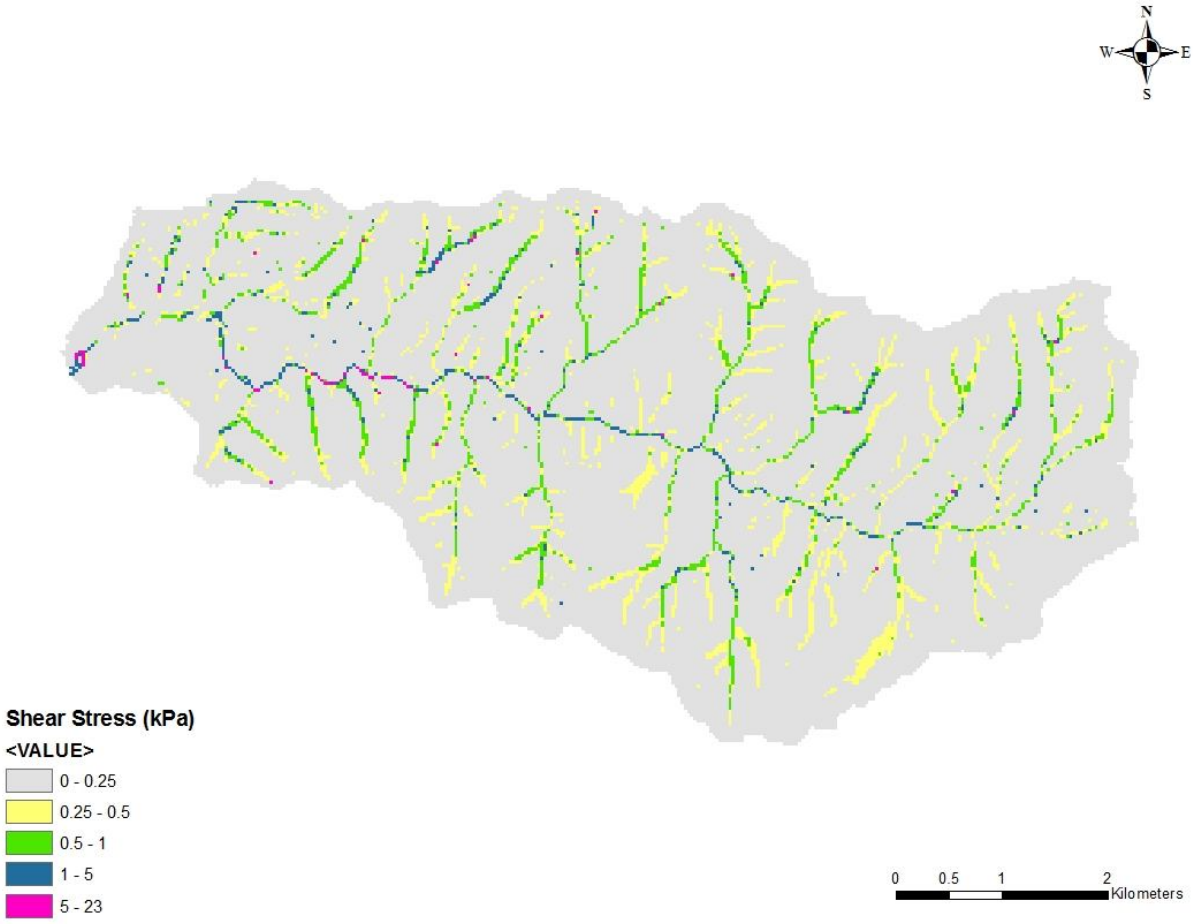

Figure 5.22. Shear Stress in the Duksan Creek watershed

Most watershed areas with grey color showed low shear stress. The shear stress was 0.5 to 1.0 kPa on the upstream of tributaries and 1.0 to 5.0 kPa on the downstream of the main channel. The shear stress was relatively low in the upstream of tributaries, increased in the downstream of tributaries, and was highest downstream of the main channel. This magnitude of shear stress is demonstrated in Table 5.8.

Table 5.8. Critical shear stress with respect to particle size (Julien, 2010)

Class name	d_s (mm)	τ_c (kPa)
Boulder		
Very large	>2,048	1.790
Large	>1,024	0.895
Medium	>512	0.447
Small	>256	0.223
Cobble		
Large	>128	0.111
Small	>64	0.053

When critical shear stress is close to 0.895 kPa, the class of particle size belongs to large boulders and the median diameter of this material is 1 m. Shear stress in the main channel area is 1 to 5 kPa, and this magnitude can move over 2.0 m of bed material.

This shear stress result was overlaid on the aerial image using GIS to describe real damaged areas of debris flow, and this is shown in Figure 5.23. The percent of each area from blue to red was 29.8 %, 41.5 %, 22.8 %, 3.5 %, and 2.5 %, respectively. The shear stress that can move the bed material up to gravel size (blue color) was mainly distributed in downstream area and upstream area with low slope. The bed material of cobble size (green) can be transported near main channel regions. The yellow colors were distributed in upstream tributary area. The high shear stress was mainly located in the main channel area. Based on the shear stress criteria in Table 5.8, the shear stress on each tributary was 0.223 to 0.895 kPa. This magnitude of shear stress assumed to move soil and woody debris from each tributary to the main channel. The higher shear stress of 1.79 to 17 kPa was presumed to make streambed damaged in the main channel. The residential and agricultural areas in downstream region occurred 0 to 0.223 kPa of shear stress. For this region, an aerial photograph was also provided to compare with the shear stress result. This is shown in Figure 5.24.

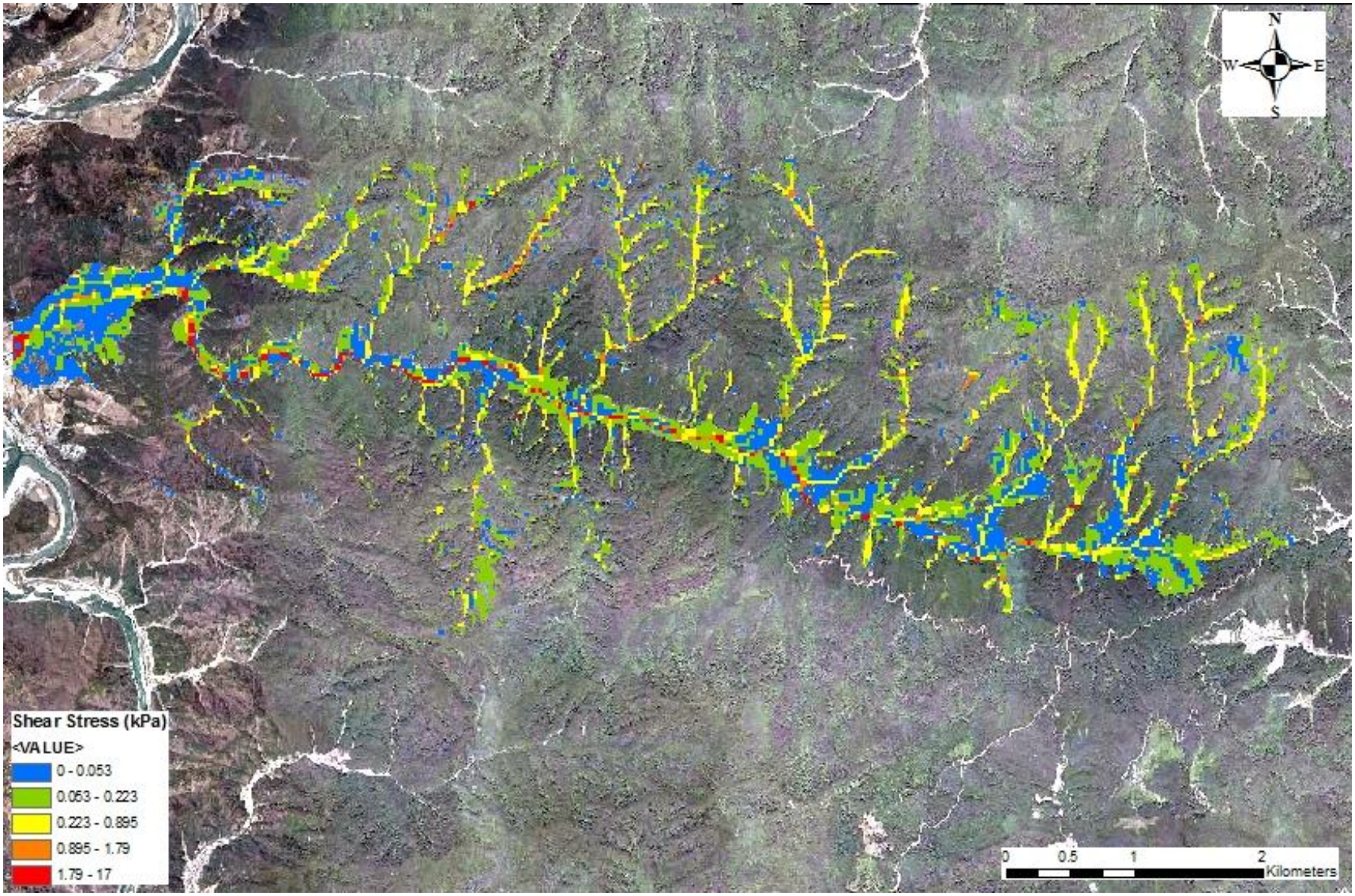

Figure 5.23. Shear stress map overlaid in an aerial image

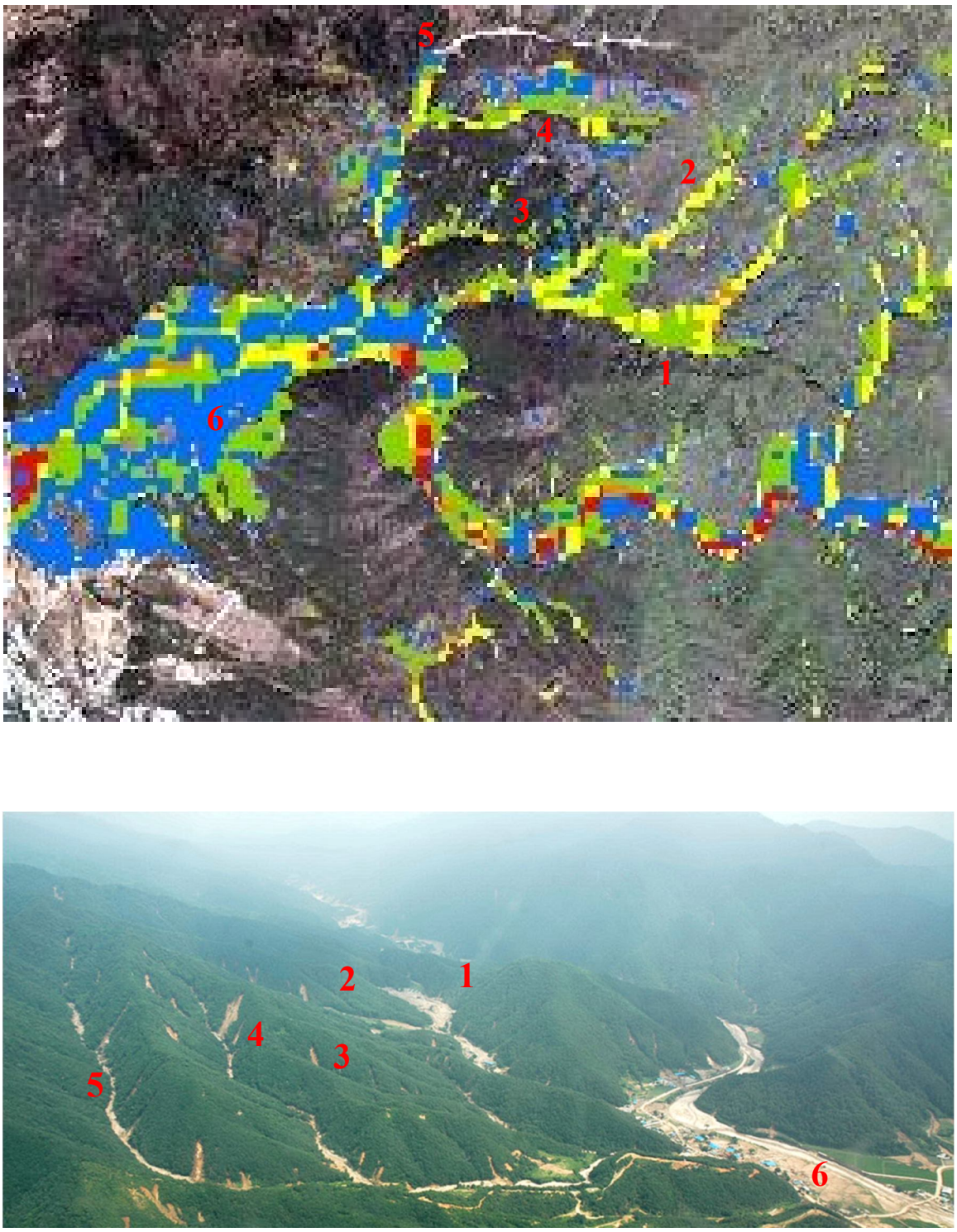

Figure 5.24. The comparison between shear stress and real damaged area

5.6.3 Field Investigation

Field investigation was carried out in the Duksan Creek watershed to compare shear stress results with field measurement data. The places where bed materials were sampled are shown in Figure 5.25.

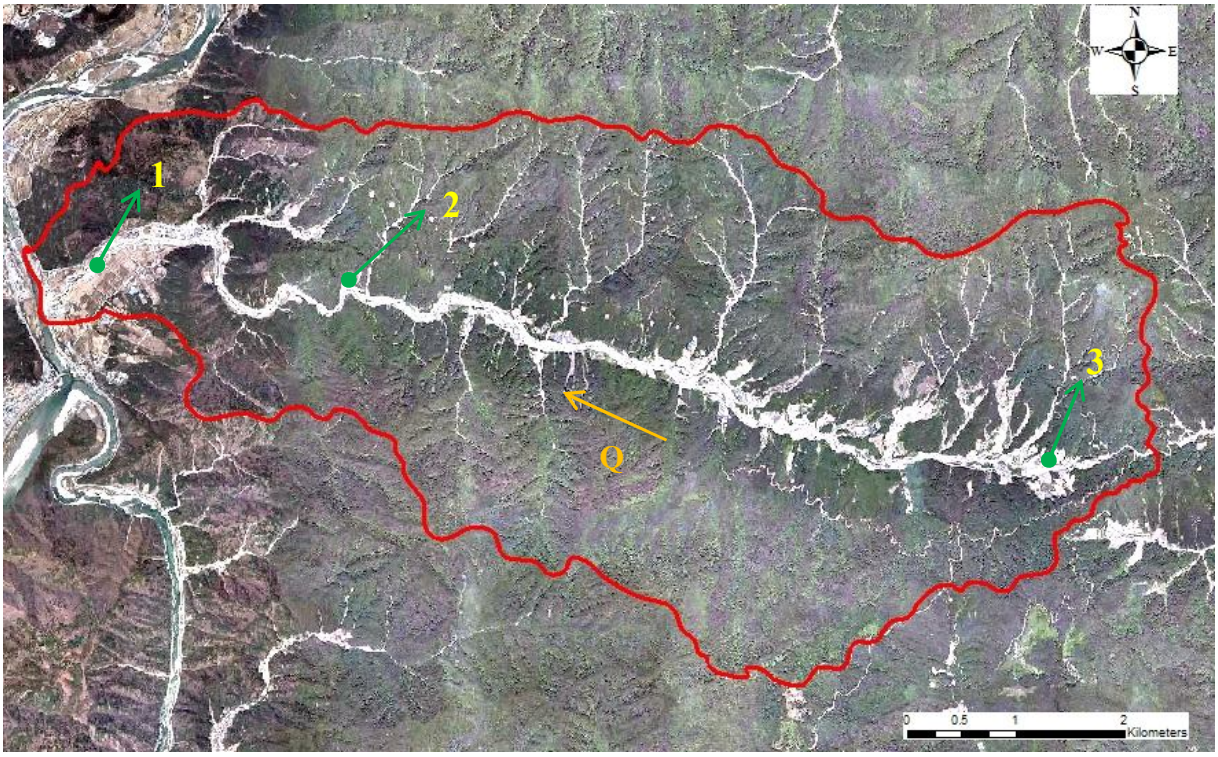

Figure 5.25. Field investigation places

A grid was established by a tape and a particle was collected in each grid at random. The bed material size from the place number 1 and 3 was 18 mm and 640 mm, respectively. This size of bed material is coarse gravel to medium boulder. The photographs at each measurement site are shown in Figure 5.26.

Figure 5.26. Bed material measurements in the Duksan Creek watershed

5.6.4 Benefits of Shear Stress Map

The damage due to extreme event started from landslides and the soil and woody debris from landslides could move to the main channel with the shear stress of 0.223 to 0.895 kPa. These materials assumed to be transported to the downstream area which caused the death of 4 people and 2 people missing within the Duksan Creek watershed. The damaged areas due to debris flows are shown in Figure 5.27. The number 1 and 2 was the location from in Figure 5.25.

Figure 5.27. Damaged areas due to debris flows

The first benefits of the shear stress map would provide not only water depth but also the magnitude of shear stress at each time step in the interested area when the TREX simulation is performed from extreme event. These results would be helpful to inform residents of the time to move to a shelter.

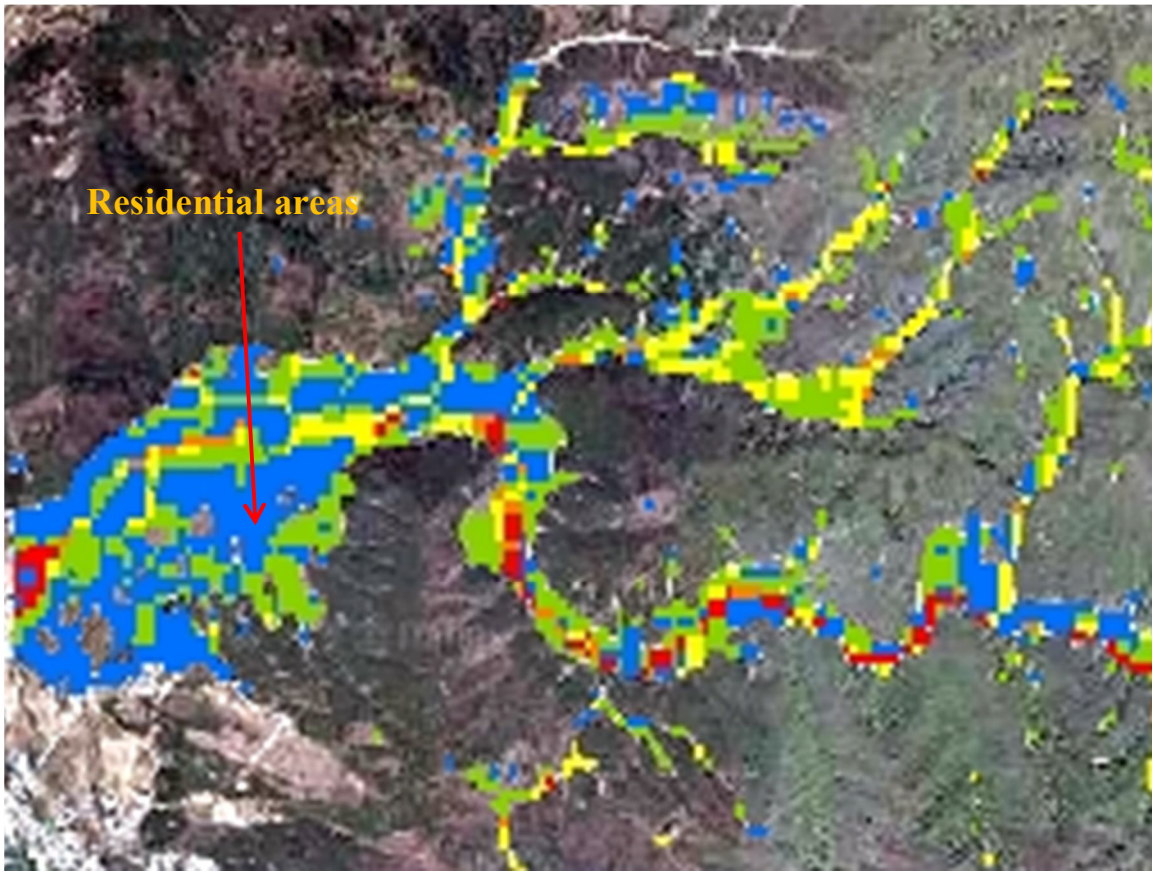

Figure 5.28. Shear stress map in the downstream of the Duksan Creek watershed

The second benefits of this map would assist to suggest the new location for houses and facilities damaged by debris flows. Shear stress map represents the magnitude of shear stress in the entire watershed. The areas where relatively low shear stress is distributed would be the best location for new residential and facility areas.

Therefore, the shear stress map would be beneficial to provide critical time for residents and to identify relatively a safe place in the interested areas due to extreme event.

CHAPTER 6 CONCLUSIONS

The objectives of this research are to simulate extreme event using TREX in mountain areas, to perform landslide and debris hazard area mapping. Surface runoff simulation using TREX produce hazard area map based on the infinite slope method. This model can also determine the maximum shear stress areas along the channel network. The conclusions for these are summarized in the following.

6.1 SURFACE RUNOFF SIMULATION USING TREX

The TREX model was calibrated in two areas, the Naerin Stream watershed and the Naesung Stream watershed. Naerin stream is located on the south eastern part of the Duksan Creek watershed. The relative percent differences of the Naerin Stream calibration for time to peak and peak discharge were 6.25 % and -2.58 % respectively. The percent differences of the Naesung Stream calibration for time to peak and peak discharge were 1.90 % and -0.25 %. Thus, the TREX model performance in South Korean mountains is in good agreement with the measured discharge data.

The TREX model simulation at the Duksan Creek watershed during the storm of July 15 in 2006 showed a peak discharge of 452 m^3/s. This result was compared with the SCS method, HEC-HMS, CLARK, and Nakayasu models. Among these the result of SCS method showed 457 m^3/s and the relative percent difference between the TREX simulation and the SCS method was -1.1 %. For this storm, the specific peak discharge of Duksan Creek was 13.7 $m^3/s/km^2$ and is consistent well with the range of peak discharges of other watersheds.

6.2 LANDSLIDE HAZARD AREA MAPPING

Hazard mapping in mountainous areas was performed using the infiltration depth from the TREX simulation and the infinite slope analysis. The infiltration depth range of 0.2 m to 1.0 m corresponds to the critical slope angle range of 19° to 29°. These results were very comparable to the failure depth of 0.3 m to 0.8 m from the field investigation and the failure slope angle of 16° to 29° from the analysis of satellite image and aerial photograph. The infiltration depth of 0.2 to 0.3m in the mountainous areas corresponds to the critical slope angle of 25° to 29°. This slope angle was very comparable with the failure slope angle of 26° from the field investigation and the analysis in satellite image and aerial photograph.

Watershed stability mapping from TREX and SINMAP were compared with a landslide hazard map developed by KFRI. The predictability of KFRI map, SINMAP and TREX was 3.5 %, 73.6 % and 44.8 %. However, the result of SINMAP predicted much larger areas as unstable regions when it compared to the result of TREX. In the analysis of the relative predictability, the TREX result was improved to 24.6 % compared to the result of SINMAP.

6.3 DEBRIS FLOWS HAZARD AREA MAPPING

Both SINMAP and KFRI maps predict unstable hill slopes and relatively stable valleys, while TREX simulation results showed very high shear stress along the tributaries and the main channel at the Duksan Creek watershed. The TREX model can calculate the distribution of water depth and shear stress in the Duksan Creek watershed at a 30 m resolution. The shear stress values from the TREX range from 0.223 kPa to 0.895 kPa on the tributaries and from 1.79 kPa to 17 kPa in the main channel. Since a critical shear stress of 0.895 kPa can move a 1 m diameter boulder, severe damage from debris flows would be expected in this steep mountainous

channel. The shear stress map was compared to aerial photographs and the location of major debris flow areas correspond very well with the calculated areas of high shear stress. Therefore, the shear stress map would be helpful to identify potential damage areas from debris flows.

REFERENCES

Abdullrazzak, M., and Morel-Seytoux, H. 1983. Recharge from an ephemeral stream following wetting front arrival to water table. Water Resources Research, 19(1), 194-200.

Alexander, L. V., Hope, P., Lynch, A., and Nicholls, N. 2007. Trends in Australia's climate means and extremes: a global context. Australian Meteorological Magazine, 56, 1-18.

Ambrose, R. B., Martin, J. L. and Wool, T. A. 1993. WASP5, A hydrodynamic and water quality model -- Model theory, user's manual, and programmer's guide. U.S. Environmental Protection Agency, Office of Research and Development, Environmental Research Laboratory, Athens, Georgia.

Bae, S. 2007. Cause analysis of 2006 concentrated heavy rain which occurred in Inje-gun. The Korean Association of Regional Geographers, 13(4), 396-408.

Baum, R. L., Savage, W. Z., and Godt, J. W. 2008. TRIGRS-A Fortran program for transient rainfall infiltration and grid-based regional slope stability analysis, version 2.0. U.S. Geological Survey, Reston, Virginia.

Bicknell, B. R., Imhoff, J.C., Kittle, J.L., Jr., Donigian, A.S., Jr., and Johanson, R.C. 1996. Hydrological Simulation Program—Fortran: User's manual for version 11. U.S. Environmental Protection Agency, National Exposure Research Laboratory, Athens, Georgia. EPA/600/R-97/080.

Byun, I. 2010. Analysis of characteristics and causes of landslides due to locally concentrated heavy rainfall in Inje area. M.S. thesis, Department of Civil Engineering, Gangwon National University, South Korea.

Casagli, N., Dapporto, S., Ibsen, M.L., Tofani, V., and Vannocci, P. 2006. Analysis of the landslide triggering mechanism during the storm of 20th-21st November 2000, in Northern Tuscany. Landslides, 3, 13-21.

Cha, E. 2010. The characteristics of long term precipitation: extreme precipitation and typhoon. Korea Society of Hazard Mitigation, 10(2), 64-73.

Chang, H. and Kwon, W. 2007. Spatial variations of summer precipitation trends in South Korea, 1973-2005. Environmental Research Letters, 2, 1-9.

Cho, Y. 2006. Characteristics and prediction model for landslides in granites of Gangneung area. Ph.D. dissertation, Department of Geology, Kyungpook National Univesity, Daegu, Korea.

Choi, J. 2011. Assessment of potential landslides in Naerin watershed: Linking eco-hydrology model and stability model. M.S. thesis, Department of Environmental Science, Gangwon National University, South Korea.

CJIC. 2006. The report of the investigation in Gangwon area. Central joint investigation committee.

Cornforth, D. H. 2005. Landslides in practice. John Wiley & Sons, Inc.

Creager, W. P., Justin, J.D., and Hinds, J.D. 1945. General design, Vol.1 of engineering for dams series. Wiley, New York.

Cruden, D. M. 1991. A simple definition of a landslide. Bulletin IAEG, 43, 27-29

Dietrich, W. E. and Montgomery, D. R. 1998. SHALSTAB: A digital terrain model for mapping shallow landslide potential. http://socrates.berkeley.edu/ ~geomorph/shalstab/.

Downer, C. W., and Ogden, F.L. 2004. GSSHA: model to simulate diverse stream flow producing processes. Journal of Hydrologic Engineering, 93(3), 161-174.

Easterling, D. R., Evans, J. L., Groisman, P. Ya., Karl, T. R., Kunkel, K. E., and Ambenje, P. 2000. Observed variability and trends in extreme climate events: a brief review. Bulletin of the American Meteorological Society, 81(3), 417-426.

England, J., Velleux, M., and Julien, P. 2007. Two-dimensional simulations of extreme floods on a large watershed. Journal of Hydrology, 347(1), 229-241.

Ewen, J., Parkin, G., and O'Connell, P.E. 2000. SHETRAN: distributed river basin flow and transport modeling system. Journal of Hydrologic Engineering, 5(3), 250-258.

Fell, R. 1994. Landslide risk assessment and acceptable risk. Canadian Geotechnical Journal. 31, 261-272.

Green, W. H., and Ampt, G. A. 1911. Studies on soil physics, 1: the flow of air and water through soils. Journal of Agricultural Sciences, 4(1), 11-24.

Groisman, P. V., Karl, T. R., Easterling, D .R., Knight, R. W., Jamason, P. F., Hennessy, K. J., Suppiah, R., Page, C. M., Wibig, J., Fortuniak, K., Razuvaev, V. N., Douglas, A., Forland, E., and Zhai, P. 1999. Changes in the probability of heavy precipitation: important indicators of climatic change. Climate Change, 42(1), 243-283.

Groisman, P. Y., Knight, R. W., and Karl, T. R. 2001. Heavy precipitation and high streamflow in the contiguous United States: Trends in the twentieth century. Bulletin of the American Meteorological Society, 82(2), 219-246.

Hammond, C., Hall, D., Miller, S., and Swetik, P. 1992. Level 1 stability analysis (LISA) documentation for version 2.0. General technical report INT-285, Intermountain Research Station, Forest Service, U.S. Department of Agriculture.

Haylock, M and Nicholls N. 2000. Trends in extreme rainfall indices for an updated high quality data set for Australia, 1910-1998. International Journal of Climatology, 20, 1533-1541.

Highland, L. M., and Bobrowsky, P. 2008. The landslide handbook - A guide to understanding landslides. United States Geological Survey.

Inje County. 2008. Duksan Creek mater plan. Inje County, Gangwon Province, South Korea.

Jin, M. 1980. Geological and isotopic contrasts of the Jurassic and Cretaceous granites in South Korea. The Journal of the Geological Society of Korea, 16(4), 205-215

Johnson, B. E., Julien, P.Y., Molnar, D.K., and Watson, C.C. 2000. The two-dimensional upland erosion model CASC2D-SED. Journal of the American Water Resources Association, 36(1), 31-42.

Julien, P. Y. 2002. River mechanics. Cambridge University Press, Cambridge, UK.

Julien, P. Y. 2010. Erosion and sedimentation (Second Edition). Cambridge University Press, UK.

Julien, P. Y., and Rojas, R. 2002. Upland erosion modeling with CASC2D-SED. International Journal of Sediment Research, 17(4), 265-274.

Julien, P. Y., Saghafian, B., and Ogden, F.L. 1995. Raster-based hydrologic modeling of spatially-varied surface runoff. Water resources bulletin, AWRA, 31(3), 523-536.

Jung, H., Choi, Y., Oh, J., and Lim, G. 2002. Recent trends in temperature and precipitation over South Korea. International Journal of Climatology, 22, 1327-1337.

Jung, I., Bae, D., and Kim, G. 2011. Recent trends of mean and extreme precipitation in Korea. International Journal of Climatology, 31, 359-370.

Karl, T.R., Knight, R. W., Easterling, D. R., and Quayle, R. G. 1996. Indices of climate change for the United States. Bulletin of the American Meteorological Society, 77 (2), 279-292.

Karl, T. R. and Knight R. W. 1998. Secular trends of precipitation amount, frequency, and intensity in the United States. Bulletin of the American Meteorological Society, 79(2), 231-241.

KFS. 2009. Erosion control manual. Korea Forest Service.

KFS. http://sansatai.forest.go.kr/dg_005.do. Korea Forest Service.

Kim, H. 2011. Investigation and statistical analyses of landslide damages in the western area of Gangwon during heavy rainfall in 2006. M.S. thesis, Department of Civil Engineering, Kangwon National University, South Korea.

Kim, K. 2010. Stability analysis of slopes in unsaturated weathered soils considering field characteristics. M.S. Thesis, Department of Civil Engineering, Yeungnam University, South Korea.

Kim, Y., and Chae, B. 2009. Characteristics of rainfall, geology and failure geometry of the landslide areas on natural terrains, Korea. The Journal of Engineering Geology, 19(3), 331-344.

Kim, K., Choo, C., Booh, S., and Jeong, G. 2005. Importance of microtextural and geochemical characterizations of soils on landslide sites. The Journal of Engineering Geology, 15(4), 447-462.

Kim, W., Kim, K., Chae, B., and Cho, Y. 2000. Case study of landslide types in Korea. The Journal of Engineering Geology, 10(2), 18-35.

Kim, Y., Lee, S., Kim, K., and Chae, B. 1998. Landslide types and susceptibilities related to geomorphic characteristics - Yeonchon, Chulwon area. The Journal of Engineering Geology, 8(2), 115-130.

Kim, Y., Shin, H., and Park, D. 2011. Variation of shear strength of unsaturated weathered granite soil with degree of saturation and disturbance at Dongrae, Inje and Yeonki sites. Korea Society of Hazard Mitigation, 11(4), 157-162.

Kim, K., Song, Y., Kim, Y., and Jeong, G. 2006. Characteristics of rainfall and landslides according to the geological condition. The Journal of Engineering Geology, 16(2), 201-214.

Klein Tank, A. M. G., and Coauthors. 2002. Daily data set of 20th century surface air temperature and precipitation series for the European climate assessment. International Journal of Climatology, 22, 1441-1453.

Klein Tank, A. M. G. and Konnen, G. P. 2003. Trends in indices of daily temperature and precipitation extremes in Europe, 1946-99. American Meteorological Society, 16(22), 3665-3680.

Kuichling, E. 1889. The relation between the rainfall and the discharge of sewers in populous districts, Transactions. American Society of Civil Engineers, 20(1), 1-56.

Kunkel, K. E., Andsager, K., and Easterling, D. R. 1999. Long-term trends in extreme precipitation events over the conterminous United States and Canada. American Meteorological Society, 12, 2515-2527.

Kunkel, K. E., Easterling, D. R., Redmond, K., and Hubbard, K. 2003. Temporal variations of extreme precipitation events in the United States: 1895-2000. Geophysical Research Letters, 30(17), 1900, doi:10.1029/2003GL018052.

KMA. http://www.kma.go.kr/weather/warning/standard.jsp. Korea Meteorological Administration

KWRA. 2009. River design criteria. Korea Water Resources Association.

Lee, C. and Yoo, N. 2009. A study on debris flow landslide disasters and restoration at Inje of Kangwon Province, Korea. Korean Society of Hazard Mitigation, 9(1), 99-105.

Li, R. M., Stevens, M.A., and Simons D.B. 1976. Solutions to Green-Ampt infiltration equations. Journal of Irrigation and Drainage Division, ASCE, 102(IR2), 239-248.

Maidment, D. R. 1993. Handbook of hydrology. McGraw-Hill, Inc.

MLTM, 2001. Water vision. Minister of Land, Transport and Maritime affairs.

MLTM, 2006. Water vision. Minister of Land, Transport and Maritime affairs.

Molnár, D. K. and Julien., P.Y. 2000. Grid size effects on surface runoff modeling. Journal of Hydrologic Engineering, 5(1), 8-16.

Montrasio, L., and Valentino, R. 2008. A model for triggering mechanisms of shallow landslides. Natural Hazards and Earth System Science, 8, 1149-1159.

Muntohar, A. S., and Liao, H.J. 2009. Analysis of rainfall-induced infinite slope failure during typhoon using a hydrological-geotechnical model. Environmental Geology, 56, 1145-1159.

Neitsch, S. L., Arnold, J. G., Kiniry, J. R., and Williams, J.R. 2009. Soil and water assessment tool theoretical documentation , version 2009. Grassland, soil and water research laboratory, Agricultural Research Service, Temple, Texas.

Oh, C., Kim, K., and Choi, C. 2009. Analysis of landslide characteristics of Inje area using SPOT5 images and GIS analysis. Korean Journal of Remote Sensing, 25(5), 445-454.

Pack, R. T., Tarboton, D. G., and Goodwin, C. N., 1998a. Terrain stability mapping with SINMAP, technical description and users guide for version 1.00. Report number 4114-0, Terratech Consulting Ltd., Salmon Arm, British Columbia, Canada.

Pack, R. T., Tarboton, D. G., and Goodwin, C. N., 1998b. The SINMAP approach to terrain stability mapping. 8th Congress of the International Association of Engineering Geology, Vancouver, British Columbia, Canada.

Pack, R. T., Tarboton, D. G., and Goodwin, C. N., 2001. Assessing terrain stability in a GIS using SINMAP. 15th annual GIS conference, GIS 2001, Vancouver, British Columbia, Canada.

Pack, R. T., Tarboton, D. G., and Goodwin, C. N., 2005. SINMAP 2. A stability index approach to terrain stability hazard mapping, technical description and users guide for version 2.0. Utah State University.

Park, D., Song, Y., and Son, Y. 2010. Assessment of infiltration phases considering ground characteristics of steep-slope. National Institute of Disaster Prevention, South Korea.

Park, N. 2008. A study on characteristics of landslide of debris flow in Kangwon-do. MS. Thesis, Department of Civil Engineering, Kangwon National University, South Korea.

Phillip, J. R. 1957. The theory of infiltration: 1. The infiltration equation and its solution. Soil Science, 83, 345-357.

Rawls, W. J., Ahuja, L.R., Brakensiek, D.L., and Shirmohammadi, A. 1993. Infiltration and soil movement. In: Handbook of Hydrology, Maidment, D.R., de. , McGraw-Hill, Inc.

Rawls, W. J., Brakensiek, D.L., and Miller, N. 1983. Green-Ampt infiltration parameters from soils data. Journal of Hydraulic Engineering, 109(1), 62-69.

Richards, L. A. 1931. Capillary conduction of liquids in porous mediums. Physics, 1, 318-333.

Rojas, R. 2002. GIS-based upland erosion modeling, geovisualization and grid size effects on erosion simulations with CASC2D-SED. Ph.D. dissertation, Department of Civil Engineering, Colorado State University, Fort Collins, Colorado.

Rojas, R., Julien, P.Y., and Johnson, B. 2003. A 2-dimensional rainfall-runoff and sediment model(Reference Manual). Colorado State University, Fort Collins, Colorado.

Salgado, R. 2006. The engineering of foundations. McGraw-Hill, Inc.

Scharffenberg, W. A., and Fleming, M. J. 2010. Hydrologic modeling system HEC-HMS user's manual. US Army Corps of Engineers.

Shieh, C. L., Chen, Y.S., Tsai, Y.J., and Wu, J.H. 2009. Variability in rainfall threshold for debris flow after the Chi-Chi earthquake in central Taiwan, China. International Journal of Sediment Research, 24(2), 177-188.

Skempton, A. W., DeLory, F. A. 1957. Stability of natural slopes in London clay. Proceedings 4th International Conference on Soil Mechanics and Foundation Engineering, 2, 378–381.

Smith, R. E., and Parlange, J.-Y. 1978. A parameter efficient hydrologic infiltrations model. Water Resources Research, 14(3), 533-538.

Solomon, S., Qin, D., and Manning, M. 2007. Climate change 2007: The physical science basis. Cambridge University Press, UK.

Son, J., Kim, K., Lee, C., and Choi, C. 2009. Analysis of landslide in Inje region using aerial photograph and GIS. The Korean Society for Geospatial Information System, 17(2), 61-69.

Spierre, S. G. and Wake, C. P. 2010. Trends in extreme precipitation events for the northeastern United States 1948-2007, Carbon Solutions New England and University of New Hampshire, Durham, NH, 03824

USGS. http://pubs.usgs.gov/fs/2004/3072/fs-2004-3072.html. U.S. Geological Survey.

Varnes, D. J. 1958. Landslides types and processes. Highway Research Board Special Report.

Varnes, D. J. 1978. Slope movement types and processes. Transportation Research Board Special Report.

Velleux, M. 2005. Spatially distributed model to assess watershed contaminant transport and fate. Ph.D. dissertation, Department of Civil Engineering, Colorado State University, Fort Collins, Colorado.

Velleux, M. 2011. TREX watershed modeling framework user's manual: Model theory and description. HDR-HydroQual, Inc, Colorado State University, and Bureau of Reclamation flood hydrology and meteorology group.

Velleux, M., England, J., and Julien, P. 2008. TREX: spatially distributed model to assess watershed contaminant transport and fate. Science of the Total Environment, 404(1), 113-128.

Velleux, M., Fanelli, C., Takamatsu, M., and Schwartz, D. 2012. TREX application to Naesung Stream : Hydrology and sediment transport calibration results. HDR|HydroQual, Mahwah, New Jersey, U.S.

Velleux, M., Julien, P. Y., Rojas-Sanchez, R., Clements, W., and England, J. 2006. Simulation of metals transport and toxicity at a mine-impacted watershed: California Gulch, Colorado. Environmental Science and Technology, 40(22), 6996-7004.

Velleux, M., Westenbroek, S., Ruppel, J., Settles, M., and Endicott, D. 2001. A user's guide to IPX, the in-place pollutant export water quality modeling framework, version 2.7.4. U.S. Environmental Protection Agency, Office of research and development, National health and environmental effects research laboratory, Mid-continent ecology division, Large Lakes research station, Grosse Ile, Michigan. 179 pp. EPA/600/R-01/079.

Viessman, J., W, and Lewis, G.L. 2003. Introduction of Hydrology, Fifth Edition, Prentice Hall.

Wang, Y. and Zhou, L. 2005. Observed trends in extreme precipitation events in China during 1961-2001 and the associated changes in large scale circulation. Geophysical Research Letters, 32, L09707, doi:10.1029/2005GL022574.

Woodward, D. E. 2007. National engineering handbook, Chapter 19 transmission losses. National Resources Conservation Service.

Woolhiser, D. A., Smith, R.E., and Goodrich, D.C. 1990. KINEROS, A kinematic runoff and erosion model: Documentation and user manual. U.S. Department of Agriculture, Agriculture Research Service. ARS-77.

Wu, W. and Sidle, R. C. 1995. A distributed slope stability model for steep forested basins. Water Resources Research, 31(8), 2097-2110.

Wu, W. and Sidle, R. C. 1997. Application of a distributed shallow landslide analysis model (dSLAM) to managed forested catchments in Oregon, USA. Human Impact on Erosion and Sedimentation, Proceedings of Rabat symposium S6, IAHS, No. 245.

Yeon, Y. 2011. Evaluation and analysis of Gwangwon-do landslide susceptibility using logistic regression. The Korea Association of Geographic Information Studies, 14(4), 116-127.

Xu, X., Du, Y., Tang, J., and Wang, Y. 2011. Variations of temperature and precipitation extremes in recent two decades over China, Atmospheric Research, 101, 143-154.

Yun. 2003. Engineering hydrology. Chungmoongak. South Korea.

APPENDICES

APPENDIX A. COUNTERMEASURES FOR HAZARD AREAS

A.1 EROSION CONTROL WORKS

Erosion control work is a general term of the project that is in operation to prevent flood disaster and landslides, to protect houses and agriculture lands, to restore damaged area and to provide water for irrigation. Until the 1980's, this works were focused on the restoration in forest denudation areas including hillside erosion control and seacoast sand dune fixation. After the 1990's, this works put emphasis on the prevention of disasters and the supply of water for irrigation, including erosion control dam and torrent erosion control. Since most forest areas have steep slopes and are vulnerable to natural disasters, erosion control work is necessary to protect people's lives and property and to preserve national land and forest resources.

A.2 EROSION CONTROL METHODS

A.2.1 Hillside Erosion Control Works

Hillside erosion control is the operation at hillside to prevent forest denudation through the restoration of vegetation in desolated forest areas or expected devastated areas. The target areas are devastated land, slipped land, creeping land, damaged land and denuded torrential stream. Hillside erosion control works can be classified as foundation work for stabilizing slope and controlling erosion and afforestation for covering slopes with vegetation and preventing soil erosion. They are summarized in Table A.1.

Table A.1. The classification of hillside erosion control works (KFS, 2009)

Classification	Detail works
Foundation works	Slope grading works Soil arresting structures Underground-laying structures Rill control structures Channel works Check dam
Afforestation	Plank-board barrier works Terrace-sodding works Stepped mini-terrace works Strip-terracing works Strip-sod works Slope mulching works Direct seeding works Tree planting works

A.2.2 Erosion Control Dams

An erosion control dam is a small scale dam which crosses a stream with 30 m to 50 m of width and 4 m to 5m of height. The main construction materials are concrete, steel, and boulder. The objective of this dam is to reduce stream bed gradient, to check longitudinal and transversal erosion, to fix foothill, to prevent hillside failure, to control debris, to maintain channel in turbulent areas and to preserve stream ecosystems. The first function of an erosion control dam is to storage sand or debris. Soil and wood debris from heavy intense rainfall can be intercepted and flow velocity also can be reduced. The effect of this dam can be estimated as 5,000 m^3 / 50 m of width. The second function of this dam is to store water. This function relies on a given condition of a constructed site, and this water can be used as the extinguishment of a forest fire and irrigation. The effect of this dam is to be estimated as 3,000 m^3 / 50 m of width. The erosion control dam can be classified as types, functions, and main structure materials. Examples for this are stone dam, screen dam, concrete dam, steel dam, cell, and slit dam.

A.2.3 Torrent Erosion Control Works

Torrent erosion control works prevent longitudinal and transversal erosion by fixing foothill and reducing flow velocity using constructions on devastated mountain streams. The target area is a denudated mountain stream where a watershed area is within 300 ha and has a stable upper stream with afforestation and is the place where landslides or agricultural land and road damages can be expected due to denudated mountain streams. The examples are revetment, stream grade stabilization structures, spur, embankment, and toe protection.

A.2.4 Seacoast Sand Dune Fixation

The purpose of seacoast erosion control is to fix sand dunes in coastal areas and to protect residence and agricultural areas from sand scatter. The methods are sand dune fixation-hedge works, sand dune mulching, tide prevention works, sand dune stabilizing hedge works, and afforestation in sand dune areas.

A.3 APPLICATION EXAMPLES IN DUKSAN CREEK

A.3.1 Hillside Control Works

Figure A.1. Hill side control works example in Duksan Creek

Several slope failures occurred in the Duksan Creek watershed, and one example in the damaged areas is shown in Figure A.1. Rill control structures can be used to prevent rill erosion on slope erosion areas due to heavy rainfall. The construction materials are stone, sod, and concrete blocks. This structure is to be installed to cross sectional direction compared to rill erosion direction. The bottom of this area is finished with gabions.

(a) (b)

Figure A.2. Channel work and grading work examples in Duksan Creek

Figure A.2 (a) shows channel works. This structure makes flows from heavy rainfall to guide into drainage for hillslope stability. Figure A.2 (b) represents slope grading works. This structure can be installed in steep slope or irregular slope.

A.3.2 Erosion Control Dams

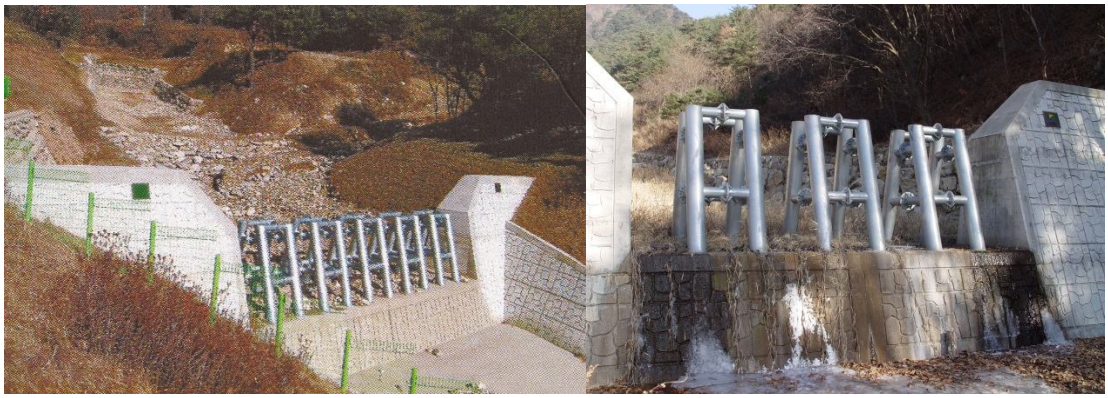

Figure A.3. Slit dam example in Duksan Creek

Four types of erosion control dams were constructed in Duksan Creek watershed. The first type of erosion control dam is slit dam and this is shown in Figure A.3. The main construction materials of slit dam are concretes or steels and these materials can be installed as columns in the erosion control dam. This dam prevents wood or soil debris at flood conditions and passes through the soil debris slowly at normal times.

Figure A.4. Buttress dam example in Duksan Creek

The second type of erosion control dam is buttress dam and is shown in Figure A.4. This is one of the screen dams and the main construction materials are concretes or steels and can be made screen shape. This dam prevents rapid soil debris at flood times and allows soil debris slowly at ordinary times.

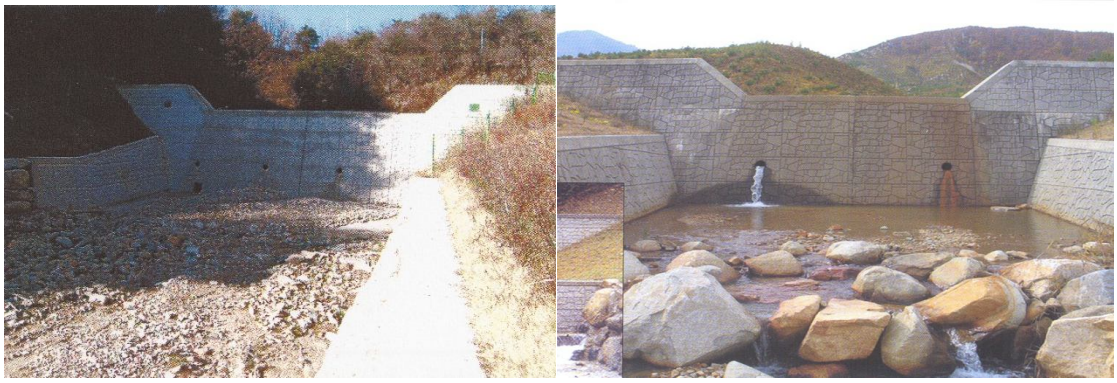

Figure A.5. Concrete dam example in Duksan Creek

The third type of erosion control dam is concrete dam and is shown in Figure A.5. This dam fills concretes into the form. The advantages of this dam are to maintain equal quality, to control the intensity of concretes when necessary and to enable the standardization of work.

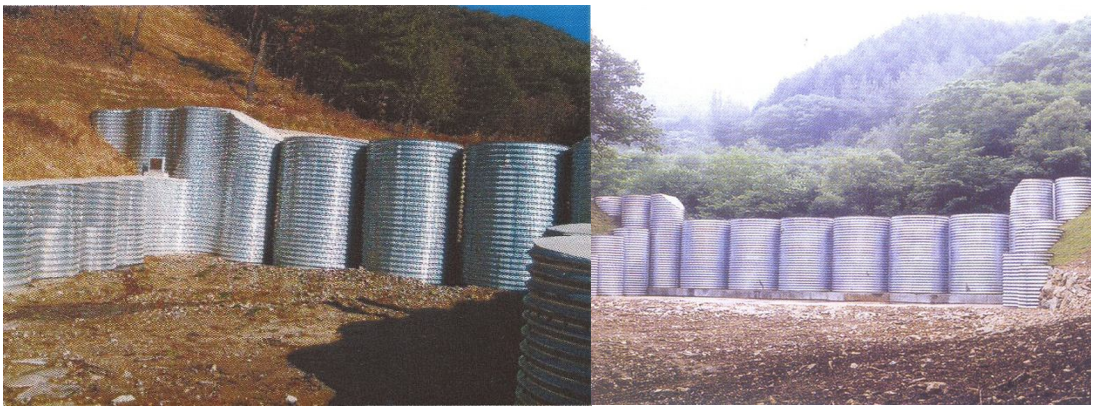

Figure A.6. Shell dam example in Duksan Creek

The fourth type of erosion control dam is shell type dam and shown in Figure A.6. This dam installs a large size of cylinder types of structure continuously. Since this structure is to save construction time, it can be used on the forest fire area or the large scale of debris flow in damaged area.

A.3.3 Torrent Erosion Control Works

(a) (b)

Figure A.7. Torrent erosion control works in Duskan Creek

Figure A.7 shows small check dam (a) and revetment (b). A small check dam reduces stream gradient and flow velocity and prevents soil debris and erosion. Revetment protects bank erosion in devastated small streams. This structure can be installed in the curvature of a stream to reduce bank shear.

The structures introduced above are appropriate to preserve residential and agricultural areas. Since these structures are constructed in steep mountain areas, they should be maintained continuously. Dredging at erosion control dams needs to be operated periodically, because soil debris can accumulate within the erosion control dam.